

2. EXPLANATORY NOTES¹

Shipboard Scientific Party²

INTRODUCTION

The “Explanatory Notes” chapter is designed to document the primary procedures and methods employed by the various shipboard laboratories in order to understand the basis of the preliminary interpretations. This information concerns only shipboard operations and analyses described in this volume.

Authorship of Site Chapters

Descriptions of individual drilling sites, summaries of operations, and preliminary results and interpretations are contained in the site chapters. This volume should be treated as a publication to which all the scientists listed in the front pages have contributed. The following shipboard scientists, listed in alphabetical order, made the principal contributions to the following sections:

Background and Objectives: Ludden, Plank
Operations: Escutia, Foss, Ludden, Plank
Site Geophysics: Abrams, Larson, Pockalny
Sedimentology: Escutia, Pletsch, Valentine
Biostratigraphy: Bartolini, Lozar
Basement: Alt, Armstrong, Barr, Honnorez, Kelley, Ludden, Plank,
Rouxel, Schmidt, Staudigel, Valentine
Paleomagnetism: Steiner
Interstitial Water Chemistry and Headspace Gas: Murray, Spivack
Microbiology: Fisk, Haveman, Murray, Smith, Spivack, Staudigel
Physical Properties: Abrams, Hirono
Downhole Measurements: Cairns, Guerin, Larson, Pockalny
NGR and Potassium Budgets: Abrams, Alt, Murray, Plank, Spivack
Sedimentation Rates: Lozar, Pletsch, Steiner.

¹Examples of how to reference the whole or part of this volume.
²Shipboard Scientific Party addresses.

Shipboard Scientific Procedures

Numbering of Sites, Holes, Cores, and Samples

Ocean Drilling Program (ODP) drill sites are numbered consecutively and refer to one or more holes drilled while the ship was positioned over one acoustic beacon. Multiple holes may be drilled at a single site by pulling the drill pipe above the seafloor (out of the hole), moving the ship some distance from the previous hole, and then drilling another hole. In some cases, the ship may return to a previously occupied site to drill additional holes or to log or deepen an existing hole. Such is the case for Hole 801C, which was first drilled during Leg 129 and was deepened during Leg 185.

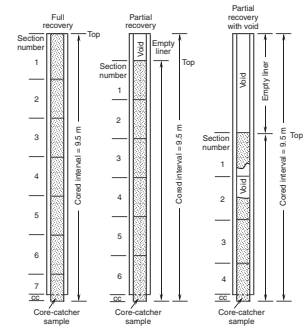
For all ODP drill sites, the letter suffix distinguishes holes drilled at the same site. For example, the first hole to be drilled is assigned the site number modified with the suffix "A," the second hole takes the site number and suffix "B," and so forth. Note that this procedure differs slightly from that used by Deep Sea Drilling Project (DSDP) (Sites 1–624) but prevents ambiguity between site- and hole-number designations. It is important to distinguish between holes drilled at a site because recovered sediments or rocks from different holes do not necessarily come from equivalent positions in the stratigraphic column.

The cored interval is measured in meters below seafloor (mbsf). The depth interval assigned to an individual begins with the depth below the seafloor at which the coring began and extends to the depth that the coring ended. Each cored interval is generally up to 9.5 m long, which is the length of a core barrel. Maximum recovery for a single core interval is 9.5 m of rock or sediment contained in a plastic liner (6.6 cm internal diameter), plus ~0.2 m (without a plastic liner) in the core catcher (Fig. F1). The core catcher is a device at the bottom of the core barrel that prevents the core from sliding out when the barrel is being retrieved from the hole. In certain situations (e.g., when coring gas-charged sediments that expand while being brought on deck), recovery may exceed the 9.5 m maximum. During Leg 185 several cores in Hole 801C (e.g., Cores 185-801C-21R, 22R, and 26R) were taken without core liners to minimize jamming by fractured rock.

A recovered core is divided into 1.5-m sections that are numbered serially from the top (Fig. F1). When full recovery is obtained, the sections are numbered from 1 through 7, with the last section possibly being shorter than 1.5 m (rarely, an unusually long core, or short sections, may require more than seven sections). When less than full recovery is obtained, as many sections as needed to accommodate the length of the core will be numbered; for example, 4 m of core would be divided into two 1.5-m sections and one 1-m section. If cores are fragmented (recovery <100%), sections are numbered serially and intervening sections are noted as void, whether or not shipboard scientists think that the fragments were contiguously in situ. In rare cases, a section <1.5 m may be cut to preserve features of interest (e.g., lithologic contacts).

By convention, material recovered from the core catcher is placed below the last section when the core is described and is labeled CC; in sedimentary cores, this is treated as a separate section. The core catcher is placed at the top of the cored interval in cases where material is recovered only in the core catcher. However, information supplied by the drillers or by other sources may allow for more precise interpretation as

F1. Examples of numbered core sections, p. 56.



to the correct position of core-catcher material within an incompletely recovered cored interval.

When the recovered core is shorter than the cored interval, by convention the top of the core is equated with the top of the cored interval to achieve consistency when handling analytical data derived from the cores. Samples removed from the cores are designated by distance measured in centimeters from the top of the section to the top and bottom of each sample removed from that section.

A complete identification number for a sample consists of the following information: leg, site, hole, core number, core type, section number, piece number (for hard rock), and interval in centimeters measured from the top of the section. For example, a sample identification of "185-1149A-10R-1, 10–12 cm," would be interpreted as representing a sample removed from the interval between 10 and 12 cm below the top of Section 1. Core 10R designates that this core was taken during drilling of Hole A with the rotary core barrel, at Site 1149, during Leg 185.

All ODP core and sample identifiers indicate core type. The following abbreviations are used: H = hydraulic piston corer (HPC, also referred to as APC, or advanced hydraulic piston corer), X = extended core barrel (XCB), R = rotary core barrel (RCB), D = diamond core barrel (DCB), W = washed-core recovery, and M = miscellaneous material.

Core Handling

Sediments

As soon as a core is retrieved on deck, a sample is taken from the core catcher and given to the paleontological laboratory for an initial age assessment. Then, the core is placed on a long horizontal rack, and gas samples may be taken by piercing the core liner and withdrawing gas into a vacuum tube. Voids within the core are sought as sites for gas sampling. Some of the gas samples are stored for shore-based study, whereas others are analyzed immediately as part of the shipboard safety and pollution-prevention program. Next, the core is marked into section lengths, each section is labeled, and the core is cut into sections. Headspace gas samples are taken from the ends of cut sections while on the catwalk and sealed in glass vials for light hydrocarbon analysis. Each section is then sealed at the top and bottom by gluing on color-coded plastic caps, blue to identify the top of a section and clear to identify the bottom. A yellow cap is placed on the section ends from which a whole-round sample has been removed. These caps are usually attached to the liner by coating the end liner and the inside rim of the cap with acetone, and then the caps are taped to the liners. Additionally, during Leg 185 sediment samples were taken on the deck for microbiology studies. Special handling of these samples is specified in "[Sampling](#)," p. 33.

Next, the cores are carried into the laboratory, where the core liners are labeled with an engraver to permanently mark the full designation of the section. The length of the core in each section and the core-catcher sample are measured to the nearest centimeter; this information is logged into the shipboard CORELOG database program. After cores have equilibrated to room temperature (~3 hr), they are run through the multisensor track (MST), thermal conductivity measurements are performed on relatively soft sediments, and the cores are split.

Cores of soft material are split lengthwise into working and archive halves. The softer cores are split with a wire or saw, depending on the degree of induration. Harder cores are split with a band saw or diamond saw. During Leg 185, the wire-cut cores were split from the bottom to top; thus, investigators should be aware that older material may have been transported up the core on the split face of each section.

The working half of the core is sampled for both shipboard and shore-based laboratory studies. Each extracted sample is recorded into CORELOG by the location and the name of the investigator receiving the sample. Records of all removed samples are kept by the curator at ODP. The extracted samples are sealed in plastic vials or bags and labeled. Samples are routinely taken for shipboard magnetic studies and physical properties analysis, calcium carbonate (coulometric method), and organic carbon (carbon-nitrogen-sulfur [CNS] elemental analyzer) analyses.

The archive half of each core is described visually. Smear slides are made from sediment samples taken from the archive half. Most archive sections are run through the cryogenic magnetometer. The archive half then is photographed using the archive multisensor track (AMST) digital camera for color shots (see “[Color](#),” p. 12) and a regular camera for black-and-white pictures. Close-up photographs (black-and-white and color) are taken of particular features for illustrations in the site summaries, as requested by individual scientists.

Both halves of the core are then placed into labeled plastic tubes, sealed, and transferred to cold-storage (4°C) space aboard the drilling vessel. At the end of the leg, the cores are usually transferred from the ship in refrigerated airfreight containers to cold storage (4°C) at the ODP Gulf Coast Repository at Texas A&M University. However, the cores obtained during Leg 185 were inadvertently shipped in unrefrigerated containers. Worst-case estimates indicate that the cores warmed from 4° to 12°C over the 10 days of shipment.

Igneous and Metamorphic Rocks

Igneous rock cores are handled differently than sedimentary cores. Once on deck, the core-catcher sample is placed at the bottom of the core liner and total core recovery is calculated by shunting the rock pieces together and measuring to the nearest centimeter. This information is logged into CORELOG. The core then is cut into 1.5-m-long sections and transferred to the laboratory. Special handling of rock samples taken for microbiology studies is detailed in “[Sampling](#),” p. 34.

The contents of each section are transferred into 1.5-m-long sections of split core liner, where the bottom of oriented pieces (i.e., pieces that clearly could not have rotated top to bottom about a horizontal axis in the liner) are marked with a red wax pencil. This is to ensure that orientation is not lost during the splitting and labeling processes. Important primary features of the cores also are recorded at this time. The core then is split into archive and working halves in such a way that important features (e.g., veins, cooling unit boundaries, breccias) are equally represented in the two halves. A plastic spacer is used to separate individual pieces and/or reconstructed groups of pieces in the core liner. These spacers may represent a substantial interval of no recovery. Each piece is numbered sequentially from the top of each section, beginning with number 1; reconstructed groups of pieces are assigned the same number, but are lettered consecutively. Pieces are labeled only on the

outer cylindrical surfaces of the core. If the piece is oriented, an arrow is added to the label pointing to the top of the section. Because pieces are free to turn about a vertical axis during drilling, azimuthal orientation during Leg 185 was possible only by using paleomagnetic or downhole logging techniques.

The working half of the core is sampled for shipboard physical properties (PP) measurements, magnetic studies, X-ray fluorescence (XRF), X-ray diffraction (XRD), and thin-section studies. Nondestructive PP measurements, such as magnetic susceptibility, are performed on the archive half of the core. Where recovery permits, samples are taken from each lithologic unit. Some of these samples are minicores. Records of all samples are kept by the curator at ODP. The archive half then is photographed using the AMST digital camera (see “**Basement**,” p. 19), and black-and-white and color film. Close-up photographs (black-and-white and color) are taken of particular features for illustrations in each site summary, as requested by individual scientists. Both halves of the core then are shrink-wrapped in plastic to prevent rock pieces from vibrating out of sequence during transit, placed into labeled plastic tubes, sealed, and transferred to cold-storage space aboard the drilling vessel. As with the other Leg 185 cores, they are housed at the ODP Gulf Coast Repository at Texas A&M University.

Depth Measurements

The measurement of depth for ODP cores and logs is subject to several uncertainties. Depths are assigned to cores and samples as a means of fixing them in space, but the “depth” values are only approximations. We do not measure depth, but provide an approximation of depth on the basis of length measurements of drill pipe and other tubulars before they become part of the drill string. The resulting vertical measurement is subject to several errors and inaccuracies.

All vertical measurements of cores, logs, and other downhole measurements (except the precision depth recorder [PDR]) are referenced to the passage of measured lengths of pipe past the driller’s datum (dual elevator stool [DES]), which is the last point at which reference marks on the pipe can be seen. Sea level is the permanent datum, and the distance from sea level to the driller’s datum can be calculated for each site by subtracting the current ship’s draft from the fixed distance between the keel and the DES—if a distance below sea level is desired. Nonetheless, official depth measurements recorded by drillers and operations personnel are based on meters below the rig floor (mbrf).

By convention, core and sample depth are given as meters below seafloor (mbsf) by the scientific party. Though the seafloor datum is convenient and helpful in visualizing the geologic setting, it is a poor datum because its depth below sea level usually is not accurately determined. Seafloor “depth” usually is established by the recovery of a partially filled core barrel containing the seafloor interface and then subtracting the length of the core from the drill pipe length to the bottom of the cored interval. It is subject to error in the assumption of 100% core recovery and to errors of drill-pipe depth (discussed below). A more accurate, though seldom used, determination is to view contact between the core bit and seafloor with the reentry television camera and to record concurrently the drill-string measurement at the DES. Sometimes neither of those determinations is available, and seafloor depth is estimated by PDR, deflection of the driller’s weight indicator, or assumption of the same depth as an offset hole.

Inaccuracies in measuring drill-string length apply to all depth measurements. They arise from several sources, with the most significant usually being the stretching of the drill string. In the past, most DSDP/ODP penetrations have been single-bit holes, and the relative depth placement of cores and logs has been of greater interest than measurement of water depth. Because most of the drill string length has been in the water column, the difference in stretch from the top of the hole to the bottom has been negligible. Stretch can be considerable, however, with long drill strings. For example, a 6-km drill string with a heavy bottom-hole assembly or casing string can stretch as much as 15 m (making seafloor depth appear 15 m shallower than it is). When multiple drill strings and varying bottom-hole assembly (BHA) weights are used in deep-water reentry installations, depth discrepancies on the order of meters can occur.

Currently, no corrections are applied for pipe stretch. Even if there were, several other inaccuracies would still be inherent in applying drill-pipe length to depth. Thermal contraction of more than 1 m would apply to the above drill string if the pipe were measured at warm tropical air temperature and then lowered into cold seawater. The tidal range in the open ocean can vary by several meters. The normal search of the dynamic positioning system can induce apparent gain and loss of drill-string depth on the scale of meters, which can change on a core-to-core basis. Other factors include vessel heave, which makes the driller's reference mark a moving target, displacement of the pipe by ocean currents, and change in vessel draft during site occupancy.

Vertical measurement to the centimeter may be useful in measuring samples and locating them relative to other samples within the core, but the vertical location of the core relative to adjacent cores or to the seafloor is unknown even to the meter.

Precision depth recorder (PDR) readings are routinely taken upon arrival at a new site. Though the PDR data are curated and sometimes used as a check on water depth as recorded on seismic records, they are not used for the depth determination of cores or measurements. The readings are taken only to ensure that the drill string is not run into the seafloor before it is time to spud the hole. In many cases, the corrected PDR reading may actually be a more accurate depth than the drill-pipe measurement because of the pipe stretch factor mentioned above. That would only apply to areas of level seafloor because the *JOIDES Resolution* broad-beam PDR gives inaccurate readings in sloping bathymetry.

Global Position

Another measurement that must be kept in perspective is that of geographic coordinates of latitude and longitude. Navigation and site location are by the Global Positioning System (GPS). For military security reasons, random errors of up to 70 m are introduced by the U.S. Department of Defense into GPS fixes. (Differential GPS is not available on the open ocean.) Those random errors can be averaged out if enough fixes are taken over time, and that is the methodology used to determine the locations of ODP holes.

The coordinates recorded for ODP holes represent the average location of the GPS antenna (corrected to the ship's moonpool) while the hole was occupied, and not the precise location of the hole. The hole cannot be assumed to be located directly beneath the moonpool. The drill string tends to swing with a pendulum motion below the ship, and the point on its trajectory at the moment of spud is not known. The

ship moves about within a circle of ~1% of water depth, and it may not have been at the averaged location when the hole was spudded. Also, the string can be offset some distance laterally by ocean currents and sustained winds.

One minute of latitude represents 1 nmi (6080 ft, or 1852 m). One minute of longitude represents that distance at the equator and proportionately less at all other latitudes. Thus 0.1' is 600 ft or less, 0.01' is 60 ft or less, and 0.001' is 6 ft or less (<2 m). The value of the third decimal of latitude/longitude is therefore highly questionable for site location. The newer practice of recording coordinates in decimals of degrees can be evaluated, considering that 1° of latitude is 60 nmi and 0.0001° is 36 ft or 11 m.

SITE GEOPHYSICS

The location of Site 1149 is based on 1976 vintage multichannel and sonobuoy seismic data and a short, single-channel seismic survey conducted on approach to the site during Leg 185. Hole 801C is a fully cased reentry site installed during Leg 129 and therefore did not require any seismic site survey data for location. Underway geophysical data were collected during transits to both Sites 801 and 1149. On board instrumentation included a precision echo sounder (3.5 kHz), magnetometer, gyrocompass (Lehmkul LR40), and global positioning satellite navigation systems (GPS).

Navigation

The GPS was used throughout Leg 185. Three GPS systems were available for operation, with output provided to the underway geophysics laboratory. GPS from Ashtech GG24 was used as the primary navigation device throughout the leg. GPS fixes were available continuously (1-s updates) and were recorded at 60-s intervals. Event data were recorded at 60-s intervals on site and in transit. Navigation data were logged by the WINFROG software system, mounted on a dedicated PC in the underway geophysics laboratory. Subsequent processing and display of navigation data were performed using the Generic Mapping Tools software package (Wessel and Smith, 1995) on shipboard Unix workstations.

Echo Sounder

One 3.5-kHz echo sounder (the PDR) was used to acquire bathymetric data as well as high-resolution reflection records of the uppermost sediment layers. Data from this system were recorded on an EPC 8082 analog line-scanning recorder. The 3.5-kHz system used a Raytheon CESP III correlator echo sounder processor driven by a Raytheon PTR105B transceiver with a 2-kW sonar transmitter and included a single EDO type 323c transducer mounted in a sonar dome on the hull 40 m forward of the center of the moonpool. This location was chosen to reduce ship-generated noise and signal attenuation from aeration beneath the hull. The recorder was annotated automatically at fixed intervals; ship speed and heading were marked every 5 min, and position every 30 min. Depth readings were taken manually every 5 min and entered into an Excel spreadsheet.

Magnetometer

Total intensity measurements of the Earth's magnetic field were obtained with a Geometrics Model G-886 proton precession magnetometer towed ~500 m astern. Magnetic data were recorded during transits at 1-min intervals on navigation files produced by WINFROG navigation software.

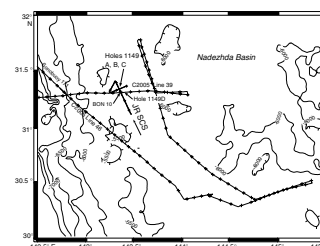
Seismic Reflection Profiling

Site selection for the second drill site of Leg 185 (proposed site BON 10, ODP Site 1149) was based on a multichannel channel seismic (MCS) and sonobuoy survey conducted during the *Robert D. Conrad* Cruise 2005 in 1976 and included two MCS lines intersecting 50 km west of the Site 1149 location (Fig. F2). Three potential sites were identified from these data, but a gap in the MCS record existed to the west of the preferred drill site (BON 10). An ~7-hr single-channel seismic (SCS) survey was conducted on approach to Site 1149 (*JOIDES Resolution* [JR] SCS Lines 1, 2, and 3) to partially fill this data gap and to ensure the correct site location by comparison of the GPS navigated SCS data with the 1976 MCS images (Fig. F2). Site 1149 is located at the intersection of JR SCS Lines 1 and 3, just 3.5 km northwest of proposed site BON 10. Hole collapse in the sedimentary section (chert and clay) and drill-string sticking problems limited basement penetration to <30 m in Holes 1149B and 1149C and prompted us to place Hole 1149D at a location where the sediment section appeared to be significantly thinned. A dome-shaped rise in basement, accompanied by a thinning of the sediment section from 0.38 to 0.28 s thick is apparent along C2005 MCS Line 39, ~5 km southeast of Holes 1149A, 1149B, and 1149C (Fig. F2). This relatively shallow basement location lies beneath a distinctive sea-floor slope, and a short 3.5-kHz survey was conducted to match the distinctive bathymetry apparent in the MCS and 3.5 kHz of C2005 Line 39. We intended to drill at the apex of the basement high; however, it is likely that we were located slightly downdip. Hole 1149D reached basement at 307 mbsf, ~100 m shallower than at Holes 1149B and 1149C, and was successful in yielding a significant basement section (~130 m thick).

The SCS data were received using a single-channel Teledyne Model 178 hydrophone streamer with a 100-m-long active section containing 60 hydrophones, a 25-m-long "stretch" section, and a 150 m lead section. The guns and streamer were both towed at 12–18 m depth. The ship speed averaged 5.4 kt during the initial approach to the site on a 337° course and averaged 5.57 kt during a second site crossing on a 70° course (see Fig. F6, p. 58, in the "Site 1149" chapter). The two synchronized 80-in³ water-gun sources operated at 1900 psi and were triggered from the WINFROG navigation system at a shot interval of 13 s, equivalent to ~36 m at 5.4 kt. The guns were towed ~24 m astern and 14 m apart. Analog data were recorded on two Raytheon Model 1807M recorders ("Analog-1" and "Analog-2"), displaying scan intervals of 4–12 s and band-pass filtered from 30 to 100 Hz throughout the seismic survey. Krohn-Hite Model 3550 analog filters were used to filter signals to both recorders.

The seismic data from each shot were sampled every 1 ms from 0 to 11 s and were digitally recorded on a Sun Sparcstation 10 in SEG Y format, using the "a2d" acquisition package after applying an anti-aliasing filter with a corner frequency at 250 Hz. Seismic data were copied to

F2. Track chart of SCS and MCS surveys, p. 57.



both 4- and 8-mm digital audio tapes during the site survey, processed using the SIOSEIS software package (Paul Henkart, Scripps Institution of Oceanography), and displayed on a HP 650C DesignJet plotter. Processing of SCS water-gun data acquired during Leg 185 included water-bottom mute, band-pass filter (30–100 Hz), weighted three-trace running mix, and automatic gain control (AGC) using a 500-ms window, and removing every other trace (see “[Site Geophysics](#),” p. 2, in the “Site 1149” chapter).

Pre-cruise Site Survey

At its November 1988 meeting in Miami, the ODP Planning Committee established the scientific drilling plan for Leg 130 to obtain geochemical reference sections at sites designated BON 8 and MAR 4 on the Pacific plate just east of the Izu-Bonin and Mariana Trenches (JOIDES proposal, Langmuir and Natland, 1986). In 1989, we (Abrams, Diebold, and Larson) reprocessed and reinterpreted MCS data collected in 1976 during a *Conrad* cruise across these two proposed sites in the western Pacific, which were scheduled for ODP drilling in January 1990. Although this geochemical reference leg was canceled, the reprocessed MCS data were used to locate Site 1149 (BON 10) seaward of the Izu-Bonin arc nearly 10 yr later.

In October and November 1976, 24-channel seismic data were acquired during *Conrad* Cruises C2005 and C2006. The motivation for C2005 was the imaging of Moho via two-ship constant offset profiling, but several single-ship profiles, along with sonobuoy data, were also recorded in the area of the Izu-Bonin Trench, including MCS Lines 39 and 46. Lines 39 and 46 intersect 50 km west of Site 1149; the final site location is on JR SCS Line 1 ~3.5 km northwest of its intersection with MCS Line 39 (see “[Site Geophysics](#),” p. 2, in the “Site 1149” chapter). C2005 was a regional survey, and both Lines 39 and 46 extend across the trench axis to the west and more than 100 km east and southeast of the site. The seismic source used during acquisition of Lines 39 and 46 consisted of four identical 466-in³ air guns, with a nominal shot spacing of 50 m. The arrivals were received by a 24-channel analog streamer with 100-m group spacing and were digitized and recorded using a DFS IV system. After acquisition, these data received “standard” processing. Since 1976, techniques and equipment enabling a higher level of interaction in choosing processing parameters, such as deconvolution operators and stacking velocities, as well as time and depth migration, have also been introduced. We, therefore, reprocessed ~220 km each of Lines 39 and 46 beginning with demultiplexed and common depth point gathered data on nine-track tapes in the Lamont-Doherty Earth Observatory (LDEO) archives. Reprocessing included repicking of stacking velocities, prestack predictive deconvolution and noise filtering, spherical divergence correction, restacking, poststack deconvolution and time-varying filtering, and, finally, migration. The resulting displayed sedimentary sections of the migrated and unmigrated data are far superior to the original data primarily because of the significant reduction in the bubble pulse from four identical air guns.

Sonobuoy 171 was acquired along Line 46 ~50 km west of Site 1149. The analog record of sonobuoy 171 was reinterpreted and indicates the onset of high velocities (>4.1 km/s) at 528 mbsf, marking the top of igneous basement (J. Diebold, pers. comm., 1989, and JOI/USSSP report JSC10-89, 1989).

SEDIMENTOLOGIC DESCRIPTION

The description of sedimentary units recovered during Leg 185 included estimates of sediment composition based on smear slides, thin sections, carbonate measurements, and XRD, documentation of sedimentary and deformational structures, drilling disturbance, presence and type of fossils, bioturbation intensity, induration, diagenetic alteration, and color. These data were recorded manually for each core section on standard visual core description (VCD) paper forms that are archived by ODP.

Barrel-Sheet Data

Information on the VCDs was summarized and entered into AppleCORE (version 0.7.5g) software, which generated a one-page graphical log of each core (“barrel sheet”). Barrel sheets are presented with core photographs (see the “Core Descriptions” contents list). A wide variety of features, such as sediment lithology, bed thickness, primary sedimentary structures, bioturbation parameters, soft-sediment deformation, and structural and diagenetic features are indicated by patterns and symbols in the graphic logs. A key to the full set of patterns and symbols used on the barrel sheets is shown in Figure F3. The symbols are schematic, but they are placed as close as possible to their proper stratigraphic position, or arrows indicate the interval for which the symbol applies. For exact positions of sedimentary features, copies of the detailed section-by-section VCD forms can be obtained from ODP. The columns on the barrel sheets are as follows.

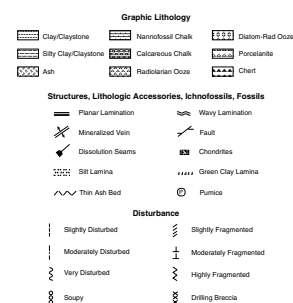
Lithology

Sediment lithologies are represented by patterns in the “Lithology” column (see the “Core Descriptions” contents list). This column may consist of up to three vertical strips, depending on the number of the major end-member constituents (see “Sediment Classification,” p. 14), thus reflecting intermixing of different components. Sediments with only one major component group (i.e., all other component groups are <10% each) are represented by one strip. Because of the limitations of the AppleCORE software, thin intervals of interbedded lithologies cannot be adequately displayed at the scale used for the barrel sheets, but they are described in the “Description” columns of the barrel sheets where appropriate.

Bioturbation, Structures, Accessories, Ichnofossils, and Fossils

Symbols in these columns are explained in Figure F3. The bulk of the clayey sediments recovered during Leg 185 was relatively homogeneous. Stratification, bioturbation, or other sedimentary structures were usually discernible only where textural or compositional differences were present (e.g., close to ash layers). In the homogeneous background sediment, however, it was difficult to distinguish the destruction of primary structures due to bioturbation from the actual absence of primary structures. Given the light gray and reddish colors of the clayey sediments, the absence of lamination, and the very low organic matter contents (see “Interstitial Water Chemistry and Headspace Gas,” p. 29), it is reasonable to assume that the remaining sediment has been perva-

F3. Key to barrel-sheet symbols, p. 58.



sively bioturbated as well because benthic burrowing activity was not limited by oxygen deficiency. To convey the maximum amount of information without confusing interpretation with observation, we used the "Bioturbation" column to display only visible bioturbation or sediment mottling. The bioturbation column of the barrel sheets shows four levels of intensity:

Homogeneous = trace fossils are either absent or invisible because they are in a completely biogenic fabric,
Low = rare, discrete burrows,
Moderate = burrows are generally isolated but locally overlap, and
Intense = abundant, overlapping burrows. Several generations of bioturbation structures cut across each other resulting in almost total disruption of sedimentary structures.

Stratification thickness was characterized by a combination of the terms given by McKee and Weir (1953) and Ingram (1954): very thick bedded (>1 m thick), thick bedded (30–100 cm thick), medium bedded (10–30 cm thick), thin bedded (3–10 cm thick), very thin bedded (1–3 cm thick), thickly laminated (3–10 mm thick), thinly laminated (1–3 mm thick), and very thinly laminated (<1 mm thick).

Drilling Disturbance

Natural structures (physical or biological) can be difficult to distinguish from disturbance created by the coring process. Deformation and disturbance of sediment that resulted from the coring process are illustrated in the "Drilling disturbance" column with the symbols shown in Figure F3. Blank regions indicate the absence of drilling disturbance. The degree of drilling disturbance for soft sediments was described using the following categories:

Slightly disturbed = bedding contacts slightly bent,
Moderately disturbed = bedding contacts bowed,
Highly disturbed = bedding hardly discernible, sometimes showing flow structures, and
Soupy = water-saturated intervals that have lost all original structure.
Fragmentation in indurated sediments and rock was described using the following categories:
Slightly fragmented = core pieces in place with little drilling slurry or brecciation,
Moderately fragmented = core pieces in place or partly displaced but original orientation preserved or recognizable (drilling slurry may surround fragments),
Highly fragmented = core pieces are from the interval cored and are probably in correct stratigraphic sequence (although they may not represent the entire section), but the original orientation is completely lost, and
Drilling breccia = core pieces have lost their original orientation and stratigraphic position and may have been mixed with drilling slurry.

Samples and Close-Up Photographs

The stratigraphic position of samples taken for shipboard analysis and the location of close-up photographs is indicated in the "Samples" column of the barrel sheet according to the following codes:

CAR = carbonate content,
PAL = biostratigraphy,
PHO = close-up photograph,
SS = smear slide,
THS = thin section,
WR = whole-round sample,
XRD = X-ray diffraction analysis, and
XRF = X-ray fluorescence analysis.

Color

Sediment color was determined visually by comparison with standard color charts (Munsell Color Company, Inc., 1975; Rock Color Chart Committee, 1991) and is reported in the "Description" column of the barrel sheets. In addition to determining color visually, all cores were scanned at 2- to 4-cm intervals using a Minolta CM-2002 spectrophotometer mounted on the AMST. The spectrophotometer measures reflectance in thirty-one 10-nm-wide bands of the visible spectrum (400–700 nm) on the archive half of each core section. Spectrophotometer readings were taken after cleaning the surface of each core section and covering it with the clear plastic film (Glad brand Cling Wrap, a brand of polyethylene food wrap). Calibration of the color scanner did not include a correction for the plastic film because we found that the effect is very minor even with very bright colored lithologies. The measurements were taken automatically and recorded by the AMST at evenly spaced intervals along each section. There was no way to program the AMST software to avoid taking measurements in intervals with a depressed core surface or in disturbed areas of core containing drilling slurry or biscuits. The data are part of the Janus database and can be obtained from ODP. Additional detailed information about measurement and interpretation of spectral data with the Minolta spectrophotometer can be found in Balsam et al. (1997, 1998, 2000).

Description

A summary of the sedimentologic data is given in the "Description" column of the barrel sheet. It consists of four parts: (1) a heading in capital letters that lists only the dominant sediment lithologies observed in the core; (2) a general description of the sediments in the core, including color, composition, sedimentary structures, bed thicknesses, drilling disturbance, as well as any other general features in the core; and (3) descriptions and locations of thin, interbedded, or minor lithologies.

Smear Slides and Thin Sections

Sediments were analyzed petrographically using smear slides and thin sections. Tables summarizing these data (see the "[Core Descriptions](#)" and "[ASCII Tables](#)" contents lists) include information about the sample location, whether the sample represents a dominant (D) or a minor (M) lithology in the core, and the percentages of sand, silt, and

clay size fractions, along with all identified components. We emphasize here that smear-slide and thin-section analyses provide only estimates of the relative abundances of the constituents. The comparison charts of Baccelle and Bosellini (1965) were used to refine abundance estimates in thin sections. However, these charts cannot be used for smear slides because they are designed to simulate a field of view that is completely and evenly covered with particles. Quantification of data from smear slides is further aggravated by the difficulty in identifying fine-grained particles using only a microscope and by the tendency to underestimate sand-sized grains because they cannot be incorporated evenly into the smear. Biogenic opal and its diagenetic modifications are particularly difficult to determine from smear slides (van Andel, 1983). Previous experience has shown that the largest variations in smear-slide determination correlate with the change from one observer to another, or with shift changes. The accuracy problem is indicated in the "Explanatory Notes" chapters of several recent ODP volumes in which sedimentologic numerical data in general, and those of smear-slide determination in particular, are consistently de-emphasized and replaced by semiquantitative categories (e.g., Shipboard Scientific Party, 1998a, 1998b, 1998c). A limitation to semiquantitative categories, such as the ones proposed during previous legs would have seemed all the more appropriate during Leg 185. Current ODP policies, however, require the input of numerical data; therefore, the reader is warned that the tabulated smear-slide results (see the "[Core Descriptions](#)" and "[ASCII Tables](#)" contents lists) largely reflect the need to comply with these regulations rather than actual accuracy. Smear-slide and thin-section data were reviewed for internal consistency and correct sedimentologic nomenclature, and the qualitative composition was confirmed by XRD. Accuracy of the carbonate content estimated from smear slides and thin sections was confirmed by chemical analyses (see "[Interstitial Water Chemistry and Headspace Gas](#)," p. 29).

X-Ray Diffraction Analysis

Selected samples were taken for qualitative mineral analysis by XRD using a Philips diffractometer with $\text{CuK}\alpha$ radiation at 40 kV and 35 mA with a focusing graphite monochromator and the following slit settings:

Focus = fine,
Irradiated length = 12 mm,
Divergence slit = automatic,
Receiving slit = 0.2 mm,
Step size = $0.02^\circ 2\theta$,
Count time per step = 1 s,
Scanning rate = $2^\circ 2\theta/\text{min}$,
Ratemeter time constant = 0.2 s,
Spinner = off,
Monochromator = on, and
Scan = continuous.

Bulk samples were freeze-dried, ground with an agate mortar and pestle, and packed in sample holders, which, together with the ship's movement, probably imparted some orientation to the mineral powder. These samples were scanned from 2° to $70^\circ 2\theta$. MacDiff software (v. 4.0.4 PPC, by Rainer Petschick) was used to display diffractograms and to identify

the minerals. Most diffractograms were corrected to match the main peaks of quartz, calcite, or clinoptilolite at 3.343, 3.035, and 8.95 Å, respectively. Identifications are based on multiple peak matches with the mineral data base provided with MacDiff. Each site chapter includes selected diffractograms to illustrate which peaks were associated with various minerals. Relative abundances reported in this volume are useful for general characterization of the sediments, but they are not quantitative concentration data.

Sediment Classification

One major goal of Leg 185 is to quantitatively assess the composition of the input material to the Izu-Bonin Trench, which includes the sedimentary cover of the oceanic crust at the drill site. Achieving this goal requires extrapolating petrographical and geochemical measurements on discrete samples over long core intervals, which, in turn relies on an accurate core description. We evaluated the methods and the classification used for sediment description and found that there is a need for a less ambiguous and more flexible classification than the proposed ODP standard classification by Mazzullo et al. (1988). Our classification is neither comprehensive nor entirely descriptive, but it is simple to use for the purpose of Leg 185, and it circumvents some of the disadvantages of the Mazzullo classification. Notably, it avoids the impression of a level of accuracy that is not achievable under the conditions of most ODP cruises. Also, we tried to use common and relatively simple names, which led us to abandon a number of ambiguous or meaningless terms like “Radiolarite” and “Mixed sediment” (see “[Sediment Nomenclature](#),” p. 14). We used three end-members (i.e., calcareous, siliceous, and silicate) (Fig. F4), similar to the classification by Dean et al. (1984). In response to the absence of reliable quantitative petrographic data mentioned above, the Leg 185 sediment classification provides only a limited number of principal sediment names supplemented by a preliminary modifier that relates to the carbonate content (e.g., calcareous, clayey) (Fig. F4). The preliminary modifiers were eventually adjusted to the corresponding measured carbonate content when those measurements were available.

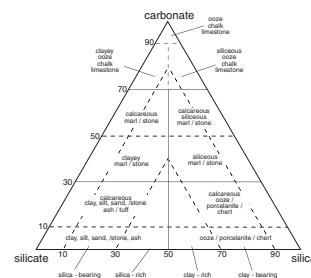
Sediment Nomenclature

Sediment names consist of a principal name relating to the dominant composition of the sediment (e.g., claystone, marl, or chert) and one or two modifiers that precede the principal name (e.g., ash-bearing siliceous clay). Besides composition, principal names vary according to the grain size and the induration of the sediment. Principal sediment names are as follows.

Calcareous Sediments

The calcareous end-member of our classification includes sediments made up of all kind of calcareous fossil shells or tests, resedimented and diagenetic carbonate grains, and cements. Sediments that contain more than ~70% calcareous components, the majority of which were secreted by pelagic organisms (planktonic foraminifers and calcareous nannofossils) are called ooze if they are soft, chalk if they are firm, and limestone if they are hard. These names may be preceded by the dominant calcareous microfossil. Mixtures of the calcareous and the silicate or the

F4. Sediment classification scheme, p. 59.



siliceous end-member that contain between 70% and 30% carbonate are called marl or marlstone, depending on their induration.

Siliceous Sediments

The siliceous end-member of our classification includes sediments rich in siliceous microfossils, as well as the diagenetic modifications of these sediments, and silica-rich hydrothermal precipitates. Sediments dominated by siliceous microfossils and indeterminate silica that contain less than ~30% carbonate are called radiolarian, diatom, or siliceous ooze if they are soft, porcelanite if they are firm to hard, and chert if they are hard enough not to be scratched by a stainless steel probe. In addition to this field classification, the terms porcelanite and chert bear a strong compositional notion. Thus, porcelanite is typically composed of opal-CT (christobalite-tridymite), but it may also contain diagenetic quartz, carbonate, and silicates (mostly clay minerals). Chert is usually dominated by quartz and tends to be a purer silica, but may also contain clay minerals and carbonate (Kastner, 1979; Isaacs, 1982; Isaacs et al., 1983).

A number of different lithologic definitions for siliceous rocks were used by the Leg 129 participants, which resulted in considerable confusion (Lancelot, Larson, et al., 1990; Behl and Smith, 1992; Fisher et al., 1992; Karl et al., 1992; Karpoff, 1992; Ogg et al., 1992). This unsatisfactory situation partly reflects the difficulty to quickly determine the composition of siliceous sediments and rocks (van Andel, 1983) but also relates to regional differences in usage of specific rock names. Thus, “radiolarite” was used during Leg 129 to describe a soft, friable sediment that contains abundant radiolarians. Most European geologists, and probably many others, use radiolarite for an extremely hard radiolarian-bearing rock (i.e., as a synonym of radiolarian chert) (e.g., Bernoulli, 1972; Baltuck, 1983, 1986; Jenkyns, 1986). In view of the intended integration of core and logging data, which involves the comparison of physical properties, we avoided the Leg 129 usage of radiolarite. Soft, friable sediments dominated by radiolarians are called radiolarian ooze or radiolarian marl, depending on their carbonate content. The more indurated forms of this sediment are called radiolarian porcelanite and radiolarian chert or radiolarian marlstone, respectively.

Silicate Sediments

Sediments dominated by nonbiogenic, mostly detrital, silicate components are further subdivided based on the relative proportion of siliciclastic and volcanoclastic sediments. If the majority of the detrital components are siliciclastic, the sediment is called sand if the average grain size is between 63 μm and 2 mm, silt (2–63 μm), or clay (<2 μm). Mixtures of sand, silt, and clay are named according to the classification of Shepard (1954). Note that the silt/clay boundary has been placed at 2 μm as suggested by Doeglas (1968). The suffix “-stone” is added if the sediment is indurated. The principal name for sediments dominated by volcanoclastic components in the silt and fine sand size range (2–250 μm) is volcanic ash.

Major and Minor Modifiers

Principal names may be preceded by a major modifier, (e.g., diatomaceous) that relates to a component group that is common or abundant,

but not dominant. Alternatively, where this makes for odd names, the modifier may be used in conjunction with the suffix “rich.” As an example, diatomaceous claystone or, alternatively, diatom-rich claystone describes a hard sediment that contains more than 50% siliciclastic clay and more than 30% diatoms. Minor modifiers were used to specify a common component group (i.e., less than ~30%, but more than ~10% of the sediment). Minor modifiers are used with the suffix “-bearing” and precede the major modifiers. Thus, a soft sediment with dominant radiolarians, abundant calcareous nannofossils, and common volcanic ash would be called an ash-bearing nannofossil-rich radiolarian marl. Note that the more specific microfossil names take the places of the terms “calcareous” and “siliceous” that are shown in Figure F4. Where appropriate, the names of important, but accessory (<10%) components, or those not covered by the end-member component groups, such as manganese oxyhydroxides, phosphate, zeolite, or barite, were added to the sediment names preceded by the word “with” (e.g., nannofossil marl with Mn micronodules).

BIOSTRATIGRAPHY

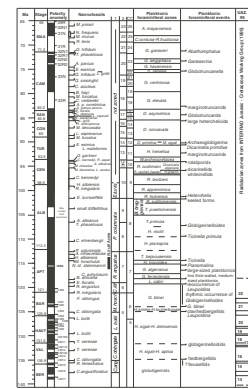
Calcareous Nannofossils, Radiolarians, and Ichthyoliths

During Leg 185 calcareous nannofossils and radiolarian assemblages were studied to provide biostratigraphic constraints on the sedimentary section at Site 1149. Clays at Sites 801 and 1149 were sampled to study ichthyolith (fish debris) assemblages. The reference time scale adopted for Leg 185 follows Gradstein et al. (1995) for the Late Cretaceous and part of the Early Cretaceous and Channell et al. (1995) for the Late Jurassic and part of the Early Cretaceous. The nannofossil biozonations adopted for the Lower and Upper Cretaceous during Leg 185 are mainly that of Thierstein (1973, 1976), Sissingh (1977), and Roth (1978) and are regarded as standards as summarized in Perch-Nielsen (1985). Additional useful bioevents as shown by Erba et al. (1995) for Leg 144 and by Erba et al. (in press) for the Cismon Apticore were also used.

INTERRAD Jurassic–Cretaceous Working Group radiolarian biochronology (1995) was adopted for Leg 185. The INTERRAD Jurassic–Cretaceous Working Group (1995) provided a synthesis of the systematics, occurrences, and biochronology of radiolarians of Middle Jurassic to Early Cretaceous age from the low-latitude Tethyan realm. Twenty-two radiolarian zones were defined by means of Unitary Associations (Guex, 1977, 1991). These zones were correlated to the standard stages using other fossil groups reported from the same sections, such as ammonites, nannofossils, calpionellids, and dinoflagellates. In particular, Upper Jurassic–Lower Cretaceous radiolarian Unitary Association zones were correlated with calpionellid and calcareous nannofossil bioevents and magnetic chrons (Jud, 1994; Dumitrica-Jud, 1995). Figure F5 shows a tentative correlation between calcareous nannofossil and radiolarian biozonations based on magnetic chrons.

Age determinations of ichthyoliths were based on Doyle et al. (1974), Doyle and Riedel (1979, 1985), and Kozarek and Orr (1979).

F5. Cretaceous biostratigraphic scale, p. 60.



Radiolarians

Methods

Radiolarians from siliceous sediments were extracted with a standard hydrofluoric (HF) acid method, by reacting samples in 5% diluted HF acid for 12–24 hr. Carbonate-rich samples were first decalcified in 10% hydrochloric (HCl) acid. The samples were sieved and the >46- μm fraction was examined.

Preservation was defined as follows:

VG (very good) = majority of specimens observed are complete, with spines intact, no overgrowths, or recrystallization. Nearly all specimens are determinable.

G (good) = many specimens are complete with spines intact, little or no overgrowths, cement or matrix infill present, but outer surface intact. Most specimens are determinable.

M (moderate) = a substantial portion of the specimens is broken, with some degree of overgrowth, etching, or replacement by minerals other than quartz or pyrite. Fifty percent of specimens are determinable.

P (poor) = specimens are mostly broken and fragmented or strongly etched or replaced by other minerals. Less than 5% of specimens are determinable.

VP (very poor) = specimens are only present as inner molds or ghosts, or fragments. None are determinable. Estimates of abundance are qualitative and were determined on the percentage of radiolarian specimens observed in the residue.

Abundance of radiolarian specimens has been defined as follows:

A (abundant) = >80%,

C (common) = 10%–80%,

F (few) = 1%–10%,

R (rare) = <1%, and

VR (very rare) = <0.1%.

Calcareous Nannofossils

Methods

Biostratigraphic Analysis

Samples for calcareous nannofossil biostratigraphic analysis were prepared using standard techniques in order to retain the composition of the original assemblage. Smear slides were examined using standard light microscope techniques under crossed polarizers and transmitted light at 1000 \times magnification. Because of calcite dissolution or overgrowth, preservation and abundance of calcareous nannofossil species may vary significantly. Thus, to characterize preservation a simple code system, which follows the shipboard ODP-PAL (paleontology analysis log) program, has been adopted and is listed below:

VG (very good) = no evidence of dissolution and/or overgrowth is present; there is no alteration of primary morphological characteristics, and specimens appear diaphanous; specimens are identifiable to the species level.

G (good) = little or no evidence of dissolution and/or overgrowth is present; primary morphological characteristics are only slightly altered; specimens are identifiable to the species level.

M (moderate) = specimens exhibit some etching and/or overgrowth; primary morphological characteristics are sometimes altered; however, most specimens are identifiable to the species level.

P (poor) = most specimens exhibit overgrowth or dissolution; primary morphological characteristics are sometimes destroyed; fragmentation has occurred; species identification is often impaired.

Estimates of the total calcareous nannofossils abundance (group abundance in PAL) were recorded as follows:

C (common) = >50% of all particles,

F (few) = 10%–50% of all particles,

R (rare) = 1%–10% of all particles,

T (trace) = <1% of all particles, and

B (barren) = no nannofossils are present.

Estimates of the relative abundance of calcareous nannofossil species in pelagic assemblages, according to those suggested in the PAL program, were determined as follows:

D (dominant) = >50% of the total assemblage,

A (abundant) = 10%–50% of the total assemblage,

C (common) = 1%–10% of the total assemblage,

F (few) = 0.1%–1% of the total assemblage, and

R (rare) = <0.1% of the total assemblage.

Data Entry

During Leg 185, data entry to the Janus database was performed with the ODP-PAL program. Data input and data query in PAL were performed in a user-friendly working window very similar to most commercial spreadsheets. The program links the data input to the scientist and the fossil group in order to retrieve the appropriate spreadsheet every time the data input or the data query are performed by the same scientist. The scientist selects the appropriate fossil group and creates a personal taxa dictionary. This can be performed either by selecting different species names from the main taxa dictionary, or adding new relevant taxa, together with their authorship, to the main dictionary. Datum events, biozones, and geologic ages can be selected and recorded as well. Data input of micropaleontological analysis records the biozone, age, preparation technique, preservation, group abundance, and bathymetry of all samples. Moreover, presence/absence, reworking/contamination, and relative abundance are recorded for every species belonging to a given sample. Queries can be performed in the Janus database to produce reports (range charts, age models, etc.) and perform data correlation between different sites.

Ichthyoliths

Methods

Samples were disaggregated in a mixture of water and hydrogen peroxide (H₂O₂) for 1 day then sieved and washed through 250- and 64-

mesh sieves. The residues were dried and the >250- and >64- μm fractions were examined. The fish remains were picked from the residue, first studied under reflected light and then permanently mounted on glass slides with Norland Optical Adhesive for detailed description of structural patterns under transmitted light.

BASEMENT

Igneous Petrology

Introduction

This section describes the technologies used for defining the lithologic units and subunits in the cores. In addition to these units, a further series of sequences were defined. These include groups of units that correspond to major lithologic changes. They are commonly coupled with changes in the physical properties of the rocks, as defined in the logs, and/or geochemical changes determined by significant shifts in geochemistry from X-ray fluorescence (XRF) or ICP analyses. In addition to the 60 lithologic units and ~250 subunits defined in Hole 801C basement, 18 geochemical units and 8 sequences were identified.

Core Curation and Shipboard Sampling

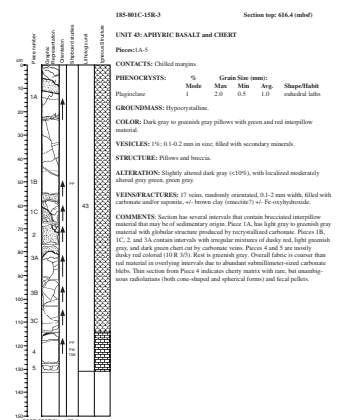
To preserve important features and structures, core sections containing igneous rocks were examined before the core was split. Contacts were examined for evidence of chilling, baking, and alteration. Each piece was numbered sequentially from the top of each core section and labeled on the outside surface. Broken core pieces that could be fitted together were assigned the same number and were lettered consecutively from the top down (e.g., 1A, 1B, 1C). Composite pieces sometimes occupied more than one section. Plastic spacers were placed between pieces with different numbers. The presence of a spacer may represent a substantial interval without recovery. If it was evident that an individual piece had not rotated about a horizontal axis during drilling, an arrow was added to the label pointing to the top of the section. The pieces were split with a diamond-impregnated saw so that important compositional and structural features were preserved in both the archive and working halves.

Nondestructive physical properties measurements, such as magnetic susceptibility and natural gamma-ray emission, were made on the core before it was split (see “Physical Properties,” p. 36). After splitting, the archive half was described on VCD forms and photographed. Digital images of the core were taken using the AMST. To minimize contamination of the core with Pt-group elements and Au, the describers removed jewelry from their hands and wrists before handling. After the core was split and described, the working half was sampled for shipboard physical properties, magnetic studies (see “Paleomagnetism,” p. 27), thin sections, XRD, XRF, and shore-based studies.

Visual Core Descriptions

VCD forms (Fig. F6) were used to document each section of the igneous rock cores. From left to right on the VCD the following were displayed: (1) a photograph of the archive half of the core, (2) a scale from 0 to 150 cm, (3) the piece numbers, (4) a graphical representation of the

F6. Example of a VCD form, p. 61.



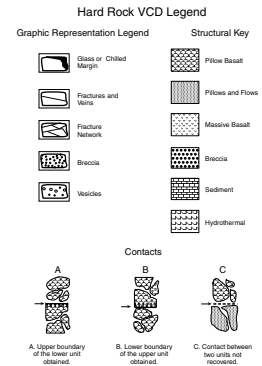
rock with structural details, (5) the piece orientation, (6) the location of samples selected for shipboard studies, (7) the boundaries of lithologic units, and (8) structure. In the graphical representation, fractures, veins, breccia, glassy contacts, and vesicles were indicated by using the symbols shown in Figure F7. A horizontal line across the entire width of this column denotes a plastic spacer. Vertically oriented pieces are indicated on the form by an upward-pointing arrow to the right of the appropriate piece. The location of samples selected for shipboard studies is indicated in the column headed "Shipboard studies," using the following notation: XRD = X-ray diffraction analysis; XRF = X-ray fluorescence analysis; TS = petrographic thin section; PP = physical properties analysis; and PM = paleomagnetic analysis. Column 7 displays the number of the lithologic unit and the location of the boundaries between units. Column 8 displays the graphical representations of structural types from the key in Figure F7.

Each section of core was examined separately by two teams of describers, igneous characteristics (discussed here) and alteration (see "Alteration," p. 22). Lithologic units and subunits (the latter representing single cooling units, breccia, or interflow sediment) were identified on the basis of the presence of contacts, chill margins (Fig. F7), changes in primary mineralogy (occurrence and abundance), color, grain size, and structural or textural variations. The boundaries of the lithologic units were drawn on the VCD, and for Hole 801C the units were numbered continuously from the end of Leg 129, starting with Unit 33. Some units were divided into subunits (-1,-2, etc.) for each cooling unit. For Site 1149 the igneous unit numbers start at 1 in Core 185-1149B-29R-1 at 407.74 mbsf. VCDs also contain a text description of each section of core that includes the (1) leg, site, hole, core number, core type, section number; (2) depth of the top of the section in mbsf; (3) unit number (consecutive downhole), number of pieces in the unit in the section, and the rock name; (4) groundmass, grain size, the Munsell color, vesicle abundance and size, structure, the nature of the alteration, information about abundance and filling of fractures, and additional comments.

Igneous Lithology and Mineralogy Logs

The lithology spreadsheet (Table T1) lists for each unit and subunit the core number, section number, piece numbers, locations of the top and bottom of the unit in mbsf and in centimeters from the top of the section, length of each unit in centimeters, unit number, rock name, texture, structure, color, comments, and whether the unit has top and/or bottom contacts. Units were defined based on major changes in lithology, texture, structure, and mineralogy. Subunits were defined by contacts and changes in lithology within the units. Types of contacts are indicated in Table T1. When a contact was unrecovered, changes in lithology were used to define units. In the spreadsheet the first subunit of each unit is highlighted in blue. The units and subunits were named on the basis of the structure and abundance of primary minerals. In the lithology column, basalts were described as aphyric (<1% phenocrysts), sparsely phyric (1%–2% phenocrysts), moderately phyric (2%–10% phenocrysts), or highly phyric (>10% phenocrysts). They were further classified by the types of phenocrysts or megascopic crystals present (e.g., sparsely plagioclase-olivine phyric in which the amount of plagioclase exceeds the amount of olivine). Sedimentary, interpillow, and rubble units were also present in the upper levels of the hole. These are indi-

F7. Hard rock VCD legend and types of igneous contacts, p. 62.



T1. Example of the igneous core description log, p. 70.

cated in yellow in the spreadsheet. Rock color was determined on a wet, cut surface of the rock using the Munsell color chart.

Pillow basalts were identified by their chilled margins or, when these margins were absent, by variolitic texture, curved fractures, and microcrystalline grain size. In some cases when the margins were not recovered, pillows could not be distinguished from thin flows, and these were called pillow and flow units. Massive units were identified by continuous sections of similar lithology that increased in grain size toward their center. In the lithology spreadsheet, structures of the basalts were subdivided into pillows, flows, breccias, and massive units; these structures were included in the barrel sheet using the key in Figure F7.

Mineralogy spreadsheets contain the core, section, piece number, depth interval (cm), depth in mbsf, lithologic unit number, groundmass grain size, and mineralogy of the rocks. At least one sample from each section and unit was examined with the binocular microscope to determine phenocryst size, abundance, morphology, and vesicle abundance and size. In addition, for Cores 185-801C-13R through 30R, the spreadsheet (Table T2) contains cells for recording the groundmass mineral abundance and grain size, and the spinel, oxide, and sulfide abundance. However, because basalts from Hole 801 were consistently fine grained and microcrystalline, this information could not be determined in hand specimen.

Groundmass character was identified as medium grained (MG) if the average grain size was 1 mm or greater, fine grained (FG) if the grains could be identified and were <1 mm, microcrystalline (M) if the groundmass crystals could be seen but were too fine to identify, cryptocrystalline (C) if crystals could not be distinguished, hypocrySTALLINE (HY) if glass was present with crystals and crystal abundance exceeded glass abundance, and hypohyaline (HH) if glass abundance exceeded crystals. Mineral morphology was indicated as anhedral (an), subhedral (su), or euhedral (eu). A hyphen indicates the absence of a phase. Maximum, minimum, and average crystal size were also estimated. An estimate of the percentage of vesicles and their average sizes was made. Mineral abundance was used in determining the rock name. The igneous lithology and mineralogy logs are included (see the **“Supplementary Materials”** contents list.

Thin Sections

Thin sections of igneous rocks were studied to complete and refine the hand-specimen observations. This included textural features that were not identified in hand specimen; precise determination of grain size of phenocrysts and groundmass; the mineralogy, abundance, and kind of glomerocrysts; the presence of inclusions within phenocrysts; and the presence of spinel, oxides, and sulfides. Crystal sizes of all primary phases were measured. In addition, mineral morphologies, grain sizes, and textural features were described. The terms heterogranular (different crystal sizes), seriate (continuous range in grain size), porphyritic (indicating presence of phenocrysts), glomerophytic (containing clusters of crystals), hypocrySTALLINE (100% crystals) to hypohyaline (100% glass), and intergranular (olivine and pyroxene grains between plagioclase laths) were used to describe the textures of the mesostasis. The same terminology was used for thin-section descriptions and the megascopic descriptions. Thin-section descriptions are included (see the **“Core Descriptions”** contents list) and are also available from the ODP Janus database.

T2. Example of the igneous mineralogy log, p. 71.

Alteration

All igneous rocks recovered during Leg 185 have undergone alteration. On the hard-rock VCD forms, rocks were graded according to whether they are fresh (<2% by volume alteration products) or have slight (2%–10%), moderate (10%–40%), high (40%–80%), very high (80%–95%), or complete (95%–100%) alteration. Alteration and vein core description logs on a piece-by-piece scale were tabulated to provide a consistent characterization of the rocks and to quantify the different alteration types (see the “Core Descriptions” contents list). Descriptions are based mostly on hand-specimen observations, and specific secondary minerals are not generally distinguished, except where crystal morphology allows unequivocal identification. Where additional mineralogical evidence is available from either thin-section descriptions and/or X-ray diffractograms, these identifications were integrated into the alteration and vein logs and the VCDs. Table T3 provides a list of abbreviations used in the alteration and vein logs.

We recorded the following information in the logs:

1. The alteration log (e.g., Table T4) was used to record the bulk-rock alteration. Each entry records the igneous unit; identifiers for the core, section, piece, subpiece; the length of each piece; and the depth below seafloor of the top of each piece. Visual estimates of the alteration type (as represented by wet rock color and calibrated by thin-section observations), the abundance (in percent), size (in millimeters), mineral fillings of vesicles, and the proportion of altered groundmass and phenocrysts with the primary and secondary minerals are documented for each piece. A column for comments is included.

2. The igneous core description log (e.g., Table T1) was used to record the presence, location, width, and mineral content of veins observed on the cut surface of the cores. Each entry records the igneous unit and the identifiers for the core, section, piece, and subpiece. For each vein the location of the top and bottom of the feature is recorded, and the mineral fillings, vein width (in millimeters), presence or absence of a related alteration halo, and the half width (in millimeters) of the halo are recorded. Data recorded for breccias include percentages of cement and clasts, and the percentages of secondary minerals and sediments present. A column for comments is included, where crosscutting relationships between veins are recorded.

IGNEOUS AND SEDIMENTARY GEOCHEMISTRY

During Leg 185, two methods were used to examine basement and sediment geochemistry: XRF and atomic absorption (AA) spectrometry.

X-Ray Fluorescence Analysis

Samples considered by the shipboard party to be representative of individual lithologic units or of unusual composition were analyzed for major and selected trace elements by XRF. We used a fully automated wavelength-dispersive ARL8420 XRF system, equipped with a 3-kW generator and a Rh-anode X-ray tube, to determine the major- and trace-element abundances in the samples. Analytical conditions used are given in Table T5. The spectrometer is calibrated using a suite of 30 well-analyzed reference standards for basement rocks and 20 for sedi-

T3. Abbreviations used in the alteration and vein logs, p. 72.

T4. Example of the alteration log, p. 73.

T5. Instrumental conditions for XRF analyses, p. 74.

ments. The values recommended by Govindaraju (1989) are used for all elements. The analytical errors (standard deviation) based on the average of replicate shipboard analyses of the U.S. Geological Survey reference standard BHVO-1 are better than 0.75% for all major elements except for N, K, and Mn, which are <2.60% (Table T5).

After cutting by either a water-cooled diamond circular saw or a 1-in-diameter diamond drill, the samples were sandblasted with alumina grit to remove saw marks or any unwanted material. The average sample taken weighed ~22 g. After sandblasting, the samples were cleaned in an ultrasonic bath in methanol and deionized water for 10 min each, followed by drying at 110°C. Larger pieces (~20 cm³) were reduced to <1 cm diameter by crushing between two disks of Delron plastic in a hydraulic press. The samples were then ground for ~1–5 min in a Spex 8510 shatterbox with a tungsten carbide barrel. Contamination of the samples with Nb during grinding was investigated before the start of Leg 152, and none was detected (Larsen, Saunders, Clift, et al., 1994), although significant contamination occurred for W, Co, and Ta (Thompson and Bankston, 1970).

Major Elements

Samples were prepared for major-element analysis using fused lithium tetraborate glass disks doped with lanthanum oxide as a heavy absorber (Norrish and Hutton, 1969). The discs were prepared from 600 mg of rock powder that had been ignited for 4 hr at ~1025°C and mixed with 7.2 g of dry flux consisting of 80% lithium tetraborate and 20% lanthanum oxide. This mixture, with 20 mL of LiBr (8.6 M) added to prevent adhesion to the Pt-Au crucible, was then melted in air at 1100°C for ~10 min with constant agitation to ensure thorough mixing and then cooled. The 12:1 flux to sample ratio and the use of the heavy absorber made matrix effects insignificant over the normal range of igneous rock compositions. Hence, the relationship between X-ray intensity and element concentration was linear.

Trace Elements

We determined trace elements with pressed-powder pellets. For the basement, these were made by mixing 5 g of rock powder with ~2 mL of a solution of Chemplex polymer in methylene chloride (100 mg/cm³) and then pressing the mixture into an aluminum cap under a load of 7 T. For the sediments, we used 6.0 g of powder. A pellet made with 5 or 6 g of powder should be infinitely thick at the shortest wavelengths used in the analysis. X-ray intensities were corrected for line overlap and interelement absorption effects. The latter corrections were based on the relationship between the mass absorption coefficient and the intensity of the Rh-K Compton scatter line (Reynolds, 1963, 1967; Walker, 1973). We measured loss on ignition from weighed powders, which were heated for 4 hr at 1025°C, then reweighed.

For more details on calibration, see the “XRF Analyses” sections in the “Explanatory Notes” chapters of Becker, Sakai, et al. (1988, pp. 9 and 10) and Dick, Erzinger, Stokking, et al. (1992, pp. 13–18).

Analysis of Potassium in Basalts by Atomic Absorption Spectrometry

Hole 801C basalt samples were analyzed for K by AA spectrometry in order to provide higher resolution data than that provided by the more complete and time-consuming XRF analyses. Potassium was measured because it is sensitive to basalt alteration and is a main contributor to the natural gamma radiation (NGR) measurements of both the down-hole logs and the MST. Thus, we were interested in obtaining a higher resolution data set for K on targeted samples and intervals to better understand the length scales of basalt alteration and to help calibrate the NGR measurements. The results of this study are described in “[Discussion](#),” p. 17, and “[Physical Properties](#),” p. 35, both in the “Site 801” chapter. There are several advantages to the AA method over the XRF protocol: (1) smaller sample sizes can be used (<0.1 g), as opposed to the >3 g required by XRF, thus allowing higher resolution sampling; (2) detection limits are lower; and (3) the prepared solutions may be used for shore-based inductively coupled plasma-atomic emission spectroscopy (ICP-AES) and ICP-mass spectrometry (ICP-MS) analyses of a greater suite of major and trace elements.

For the shipboard AA analyses, small chips of rock samples were taken on the sampling table, cleaned in an ultrasonic bath in nanopure water (DI), and oven dried at 105°C for several hours. These sample chips were subsequently crushed between Delron plastic dishes and powdered by hand in an agate mortar and pestle. Approximately 0.10 ± 0.01 g of dried sample powder was used in the analysis. The precise weight was recorded to four decimal places and was used in calculations of final individual dilution factors on a per sample basis. The precision parameter on the Scientech Balance Control was set to 0.0005 to provide an effective precision of weighing to better than 1% of the measured value. The precision of the weighing was aided by the calm seas of the balmy, tropical climate at Site 801 during this leg.

The sample powder was poured directly into 6 mL of 8 N (35%) nitric acid in a Teflon beaker, into which was added 2 mL of concentrated HF acid. Both small (3 mL) and large (100 mL) Teflon beakers were used for the dissolution, with no difference in decomposition quality. Samples were heated and dried on a hot plate to a hard residue at ~60°C over 5–8 hr. The commonly yellow-colored residue resulting from the drydown was redissolved in 6 mL of 8 N (35%) nitric acid for ~30 min. Even at this stage, a yellow residue was commonly visible. The 6 mL of acid solution, along with the residue, was diluted in a 60 mL acid-cleaned bottle by adding 12 mL of DI. This primary dilution was achieved by successive DI additions of 3 mL each to thoroughly clean the Teflon beaker. During this dilution, the yellow residues dissolved. From this initial dilution, 3 mL was taken and added to 18 mL of 0.35% CsCl solution to arrive at a final aliquot for AA analysis. This dilution worked well for the lowest concentration samples only, with the remaining ones requiring a further 11-fold dilution. The final dilution factor in the majority of the samples, therefore, was ~13,860-fold.

The AA was operated in flame emission mode, using the 766.5-nm wavelength and a slit width of 0.2 nm. The AA conditions, and the use of the CsCl matrix, were selected on the basis of the operating conditions suggested by Gieskes et al. (1991) for the analysis of interstitial water.

Blanks and standard reference materials (SRMs) were prepared along with the samples. Several SRMs and natural samples were analyzed in

replicate to assess procedural and analytical precision, as well as for a final correction. Precision was quantified to be better than 10% of the measured value. Matrix matched (in terms of the nitric acid and CsCl concentrations) calibration standards at K concentrations of 0, 0.1, 0.2, 0.5, and 1 ppm were used. The calibration was fit with a second order polynomial equation over this concentration range with a correlation coefficient (r^2) >0.995 . Data from all unknown samples, known samples (previously analyzed by XRF), and SRMs were analyzed, and the data were reduced in this fashion.

Accuracy was also assessed by the analyses of the SRMs. As long as the same pipettes and all other laboratory apparatus were used during the preparation of the SRMs and the unknowns, then uncertainties caused by the volumetric (as opposed to mass) dilutions and vagaries of the dissolution procedure were minimized. Comparison of the AA results of the analysis and the accepted values of the SRMs shows a strongly linear relationship, with the shipboard measurements agreeing to within 10% of the accepted values. The shipboard values were corrected by this offset to arrive at the final concentrations.

PREPARATION OF COMPOSITES

Introduction

The net chemical changes to the oceanic crust during plate creation and destruction are poorly understood because of our inability to constrain its bulk composition on length scales that are relevant to global geochemical budgets. Such large-scale chemical compositions can be relatively easily determined for thick homogeneous sedimentary strata or for unaltered lava flows that may represent total volumes of several cubic kilometers or more. However, rock units in the oceanic crust are heterogeneous either because of original conditions during their formation or as a result of secondary processes such as weathering or metamorphism. Special efforts have to be made to bridge the gap in scale from a geochemical sample size (centimeter scale) and a geologically mappable unit to allow extrapolation of geochemical data on a regional scale (hundreds to thousands of meters). This extrapolation requires a detailed analysis of the heterogeneity on the scale of an outcrop or drilled section. All representative units need to be sampled and integrated in their respective proportions to determine the bulk geochemical composition of a particular reservoir.

Integration of multiple samples for large-scale geochemical budgets can be done in two ways: (1) by physical integration (i.e., mixing) of samples in their respective proportions to form large composite samples for chemical analysis or (2) by geochemical analysis of each sample and numerical integration of the chemical data to determine large-scale chemical composition. The result of these two different procedures should yield an identical geochemical mean; nonetheless, the two approaches differ in terms of their practical and scientific benefits.

The physical composite approach has the advantage that it requires fewer chemical analyses. Small amounts of material from a large number of samples are combined in one or several large composite samples. This is particularly important in ODP sampling, where very little core often has to be shared by a large group of scientists. A small number of composites provides a focus of analytical effort that permits correlation

of geochemical data that are usually performed by different laboratories on different samples.

However, composite samples also have potential problems. Once a composite is mixed, it is impossible to resolve whether a particular element is homogeneously distributed between contributing samples or whether it is dominated by a few samples with extreme composition. Thus, by analyzing each sample, bulk compositions can be constructed knowing the composition of each component and permitting cross-checks for samples of extreme composition. Analyzing each sample also has the advantage that the geochemical covariation between individual samples is known, which may help constrain the processes that control the bulk composition.

In our approach, we chose a path between these extremes: samples taken shipboard will be analyzed on shore for the less labor intensive analytical steps (such as major and trace elements), whereas composites will be analyzed for all chemical and isotopic parameters and curated for future investigators. Furthermore, we will prepare several composites that allow us to identify some of the heterogeneity, in particular between moderately altered lava flows and the extremely altered compositions in intercalated sediments, breccias, and hyaloclastites.

Sample Selection and Preparation of Powders

For the preparation of composites, we selected 118 individual samples from Hole 801C, ~25 samples per 100 m drilled, including 58 samples from cores drilled during Leg 129 (see the “[Supplementary Materials](#)” contents list). All samples were characterized and powdered on board; the mixing and homogenization of composite powders will be completed onshore. Individual core samples were chosen as representative samples of the different alteration domains. Typically, we selected one characteristic minimally altered sample per major igneous unit or at least every ~20 m drilled (total 28 samples). About 50 samples were taken to represent the average altered portion of the core in terms of its colors, halos, and type of veins. We also sampled characteristic, highly altered intraflow materials (IFMs) based on lithologic type (sedimentary or igneous), color, and texture. Most samples were taken as 4- to 6-cm-long, quarter-core sections and were subsequently split into three 4- to 6-mm-thick slabs for the composite powder, a thin section, and an archive sample. In some cases we used representative grains from the coarsely crushed samples for the archive sample.

We recorded the color, vein mineral content, and primary and secondary mineralogy of each sample included in composites. After describing each sample, we used an Al grit in a sandblaster to remove surface contamination, eroding 0.1–0.5 mm of the outermost surface of the sample. Subsequently, individual slabs were cleaned ultrasonically for ~10–20 min in DI and air dried. The dry slabs were sandwiched between two plastic discs, placed in a hydraulic press, and reduced to 2- to 4-mm-sized particles by applying 5–8 T of pressure. Coarsely crushed rocks were then freeze-dried for 3 hr and powdered for 15 min in an alumina-ball mill. Separately ground powder batches of individual samples were combined and mixed for an additional 5 min for homogenization in order to obtain ~10 g of powder for each composite sample.

Composite Make-Up Strategy

Overall, we have chosen a procedure that allows us to compare composite data to previous estimates of this type at Sites 417 and 418. A total of 12 composites was prepared to define the bulk chemical composition on different scale lengths. The largest scale is represented in the top alkali basalt composite (Sequence I), the total tholeiite section composite (Sequences III–VIII), and the total drilled section at Site 801. In addition, we will prepare nine other composites, three from each of the three depth intervals (upper, intermediate, and lower tholeiite section). For each of these depth intervals, we will prepare a pillow/flow composite (FLO), an IFM composite, and a depth composite that is a mix of FLO and IFM materials in the proportions in which they occur in each interval. FLO composites are made of a representative mix of basalt samples and quenched margins (plus a minor amount of inter-pillow material), as is typical for most sequences of submarine pillows and flows. Here, flows may include some shallow intrusions that are hard to distinguish from flows where contacts are not completely recovered. Individual samples were chosen to represent the proportions of different alteration types and vein mineral abundances, as they were described for the whole core. IFMs include epiclastic, volcanoclastic, and hydrothermal units that are deposited between igneous cooling units. These IFMs are often poorly recovered, and their proportions are difficult to determine. Whenever possible, we used logging data to determine the volume of the different units. However, much of this analysis will be conducted onshore; thus, the final composition of the composites will be determined once the log analysis is completed.

PALEOMAGNETISM

Instrumentation Used

Remanent magnetization was measured using the shipboard 2-G Enterprises (Model 760R) long-core cryogenic magnetometer that is equipped with direct current superconducting quantum interference devices (DC SQUIDS) and has in-line, automated alternating-field (AF) demagnetization capability. The sense coils of the cryogenic magnetometer measure over a width of a little more than 30 cm, although ~85% of the remanence is sensed from a 20-cm width of a core section. Measurements were made at 5-cm intervals in basalt and other basement materials and at 2–4 cm in sedimentary sequences. A background resolution limit is imposed on measurement of rock remanence by the magnetization of the core liner itself, which is $\sim 3 \times 10^{-5}$ A/m.

The measurement coordinate system, which is standard for ODP legs, was used: +x = upward (downward) from the split face of the archive (working) half of the core; +y = left looking upcore along the split surface of the archive half; +z = downcore.

AF demagnetization on the archive halves was performed routinely with the automated cryogenic magnetometer and attached AF coils; most core sections were demagnetized at 5, 10, 15, 20, 25, 30, and 35 mT; additional steps of 3, 8, 40, 45, and 50 mT also were tested. Discrete samples were not demagnetized on board, however, because of an anhysteretic remanence magnetization (ARM) that is imparted by the in-line demagnetization apparatus of the cryogenic magnetometer. The ARM probably results from the poor shielding from magnetic fields in

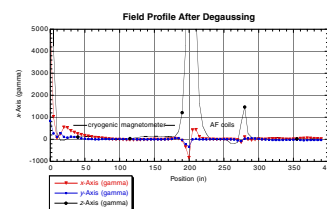
the demagnetization region (Fig. F8); the fields are a result of two prominent leaks in the magnetic shielding at the two points where the magnetic shielding cans are bolted together. Comparisons of sequential demagnetization steps show that in many samples, the ARM becomes prominent just as the drill-string remanence is removed. In more magnetically susceptible samples (e.g., medium-grained basalts), the ARM becomes visible at low demagnetizing fields (between 8 and 10 mT). In less susceptible rocks, such as chilled margins of pillow basalts, the ARM can remain obscure until 35–40 mT (Fig. F9).

Magnetic susceptibility is measured routinely as a part of several shipboard procedures. The susceptibility meter for all measurements was the same, a Bartington Instruments model MS-2. Whole-core sections were run through the MST (see “Physical Properties,” p. 36), on which is mounted a Bartington Instruments susceptibility ring sensor (MS-2C), an 8-cm ID coil through which the whole core (~5.5–6.5 cm) passes; susceptibility was measured every 5 cm. Susceptibility was measured again on the archive half of all cores with a Bartington probe sensor (MS-2F), a cylindrical probe of 2-cm length attached to the AMST (see “Sedimentologic Description,” p. 10). This sensor can probe to a depth of ~2 cm. The AMST permits measurements at only evenly spaced intervals along core sections and automatically excludes missing sections of core; spacing can vary from 2 to 10 cm. AMST measurements again were made every 5 cm on basalts and other basement rocks and every 2 to 4 cm for sedimentary rocks. Susceptibilities of discrete samples also used a Bartington MS-2 meter in combination with a hollow cylindrical sensor, the MS-1B dual frequency sensor (ID = 3.6 cm).

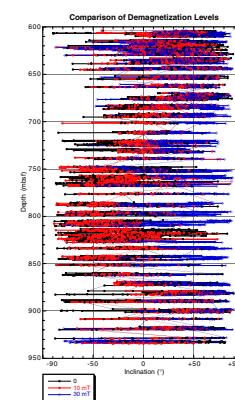
Comparison among the three types of susceptibility measurements has been undertaken numerous times during previous ODP legs, most recently Leg 183. Shipboard Scientific Party (2000) report that the variation with depth by the three independent susceptibility measurements was consistent throughout the leg but that the MST and AMST data sometimes showed lower values than those of discrete samples. The most significant differences were in the AMST measurements. They speculate that the lower values were probably the result of gaps in core sections, although sensor calibrations also may not have been uniform. Gaps in core material create low values, which are significant additions to the whole-core signatures because of the volume of the ~6.5-cm diameter of whole cores. Although scientists from Leg 183 were unable to reprogram the AMST software to ignore measurements from missing sections or disturbed intervals of core, the software was reprogrammed just before the start of Leg 185 to skip missing sections.

A seafloor punch core taken for microbial studies recovered a very homogeneous brown clay; the homogeneous nature made this material ideal for testing the instruments. The seven sections of the core, Core 185-801D-1W, were measured with each instrument, as a whole core, a half core, and then as discrete samples taken from each section. Figure F10A shows the direct output of each of the three susceptibility devices. The discrete and AMST sensors gave quite similar values. The MST data must be corrected for the difference between diameter of the core and the inner diameter of the ring sensor. The correction requires an estimate of the differences in diameters and the use of a table or graph of correction factors supplied by Bartington Instruments to determine the correction factor. The measured susceptibility values are divided by the correction factor. Use of this correction method improves the agreement between the results from the MST and the other methods (Fig.

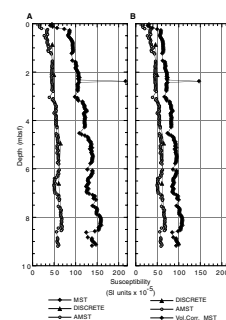
F8. Field profile after degaussing, p. 63.



F9. Comparison of demagnetization levels, p. 64.



F10. Whole-core and half-core susceptibility measurements, p. 65.



F10B). Lack of perfect agreement is most likely because of imperfect assessment of the whole-core volume.

Measurements and Procedures

Measurements of natural remanent magnetization (NRM) and magnetic susceptibility were routinely conducted on the igneous and sedimentary rocks on board the *JOIDES Resolution* during Leg 185. NRM was measured on all archive halves and on discrete samples from the working halves. Susceptibility was measured for all whole cores using the MST, on all archive halves using the AMST, and on all discrete samples with the dual-frequency sensor. Stepwise AF demagnetization was conducted on all archive halves of the cores; however, discrete samples were not demagnetized on the ship because of the ARM problem. They will be demagnetized onshore at the University of Wyoming.

Basalt data are presented as the direct output of the long-core magnetometer; principal component analysis of this data will be performed onshore. Together with the discrete sample analyzed onshore, this complete data set will be presented in the Leg 185 *Scientific Results* volume of the ODP *Proceedings*. Magnetostratigraphic results from Site 1149 are based on the time scales of Berggren et al. (1995) for the Cenozoic, Gradstein et al. (1995) for the Late Cretaceous, and Channell et al. (1995) for the Early Cretaceous. Paleolatitudes for the Pacific plate will be determined from a complete discrete sampling of the sedimentary section at Site 1149. Discrete samples will be measured onshore to utilize thermal demagnetization, and the results will be compiled with those obtained from Hole 801B of Leg 129 (Steiner and Wallick, 1992) for the *Scientific Results* volume.

INTERSTITIAL WATER CHEMISTRY AND HEADSPACE GAS

The shipboard inorganic and organic geochemistry program for Leg 185 focused on Site 1149 because Site 801 was reoccupied predominantly for igneous rock drilling. In Hole 801C, the water sampling temperature probe (WSTP) was run to sample borehole water on three different occasions, as described in "*Microbiology*," p. 31. A single pushcore (designated as Hole 801D) taken with the RCB at Site 801 was analyzed for interstitial waters. At Site 1149 the combined inorganic and organic program included (1) real-time monitoring of carbon dioxide and volatile hydrocarbons (HC), as required by ODP safety regulations, (2) measurement of inorganic carbon and carbonate content of the sediments, (3) elemental analyses of total carbon, nitrogen, and sulfur, and (4) a comprehensive interstitial water protocol.

Volatile Hydrocarbons

For safety and pollution prevention, concentrations and ratios of light HC gases, mainly methane (C_1), ethane (C_2), and propane (C_3), were monitored for each core following the standard headspace sampling method described by Kvenvolden and McDonald (1986). Immediately after core retrieval on deck, a sediment sample of $\sim 5 \text{ cm}^3$ was collected using a calibrated borer tool, placed in a 21.5-cm^3 glass serum vial, and sealed immediately with a septum and metal crimp cap. When

consolidated or lithified samples were encountered, chips of material were placed in the vial and sealed. Before gas analyses, the vial was heated at 70°C for a minimum of 20 min. A 5-cm³ subsample of the headspace gas was extracted from each vial using a 5-cm³ glass gas syringe for gas chromatography (GC) analysis. When gas pockets and expansion voids were encountered, gas samples were collected by penetrating the liner using a 50-cm³ plastic syringe with a plastic three-way valve connected to a steel penetration tool. Gas HC constituents were analyzed using a HP6890 gas chromatograph equipped with a flame ionization detector.

Inorganic Carbon

Inorganic carbon was determined at a frequency of one sample per core (and occasionally more frequently) using a Coulometrics 5011 carbon dioxide coulometer equipped with a System 140 carbonate carbon analyzer. Ten to 12 mg of freeze-dried ground sediment was reacted with 2 M HCl acid to liberate CO₂. The CO₂ was titrated and the change in light transmittance monitored by a photo detection cell. The weight percentage of calcium carbonate was calculated from the inorganic carbon content assuming that all the CO₂ evolved was derived from dissolution of calcium carbonate by the following equation:

$$\text{wt\% CaCO}_2 = \text{wt\% IC (inorganic carbon)} \times 8.33. \quad (1)$$

The amount of carbonate is expressed as weight percent, assuming all the carbonate was present as calcite. No corrections were made for other carbonate minerals.

Elemental Analysis

Total carbon, nitrogen, and sulfur were determined using a Carlo Erba 1500 CNS analyzer. An aliquot of 5–15 mg freeze-dried, crushed sediment with ~10 mg V₂O₅ oxidant were combusted at 1000°C in a stream of oxygen. Nitrogen oxides were reduced to N₂ and the mixture of N₂, CO₂, H₂O, and SO₂ gases was separated by GC and detection performed by a thermal conductivity detector. The H₂ value is not useful because it represents hydrogen from both organic matter and minerals (clay). All measurements were calibrated by comparison to pure sulfanilamide as standard. The amount of total organic carbon was calculated as the difference between total carbon and inorganic carbon, as follows:

$$\text{wt\% TOC} = \text{wt\% TC} - \text{wt\% IC}. \quad (2)$$

Interstitial Waters

Interstitial waters were extracted from 10- to 15-cm-long whole-round sections cut immediately after core retrieval on deck. At Site 1149, samples were gathered at a frequency of one per section of core in the upper 60 mbsf, one per core from 60 to 100 mbsf, and approximately every second core until interstitial water could no longer be extracted. These samples were coordinated closely with those taken by the microbiologists. After extruding the sediment from the core liner, the surface of each whole round was carefully scraped with a spatula to re-

move potential contamination. Interstitial waters were extracted by placing the sediment in a titanium squeezer and applying pressures up to 40,000 lb (~4150 psi) using a Carver hydraulic press. Water samples were collected into acid-cleaned plastic syringes and filtered through sterile 0.45- μm Gelman polysulfone disposable filters. Samples for shipboard analyses were stored in plastic vials. Aliquots for shore-based analyses were stored in heat-sealed acid-washed plastic tubes and/or glass vials, as requested by the given investigators.

Interstitial-water analyses followed the procedures outlined by Gieskes et al. (1991). Salinity was measured with a Goldberg optical handheld refractometer. The pH and alkalinity were measured by Gran titration with a Brinkmann pH electrode and a Metrohm autotitrator. The Cl^- concentration was measured by titration. Concentrations of H_4SiO_4 , PO_4^{3-} , and NH_4^+ were measured by spectrophotometric methods with a Milton Roy Spectronic 301 spectrophotometer. Concentrations of K^+ , Mg^{2+} , Ca^{2+} , and SO_4^{2-} were measured by ion chromatography using a Dionex DX-100 instrument. Concentrations of Li^+ , Sr^{2+} , Fe^{3+} , Mn^{2+} , and Rb^+ were measured by flame atomic absorption spectrophotometry using a Varian SpectrAA-20.

Analytical precision was determined by replicate analyses of natural samples as well as of calibration standards reanalyzed as unknowns. Values of precision, expressed as percent of the measured value, are as follows for the respective constituents: alkalinity, <1.5%; Cl^- , 0.4%; Ca^{2+} , <1%; Mg^{2+} , 0.5%; Si^+ and NH_4^+ , ~5%; K^+ , <3%; SO_4^{2-} , <4%; and Na^+ , <5%.

MICROBIOLOGY

The primary microbiology objective for Leg 185 was to determine the types and abundance of microbes in unconsolidated sediments, sedimentary rocks, and igneous rocks of the oceanic crust. To do this, water, sediment, and rock samples were collected to determine cell abundance and total biomass, to extract and characterize DNA contained within the samples, and to establish cultures of microorganisms inhabiting these environments. Interpretation of results is complicated by the possibility of contamination of samples with microbes from the seawater, the drilling fluid, the ship and drilling equipment, and from postcollection processing of samples. A sample handling protocol was established to minimize postcollection contamination and tracer tests were conducted to determine the extent of microbial contamination during drilling and sample preparation. Methods for tracer tests are detailed in “[Materials and Methods](#)” in “Methods for Quantifying Potential Microbial Contamination during Deep Ocean Coring” (Smith et al., 2000).

Water

Sampling

Surface-water samples were collected at each site using a sterile flask lowered from the bow of the ship to avoid encountering waste and cooling water from the ship. In addition, a sample of surface water was collected at Site 801 in a flask lowered from the small launch at ~1 km

upwind of the ship. Drill water was collected in a bucket from the drill string when it was opened to retrieve cores.

Water samples from near the bottom of Hole 801C were collected using the WSTP tool (Barnes, 1988). This water had not been disturbed since the hole was logged in June 1992 during Leg 144. The microbial content of the WSTP water sample was compared to that of surface water, sediments, and basement rocks. The chemistry of the WSTP sample was used to determine the origin of the water sampled.

Before deployment, the WSTP tool was flushed with a chlorine dioxide solution (FreeBact, Xenex Europe AB, Stockholm, Sweden; 1 ppm final concentration) and subsequently flushed with filtered (0.2- μm pore size) distilled water. The total abundance of microbial cells in the water used to flush the tool before and after it passed through the WSTP was determined by epifluorescence microscopy. The coil of the WSTP contained filtered distilled water at the time of deployment. Before it was sealed, the WSTP reservoir was flushed with nitrogen gas to reduce the concentration of oxygen. The Hole 801C water sample was taken with the WSTP sampler extended ~50 cm ahead of the bottom of the drill string. Special care was taken not to flush the hole while lowering the drill string. Water from the overflow reservoir was extracted with syringes from the pressure relief valve at the top of the reservoir. Samples from the coil reservoir were extracted in the anaerobic glove box after the coil was removed from the sampler. Temperature measurements were also obtained during the period the WSTP tools were in the borehole.

Microbial Abundance

WSTP, drill water, and seawater samples were fixed in 0.2- μm -filtered formalin (2% final concentration) and stained with DNA fluorochromes 4',6-diamidino-2-phenylindole (DAPI; 0.1 mg/mL final concentration) or Acridine orange (AO; 0.1 mg/mL final concentration) for 10 min. Stained cells were filtered onto black polycarbonate filters (Poretics or Nuclepore; 0.2- μm pore size) and examined with a Zeiss Axiophot microscope at 1000 \times final magnification (100 \times Plan-NEOF-LUAR objective) using epifluorescence illumination (100-W Hg bulb) with UV and blue filter sets for DAPI and AO, respectively. Cells were enumerated and normalized to the volume of water filtered.

Enrichment Cultures

WSTP, drill water, and seawater samples were inoculated into 12 types of anaerobic liquid culture media. The media were based on the composition of seawater, reduced with sulfide and cysteine, and buffered to pH 8.0. Media also contained vitamins and trace elements. Electron acceptors were Mn(IV), Fe(III), sulfate, and bicarbonate. Electron donors were organic carbon (acetate, lactate, and pyruvate), hydrogen, and methane. Eleven different combinations of electron donors and acceptors were used to enrich manganese reducers, iron reducers, sulfate reducers, acetogens, and methanogens. Fermenters were enriched in the same medium base with the organic nutrients of R2A medium (Reasoner and Geldreich, 1985). One bottle of each medium type was inoculated with 0.25 mL of water from the WSTP coil, or 1 mL of drill water or seawater. Cultures were incubated at 25°C for the WSTP sample and 30°C for the drill-water and seawater samples and monitored for growth. Uninoculated negative controls were incubated at the same

temperature. Cultures were shipped to Göteborg University, where growth will be detected by analysis of metabolic products and staining of microbial cells with DAPI and AO.

High-Pressure Archiving

WSTP and seawater samples were stored in polycarbonate tubes capped with tight-fitting polyethylene lids and sealed with at least two layers of stretched Parafilm. Vials were placed into stainless steel high-pressure vessels with an ID of 2 cm and a tube length of 10 cm (Fig. F11). Vials were immersed in water (distilled for the WSTP sample and NaCl solution (3.1%) for the seawater sample), eliminating air space inside the high-pressure vessel. High-pressure vessels were capped with a stainless steel plug that was screwed into the vessel, sealing it while ejecting air and excess water. The high-pressure seal was accomplished with a Vytan plug-to-wall gasket. Pressure vessels were connected to 1/8-in stainless steel tubing and sealed with a pin valve. Pressurization was accomplished with a piston-stroke pump, using distilled water as a pressure medium. Pressures were restored to ~100–200 psi above the in situ conditions. High-pressure samples were transported to Scripps Institution of Oceanography for shore-based studies.

DNA Extraction

Aliquots of water extracted from the WSTP coil and reservoir, as well as the drill-water and seawater samples, were immediately frozen in liquid nitrogen and stored at -70°C . Drill-water and seawater samples were also filtered through capsule filters (Sterivex-GS 0.22 μm ; Millipore), and the filters were immediately frozen in liquid nitrogen and stored at -70°C . Frozen samples were shipped to the Graduate School of Oceanography, University of Rhode Island, for DNA extraction and characterization.

Chemistry

Methods for chemical analyses of the WSTP samples are described in “[Interstitial Water Chemistry and Headspace Gas](#),” p. 29.

Sediments

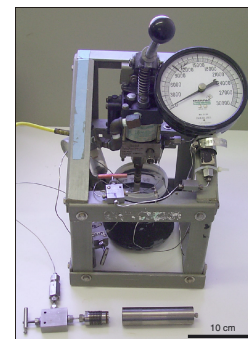
Sampling

Whole rounds cut from the cores were first sampled for microbiology and then for interstitial water analyses. The cores were cut and capped on the catwalk and immediately transported to the microbiology lab. Subsamples of the whole rounds were taken using cutoff sterile 1-mL syringes for the analyses listed below. Immediately after microbiological sampling, whole-round cores were taken to the chemistry lab where interstitial water was extracted. When the sediments were too hard to be sampled with a syringe, samples from the interior of the core were taken using sterile spatulas and spoons.

Microbial Abundance

Plugs (0.5 cm^3) taken from the interior of the whole rounds were fixed in formalin (2% final concentration) and stored at 5°C . Duplicate

F11. Photograph of equipment for high-pressure archiving, p. 66.



samples were stained with AO or DAPI, filtered onto polycarbonate filters, and examined with epifluorescence microscopy. Additionally, separate samples were preserved in formalin to be analyzed by shore-based participants.

Total Biomass

Adenosine triphosphate (ATP) was quantified in subsamples from the whole rounds to estimate total biomass. The assays were performed in a luminometer (Turner Designs 20/20) using the luciferin-luciferase analysis method. Sediment slurries were made by diluting 0.5 cm³ of sediment with 1.0 cm³ of autoclaved distilled water. A subsample (50 µL) of the slurry was placed in a 12 mm × 50 mm polypropylene vial. An ATP releasing agent (50 µL; Turner Designs) was added to the vial and mixed, after which 50 µL of HEPES buffer was added to the vial and mixed again. Luciferin-luciferase solution (100 µL) was then added to the vial and mixed, and light production was immediately quantified in the luminometer. Blanks were determined using 50 µL of the sterile, distilled water, and standards were analyzed using purified ATP (Turner Designs).

Enrichment Cultures

Subsamples of the plugs taken from the interior of the whole rounds were distributed into anaerobic growth media designed to select for sulfate reducers and methanogens or fermentative microbes. The samples were serially diluted in the growth medium to estimate total abundance using the most probable number method. The tubes were incubated at 10°C.

High-Pressure Archiving

Selected samples were returned to their ambient pressure using the high-pressure vessels described above. Sediment samples were placed in polycarbonate vials and sealed using Parafilm. The space inside the pressure vessels was filled with anaerobic 0.2-µm filtered seawater. Pressure vessels were stored at in situ temperature and transported at high pressure to Scripps Institution of Oceanography for further study.

DNA Extraction

Plugs (~1–4 cm³) taken from the interior of the core were placed in prebaked (450°C for 2 hr) glass vials, immediately frozen in liquid nitrogen, and then stored at –70°C. These frozen samples were transported to the University of Rhode Island for DNA extraction and characterization.

Igneous Rocks

Sampling

Whole-round cores were collected on the catwalk through the ends of unsplit core liners or in the core-splitting room immediately after the core liner was split. Cores were handled with latex gloves, placed in nitrogen-flushed plastic bags (Ziploc), and taken immediately to the

anaerobic chamber (Coy) in the microbiology laboratory. Samples were in anaerobic conditions within 40 min of the core arriving on deck.

In the anaerobic chamber, a hydraulic rock trimmer (Ward) was used to split off the outside of the cores. Inside core pieces were handled using sterile techniques. Interior pieces of core, kept moist with 1 mL of culture medium without growth substrates, were crushed in a sterile percussion mortar (Rock Labs). Additional interior pieces of core were used whole as described below.

Microbial Abundance

Crushed rock (1–2 cm³) was preserved in phosphate-buffered saline (PBS; NaH₂PO₄, 2 mM; Na₂HPO₄, 8 mM; NaCl, 130 mM; pH 7.2) containing 2% formalin. Cells were stained with AO or DAPI, filtered onto polycarbonate filters, and examined with epifluorescence microscopy. Unstained samples were examined for the presence of fluorescent microspheres, as described in “[Quantification of Microspheres](#)” in “[Methods for Quantifying Potential Microbial Contamination During Deep Ocean Coring](#)” (Smith et al., 2000).

Enrichment Cultures

The 12 types of anaerobic culture media described above were used to enrich viable microbial populations from the rock samples. Approximately 50 mg of crushed rock was added to each of four bottles of each type of culture media. Formalin (2% final concentration) was added to one of the four bottles of each medium type to inhibit all biological reactions in that bottle. These controls allow differentiation of abiotic and biotic reactions in the growth media. For Site 801, the sample in situ temperatures were calculated according to Larson et al. (1993). Samples were incubated at 25° or 30°C, whichever was nearest to the in situ temperature. For Site 1149, the temperature gradient was estimated using Adara temperature tool (Adara) measurements, and cultures were incubated within 5°C of in situ temperature. Uninoculated negative controls were incubated at each temperature to ensure sterility of growth media. Some culture media were inoculated with crushed rock and incubated at ~9000 psi and 25°C in the high-pressure vessels described above. Growth is confirmed by the accumulation of metabolic products and of microbial cells; these analyses will be performed at Göteborg University.

High-Pressure Archiving

Rock samples were crushed in the anaerobic chamber and sample splits and individual rock specimens were maintained under high pressure. The samples were placed in polycarbonate tubes and overlaid with filtered (0.2 µm) 3.1% NaCl. The same solution was used to fill the high-pressure vessels, which were pressurized to ~100–200 psi above the in situ conditions. Pressurization was typically achieved within ~1 hr of arrival of the cores at the rig floor. The decompression time from departure from ambient pressures at 6500 meters below sea level to atmospheric pressure at the rig floor is ~30–45 min. Pressurized samples were transported to Scripps Institution of Oceanography for shore-based studies.

DNA Extraction and In Situ Hybridization

Whole-rock pieces split from the interior of cores were preserved for shore-based DNA extraction and in situ hybridization. For DNA extraction, rocks were covered with Cell Resuspension Buffer (20 mM Tris, 20 mM EDTA, 0.35 M sucrose), immediately frozen in liquid nitrogen, and stored in a -70°C freezer. Samples for in situ hybridization were fixed in 4% paraformaldehyde for 5–18 hr at 4°C . The rocks were washed twice with PBS and covered with a 50:50 mixture of PBS and 98% ethanol. Tubes were frozen in liquid nitrogen and stored at -70°C . Samples were transported frozen to Göteborg University for shore-based analysis.

Scanning Electron Microscopy and Thin Sections

Samples were collected from areas of volcanic ash, glass, crystalline basalt, hydrothermally deposited minerals, fractures, and veins for examination by scanning electron microscopy (SEM) and in thin section for evidence of extant and fossil microbial activity. Some of the samples were subsamples of those collected for other microbial studies. Thin sections were prepared on board ship, and chips were preserved in alcohol. Additional crushed rock was preserved in 0.2- μm sterile filtered 3.1% NaCl containing 2% formalin for future shore-based SEM examination.

Contamination Tests

Two types of tracer tests were conducted to determine the level of contamination of samples recovered by drilling: perfluorocarbon tracer and 0.5- μm fluorescent microspheres. Methods for these tests are described in “[Materials and Methods](#)” in “Methods for Quantifying Potential Microbial Contamination During Deep Ocean Coring” (Smith et al., 2000).

PHYSICAL PROPERTIES

Introduction

Shipboard measurements of physical properties provide information that assists in characterizing lithologic units, correlating cored material with downhole logging data, understanding the nature of consolidation, and interpreting seismic reflection profiles.

First, nondestructive measurements of bulk density, magnetic susceptibility, transverse compressional wave velocity, and NGR were made using the MST on whole-round sections after the core equilibrated to room temperature ($\sim 25^{\circ}\text{C}$). Next, thermal conductivity in soft sediment was measured on whole-core sections or on split-core pieces (working half) if the core material was too hard to be penetrated by the needle without excessive force. After the sections were split, compressional wave velocity was measured on all lithologies, whereas undrained shear strength was measured only on soft-sediment cores. Finally, discrete samples were selected for the measurement of index properties including wet bulk density, dry bulk density, grain density, water content, porosity, and void ratio as well as compressional wave velocity.

MST Measurements

The MST included four physical properties sensors: a magnetic susceptibility meter (MSM), gamma-ray attenuation porosity evaluator (GRAPE), *P*-wave logger (PWL), and NGR detector. MST data were sampled at discrete intervals, with the sampling interval and count time chosen to optimize the resolution of the data and the time necessary to run each core section through the device. The MSM, GRAPE, and NGR were measured on all cores regardless of collection method, (i.e., APC, XCB, or RCB). The PWL was used only on APC-cored intervals because of the likelihood of discontinuous core, core disturbance, and/or a loss of coupling between the liner and the core with XCB and RCB drilling. MST measurements were also conducted on previously sampled half cores of igneous basement drilled during Leg 129 during the transit from Hong Kong to Site 801 (see “Background and Objectives,” p. 1, in the “Site 801” chapter).

Magnetic Susceptibility

Magnetic susceptibility is the degree to which material can be magnetized in an external magnetic field. The MSM aids in the detection of fine variations in magnetic intensity associated with magnetic reversals or lithologic changes (alteration or grain size). The quality of the results is degraded in RCB sections if the core liner is not completely filled and/or the core is disturbed. However, general downhole trends may still be used for laboratory to well log correlation. Magnetic susceptibility was determined on all sections at an interval of 4 cm with 4-s acquisition times using the 1.0-s integration time range on the Bartington meter (model MS2C), which has an 8-cm diameter loop.

Gamma Ray Attenuation Porosity Evaluator

GRAPE was used for the estimation of sediment bulk density. This measurement is based on the principle that the density of material is related to attenuation, mainly by Compton scattering, of a collimated beam of gamma rays (produced by a ¹³⁷Ce source) passing through a known volume of sediment (Boyce, 1976). GRAPE data were acquired every 4 cm for a 4-s period. GRAPE data are most reliable in undisturbed cores (i.e., APC) and offer the potential of direct correlation with downhole bulk density logs. For discontinuous and/or fragmented core (i.e., RCB) for which the core liner was not completely filled, GRAPE data are unreliable.

P-Wave Velocity

The measurement of *P*-wave velocity provides information that assists in the interpretation of seismic reflection profiles and the correlation of lithology with downhole logging data. The PWL on the MST transmits a 500-kHz compressional wave pulse through the core, where the transmitting and receiving transducers are aligned perpendicular to the long axis of the core. A pair of displacement transducers monitors the separation between the compressional wave transducers. *P*-wave velocity measurements were taken on APC cores every 4 cm for a 4-s period.

Natural Gamma Radiation Detector

NGR emission was recorded for all core sections to measure variations in radioactive counts of sample rocks (alteration and pelagic clay) and to provide a correlation with the downhole measurements of NGR emissions. The NGR system records radioactive decay of ^{40}K , ^{232}Th , and ^{238}U , three long-period isotopes that decay at an essentially constant rate within measurable time scales. The installation and operating principles of the NGR system used during Leg 185 are discussed by Hoppie et al. (1994).

NGR emission was measured every 10 cm for a 20-s period. The area of influence for the four NGR sensors was about ± 10 cm from the points of measurements along the core axis. As gamma-ray emission is a random event, count times have to be sufficiently long to average short-period variation. This was achieved on the MST system by utilizing the long area of influence on the sensors and using a moving average window to smooth count rate variations and to achieve a statistically valid sample.

The NGR instrument was calibrated with a thorium source during transit to the first drill site. Background counts measured using a core liner filled with distilled water averaged 11.75 cps over a 30-min measurement period. No corrections were made to account for sediment incompletely filling the core liner in XCB cores. Results were output in counts per second, which can be qualitatively compared to the API units obtained from borehole logging.

P-Wave Velocity (W-Logger)

P-wave velocity is measured using the contact probe systems (PWS1, PWS2, and PWS3) (Hamilton Frame). The choice of method and sampling frequency of discrete compressional wave velocity (V_p) measurements depends on the hardness of the sediment and rock.

PWS1 and PWS2 Insertion Probe Systems for Soft Sediment

Compressional wave velocity was measured using two pairs of the digital sound velocimeters for soft sediments. One pair was aligned along the core axis (PWS1; z direction), and the other one across the core (PWS2; y direction). The transducer pairs had a fixed spacing of 7 cm (z direction) and 3.5 cm (y direction) and were inserted into the split cores of soft sediment. An acoustic signal of 500 kHz was emitted and received by the two transducers. This signal was then digitized by an oscilloscope so that the first arrival waveform could be picked manually and velocity calculated.

Additionally, the PWS3 contact probe system (Hamilton Frame velocimeter) was conducted through the split core (x direction) using vertically oriented transducer pairs (500 kHz), with the upper transducer pressed against the split surface and the lower transducer pressed against the core liner. These velocities were measured at an interval of one or two per split-core section (working half).

PWS3 Contact Probe System for Lithified Sediment and Hard Rock

Compressional velocity on sedimentary and igneous rocks was measured using the PWS3 contact probe system. The PWS3 data were mea-

sured through the split core (x direction) as described in the previous paragraph. Selected igneous rocks and sedimentary rocks were sawed into oriented cubes (minicores) and velocities were measured in three mutually perpendicular directions (x, y, and z). The magnitude of velocity anisotropy was estimated according to the relationship

$$\text{Anisotropy} = 3(V_{\max} - V_{\min}) / (V_x + V_y + V_z), \quad (3)$$

where, V_z (direction along the core), V_x (direction into the split core, perpendicular to core axis), V_y (direction across the split core), and V_{\max} and V_{\min} are the maximum and minimum velocities (among V_x , V_y , and V_z).

Both split-core and discrete-sample thickness were measured by a digital caliper that was directly mounted on the transducer pair. Zero traveltimes for the velocity transducers were measured with a series of polycarbonate standards of known length. The pressure cell that monitors the axial pressure applied between sample and transducer was not operational. Pressure was applied until a measurable waveform appeared on the oscilloscope. To improve the coupling between the transducer and sample, distilled water was applied to the top and bottom of the sample and transducer heads. Measurements were corrected for the additional traveltime passing through the core liner.

Undrained Shear Strength

The peak undrained and residual shear strength of soft sediment was measured at an interval of one per split-core section (working half), using a Wykeham-Farrance motorized vane shear apparatus following the procedures of Boyce (1977). The vane rotation rate was set to 90°/min, and the vane used for all measurements had a 1:1 blade ratio with a dimension of 1.28 cm. This instrument measures the torque and strain at the vane shaft using a torque transducer and potentiometer, respectively. Output for torque and strain were recorded in volts on a Hewlett-Packard X-Y recorder. The shear strength reported was the peak strength determined from the torque vs. strain plot.

In the interpretation of shear vane measurements, it is assumed that a cylinder of sediment is uniformly sheared around the axis of the vane in an undrained condition, with cohesion as the principal contributor to shear strength. Departures from this assumption include progressive cracking within and outside of the failing specimen, uplift of the failing core cylinder, drainage of local pore pressures, and stick-slip behavior.

Index Properties

Samples of ~2–4 cm³ (5–15 g) were taken from each section adjacent to cut cubes and minicores and were used for velocity determination. Additional samples were taken to characterize the core where sawing cubes was not possible. All basalt and interpillow material samples were soaked in seawater for 24 hr before determination of index properties, whereas index properties of chert, chalk, marl, and pelagic clay were made directly after sampling. Bulk density, grain density, water content, porosity, and dry density were calculated from wet and dry sample weights and dry volumes. Sample mass was determined to a precision of ±0.001 g using two Scitech electronic balances. The balances were equipped with a computer averaging system that corrected for ship ac-

celerations. The sample mass on one balance was counterbalanced by a known mass on an adjacent balance such that the mass differentials generally were <2 g. Sample volumes were determined using a Quantachrome Penta-Pycnometer, a helium-displacement pycnometer with a nominal precision of $\pm 0.01 \text{ cm}^3$. Sample volumes were determined at least three times and then averaged. Three of the five measurement cells were operational during Leg 185 (cells 1, 2, and 4). A standard reference volume sphere was run in each of three operating cells after nine consecutive measurements. The cell volume was recalibrated if the measured volume was not within 0.02 cm^3 of the calibration sphere volume. The sample beakers used for discrete determinations of index properties of sediment were calibrated carefully before the cruise. Dry weight and volume measurements were performed after the samples were oven dried at $105^\circ \pm 5^\circ\text{C}$ for 24 hr and allowed to cool in a desiccator. The main problem with this drying temperature is that chemically bound water in some clay minerals can be lost in addition to interstitial water.

Water Content

The determination of water content as a fraction of total mass or as a ratio of water mass to solid mass followed the methods of the American Society for Testing and Materials (ASTM) designation (D) 2216 (ASTM, 1989). Total mass (M_t) and dry mass (M_d) were measured using the electronic balance and the difference was taken as the uncorrected water mass. Measurements were corrected for salt assuming a pore-water salinity (r) of 0.35%, following the discussion by Boyce (1976). The equations for the two water content (W) calculations are

$$W_d (\% \text{ dry mass}) = [(M_t - M_d) / (M_d - rM_t)] \times 100, \text{ and} \quad (4)$$

$$W_w (\% \text{ wet mass}) = \{(M_t - M_d) / [(1 - r) M_t]\} \times 100, \quad (5)$$

where M_t and M_d are measured in grams.

Bulk Density

Bulk density (ρ_{bulk}) is the density of the total sample including the pore fluid (i.e., $\rho_{\text{bulk}} = M_t / V_b$, where V_b is the bulk volume (in cubic centimeters)).

Grain Density

Grain density (ρ_g) was determined from the dry mass and dry volume measurements. Both mass and volume must be corrected for salt, based on the following equation:

$$\rho_g = (M_d - M_s) / [V_d - (M_s / \rho_s)], \quad (6)$$

where M_d is the dry mass (in grams) and ρ_s is the density of salt (2.257 g/cm^3), V_d is dry volume, $M_s = rM_w$ (in grams) is the mass of salt in the pore fluid, M_w (in grams) is the salt-corrected mass of the seawater:

$$M_w = (M_t - M_d) / (1 - r). \quad (7)$$

Porosity

Porosity (Φ), represents the ratio of pore-water volume to total volume. The following relationship using calculated grain density and bulk density was employed:

$$\Phi = [(\rho_g - \rho_{\text{bulk}}) / (\rho_g - \rho_w)] \times 100, \quad (8)$$

where ρ_g represents the grain density, ρ_{bulk} is the bulk density, and ρ_w is the density of seawater.

Dry Density

The dry density (ρ_d) is the ratio of the dry mass (M_d) to the total volume (V). The dry density was calculated using the corrected water content (W_d) and porosity (Φ) as follows:

$$\rho_d = (\Phi / W_d) \times \rho_w \quad (9)$$

A complete description of density and porosity calculations is given by Blum (1997).

Thermal Conductivity

Thermal conductivity is measured by transient heating of a material with a known heating power generated from a source of known geometry and then measuring the temperature change with time, using the TK04 system described by Blum (1997). Thermal conductivity profiles of sediments and rock sections are mainly used, along with temperature measurements, to determine heat flow. Heat flow is not only characteristic of the material, but an indicator of type and age of oceanic crust and fluid circulation processes at shallow and great depth (Blum, 1997). Whole-round core sections were allowed to adjust to room temperature for at least 2 hr in preparation for thermal conductivity measurements. In the case of soft sediment, thermal conductivity was measured on whole-core sections. However, if the core material was too hard to be penetrated by the needle without excessive force, thermal conductivity was measured on split-core pieces (working half). The needle-probe method was used in full-space configuration for soft sediments (von Herzen and Maxwell, 1959), and in half-space mode (Vacquier, 1985) for lithified sediment and hard-rock samples. Measurements were made at an interval of one per core (whole-round core or split core).

Full-Space Determinations for Soft Sediment

A needle probe, containing a heater wire and a calibrated thermistor, was inserted into the sediment through a small hole drilled in the core liner before the sections were split. At the beginning of each measurement, temperatures in the samples were monitored without applying current to the heating element to verify that temperature drift was $<0.04^\circ\text{C}/\text{min}$. The heater was then turned on and the temperature rise in the probes recorded. After heating for ~ 60 s, the needle probe behaves nearly as a line source with constant heat generation per unit length. Temperatures recorded between 60 and 240 s were fitted to the

following equation using a least-squares method (von Herzen and Maxwell, 1959):

$$T(t) = (q/4\pi k) \times \ln(t) + L(t), \quad (10)$$

where k is the apparent thermal conductivity (W/[m·K]), T is temperature (°C), t is time (s), and q is the heat input per unit length of wire (W/m). The term $L(t)$ corrects for temperature drift, described by the following equation:

$$L(t) = At + T_e, \quad (11)$$

where A represents the rate of temperature change, and T_e is the equilibrium temperature. $L(t)$ therefore corrects for the background temperature drift, systematic instrumental errors, probe response, and sample geometry. The best fit to the data determines the unknown terms k and A .

Half-Space Determinations for Lithified Sediment and Hard Rock

Half-space determinations were made on selected lithified sediments and basaltic rock samples after the cores were split and their faces polished. The needle probe encased in a grooved epoxy block with relatively low conductivity (Sass et al., 1984; Vacquier, 1985) was placed onto the polished surface. Half-space measurements were conducted in a water bath to keep the samples saturated, to improve the thermal contact between the needle and the sample, and to reduce thermal drift. Data collection and reduction procedures for half-space tests were similar to those for full-space tests except for a multiplicative constant in Equation 4, which accounted for the different experimental geometry.

DOWNHOLE MEASUREMENTS

Introduction

Downhole logs are spatially continuous records of physical, chemical, and structural properties of the formation penetrated by a borehole. The logs are made using a variety of probes combined into several tool strings. These strings are lowered down the hole on a heave-compensated electrical wireline and then pulled up at constant speed to provide continuous measurements as a function of depth of several properties simultaneously. Logs can be used to interpret the stratigraphy, lithology, mineralogy, and geochemical composition of the penetrated formation. Where core recovery is incomplete or disturbed, log data may provide the only way to characterize the borehole section. Where core recovery is good, log and core data complement one another and may be interpreted jointly. Finally, downhole logs are sensitive to formation properties on a scale that is intermediate between those obtained from laboratory measurements on core samples and geophysical surveys. They are useful to calibrate the interpretation of geophysical survey data (e.g., through the use of synthetic seismograms) and provide a necessary link for the integrated understanding of physical properties on all scales.

Three logging tool strings were used during Leg 185: the triple combination tool (triple combo), the Formation MicroScanner (FMS)/sonic, and the geochemical logging tool. In addition to wireline logs, in situ temperature measurements were made with the Adara tool, which is located in the coring shoe of the APC during piston-coring operations.

Logging Tools

The tool strings used on Leg 185 were

1. The triple combo (resistivity, density, and porosity) tool string (Fig. F12), which consists of the accelerator porosity sonde (APS), the high-temperature lithodensity tool (HLDT), and either the dual laterolog (DLL) or the phasor dual induction-spherically focused resistivity tool (DIT-E), depending on formation resistivity. The hostile environment natural gamma sonde (HNGS) was included at the top of the string, and the LDEO temperature/acceleration/pressure tool (TAP) at the bottom.
2. The FMS/sonic tool string (Fig. F12), which consists of the FMS, the general purpose inclinometer tool (GPIT), and a sonic sonde. Because of malfunctions, the dipole shear sonic imager (DSI), which is normally used, was replaced by the long spacing sonic sonde (LSS). The natural gamma-ray tool (NGT) was included at the top of this tool string.
3. The geochemical logging tool (GLT) string (Fig. F13), which consists of the NGT, the compensated neutron log (CNT-G), the aluminum activation clay tool (AACT), and the induced gamma spectrometry tool (GST). The GLT is a specialty string that provides measurements of some of the major elemental constituents of sedimentary and igneous rocks (Fig. F13). It was used to address the specific objectives of Leg 185: to constrain the geochemical fluxes being subducted as sediment and oceanic crust at the Izu-Mariana Trench.

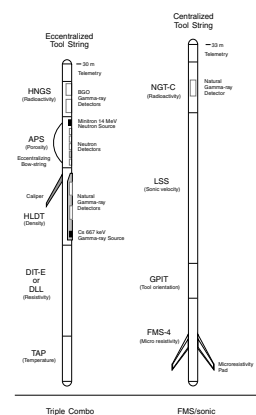
Each tool string includes a telemetry cartridge for communicating through the wireline with the logging laboratory on the drillship, and a natural gamma-ray sonde that is used to identify lithologic markers that provide a common reference for correlation and depth shifting between multiple logging runs. Logging runs are typically conducted at 250–275 m/hr, except for the GLT, which is run at ~150 m/hr.

The logging tools are briefly described below, and their operating principles, applications, and approximate vertical resolution are summarized in Table T6. Some of the principal data channels of the tools, their physical significance, and units of measure are listed in Table T7. More detailed information on individual tools and their geological applications may be found in Ellis (1987), Goldberg (1997), Lovell et al. (1998), Rider (1996), Schlumberger (1989a, 1989b, 1994), Serra (1984, 1986, 1989), and the LDEO-Borehole Research Group (BGR) Wireline Logging Services Guide (1994).

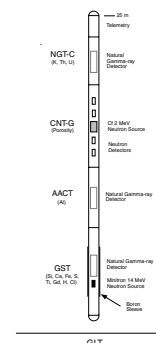
Natural Radioactivity

Two spectral gamma-ray tools were used to measure and classify natural radioactivity in the formation: the HNGS and the NGT. The NGT uses a sodium iodide scintillation detector and five-window spectroscopy to determine concentrations of K (in weight percent), Th (in parts

F12. Triple combo and Formation MicroScanner/sonic tool strings, p. 67.



F13. Geochemical logging tool string, p. 68.



T6. Logging tools and their applications, p. 75.

T7. Principal channels of the logging tools, p. 76.

per million), and U (in parts per million), the three elements whose isotopes dominate the natural radiation spectrum. The HNGS is similar to the NGT, but it uses two bismuth germanate scintillation detectors for a significantly improved tool precision. Spectral analysis in the HNGS filters out gamma-ray energies below 500 keV, eliminating sensitivity to bentonite or KCl in the drilling mud and improving measurement accuracy.

Although the NGT response is sensitive to borehole diameter and the weight and concentration of bentonite or KCl present in the drilling mud, these effects are routinely corrected for during processing at LDEO.

Density

Formation density was determined from the density of electrons in the formation, which was measured with the hostile environment lithodensity sonde (HLDS). The sonde contains a radioactive cesium (^{137}Cs) gamma-ray source (622 keV) and far and near gamma-ray detectors mounted on a shielded skid, which is pressed against the borehole wall by a hydraulically activated eccentricizing arm. Gamma rays emitted by the source experience Compton scattering, which involves the transfer of energy from gamma rays to the electrons in the formation via elastic collision. The number of scattered gamma rays that reach the detectors is directly related to the number of electrons in the formation, which is in turn related to bulk density. Porosity may also be derived from the bulk density, if the matrix density is known.

The HLDS also measures the photoelectric effect factor (PEF) caused by absorption of low-energy gamma rays. Photoelectric absorption occurs when gamma rays reach <150 keV after being repeatedly scattered by electrons in the formation. Because PEF depends on the atomic number of the elements in the formation, it varies according to the chemical composition and is essentially independent of porosity. For example, the PEF of pure calcite = 5.08 barn/e⁻; illite = 3.03 barn/e⁻; quartz = 1.81 barn/e⁻; and kaolinite = 1.49 barn/e⁻. PEF values can be used in combination with NGT curves to identify different types of clay minerals. Coupling between the tool and borehole wall is essential for good HLDS logs. Poor contact results in underestimation of density values.

The depth of investigation of the lithodensity tool is on the order of tens of centimeters, depending on the density of the rock.

Porosity

Formation porosity was measured with the APS. The sonde incorporates a minitron neutron generator that produces fast (14.4 MeV) neutrons, and five neutron detectors (four epithermal and one thermal), positioned at different spacings. The tool is pressed against the borehole wall by an eccentricizing bow spring. Emitted neutrons are slowed down by collisions. The amount of energy lost per collision depends on the relative mass of the nucleus with which the neutron collides. The greater energy loss occurs when the neutron strikes a nucleus nearly equal to its own mass, such as hydrogen, which is present mainly in the pore water. The neutron detectors record both the numbers of neutrons arriving at various distances from the source and neutron arrival times that act as a measure of formation porosity. However, as hydrogen

bound in minerals, such as clays or in hydrocarbons, also contributes to the measurement, the raw porosity value is often an overestimate.

Electrical Resistivity

Two tools were used to measure the formation electrical resistivity: the DIT-E and the DLL. The DIT-E provides three measurements of electrical resistivity, each with a different depth of investigation into the formation. Deep- and medium-penetration measurements are made inductively using transmitter coils that are energized with high-frequency alternating currents, creating time-varying magnetic fields that induce secondary Foucault currents in the formation. The strength of these induced ground currents is inversely proportional to the resistivity of the formation through which they circulate, as are the secondary inductive fields that they create. The amplitude and phase of the secondary magnetic fields, measured with receiving coils, are used as a proxy for the formation resistivity. Shallow-penetration measurements with a high vertical resolution are made with a spherically focused laterolog. This measures the current necessary to maintain a constant voltage drop across a small fixed interval. Because of the inductive nature of the deep- and medium-penetration measurements, DIT-E logs are accurate only for formations with resistivities less than $\sim 100 \Omega\text{m}$, such as sediments. In more resistive formations measurement error becomes significant ($>20\%$), and it is more suitable to use the DLL (Schlumberger, 1989b).

The DLL provides two measurements of formation electrical resistivity, labeled “deep” (LLd) and “shallow” (LLs) on the basis of their respective depths of investigation. In both devices, a current beam 61 cm thick is forced horizontally into the formation by using focusing (also called bucking) currents. For the deep measurement both focusing and measurement currents return to a remote electrode on the surface; thus, the depth of investigation is considerable, and the effect of borehole conductivity and of adjacent formations is reduced. In the shallow laterolog, the return electrodes that measure the bucking currents are located on the sonde, and, therefore, the current sheet retains focus over a shorter distance than the deep laterolog. Fracture porosity can be estimated from the separation between the deep and shallow measurements based on the observation that the deep measurement is sensitive to the presence of horizontal conductive fractures only, whereas the shallow measurement responds to both horizontal and vertical conductive structures. The DLL has a response range of $0.2\text{--}40,000 \Omega\text{m}$.

The depth of investigation of both the DIT-E and the DLL depends on the resistivity of the rock and on the resistivity contrast between the zone invaded by drilling fluid and the uninvaded zone. In formations with resistivity higher than $100 \Omega\text{m}$ the average radial depth of investigation of the DIT-E is ~ 1.5 m for the deep induction (IDPH), 76 cm for the medium induction (IMPH), and 38 cm for the spherically focused log. These values drop by $\sim 20\%$ for a $0.1 \Omega\text{m}$ formation resistivity. The depth of investigation of the DLL will vary with the separation between the sonde and the remote current return at the surface.

In most rocks, electrical conduction occurs primarily by ion transport through pore fluids and is strongly dependent on porosity. Electrical resistivity data can therefore be used to estimate formation porosity using Archie's Law (Archie, 1942) if the formation does not contain clay. Archie's Law is expressed as $FF = a\Phi^{-m}$, where FF is the formation factor (i.e., the ratio of the formation resistivity to that of the pore flu-

ids), Φ is the porosity, m is known as the cementation factor and is dependent on the tortuosity and connectivity of pore spaces, and a is a constant that varies based upon rock type. For a first order interpretation, a is conventionally taken as 1 and m as 2, but more rigorous values can be determined from resistivity and porosity measurements on core samples (see “Physical Properties,” p. 36). For example, laboratory measurements from core samples from DSDP Hole 504B led to values of $a = 10.0$ and $m = 1.0$ in the massive units of layers 2A and 2B, indicating that current conduction was occurring in cracks and microcracks present at mineral scale throughout the rock (Pezard, 1990). In the presence of chlorites, zeolites, and particularly smectites as alteration products of mid-ocean-ridge basalt, surface conduction through the Stern-Gouy layer may also play a significant role. Archie’s Law will overestimate the porosity in this case, and a more sophisticated conductivity model should be used (Pezard, 1990).

The DIT-E also measures spontaneous potential (SP) fields. SPs can originate from a variety of causes—electrochemical, electrothermal, electrokinetic streaming potentials, and membrane potentials—related to differences in the mobility of ions in the pore and drilling fluids. The interpretation of SP logs remains problematic because of this multiplicity of sources.

Temperature, Acceleration, and Pressure

Downhole temperature, acceleration, and pressure were measured with the LDEO high-resolution TAP tool. When attached to the bottom of the triple-combo string, the TAP is run in an autonomous mode, with data stored in built-in memory. Two thermistors are mounted near the bottom of the tool to detect borehole fluid temperatures at different rates. A thin fast-response thermistor is able to detect small, abrupt changes in temperature. A thicker slow-response thermistor is used to estimate temperature gradients and thermal regimes more accurately. The pressure transducer is included to activate the tool at a specified depth. A three-axis accelerometer measures tool movement downhole, providing data for analyzing the effects of heave on a deployed tool string that should eventually lead to the fine tuning of the wireline heave compensator (WHC).

The borehole temperature record provides information on the thermal regime of the surrounding formation. The vertical heat flow can be estimated from the vertical temperature gradient combined with measurements of the thermal conductivity from core samples. Packer tests in Hole 801C during Leg 144 indicated a region of high permeability beneath the hydrothermal mineralization. Temperature logs in such environments can help differentiate between convective and conductive heat transfer regimes.

The temperature record must be interpreted with caution, because the amount of time elapsed between the end of drilling and the logging operation is generally not sufficient to allow the borehole to recover thermally from the influence of drilling-fluid circulations. The data recorded under such circumstances may differ significantly from the thermal equilibrium of that environment. Nevertheless, from the spatial temperature gradient it is possible to identify abrupt temperature changes that may represent localized fluid flow into the borehole indicative of fluid pathways and fracturing, and/or breaks in the temperature gradient that may correspond to contrasts in permeability at lithologic boundaries.

Acoustic Velocity

The DSI, which is conventionally used on the FMS/sonic string, was not functional during Leg 185. The LSS was therefore used to measure elastic compressional wave velocity in the formation. The LSS provides long-spacing measurements through the “depth-derived” borehole compensation principle. Acoustic traveltime readings between two sources and two receivers are memorized at one depth and combined with a second set of readings made after the sonde has been pulled the appropriate distance along the borehole. The LSS records the full waveform for each source-receiver pair, in addition to its automatic determination of arrival time.

The depth of investigation for sonic tools depends on the spacing of the detectors and on the petrophysical characteristics of the rock, such as rock type, porosity, and alteration, but is of the order of tens of centimeters.

Formation MicroScanner

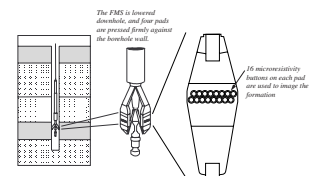
The FMS provides high-resolution electrical resistivity-based images of borehole walls. The tool has four orthogonal arms (pads) each containing 16 microelectrodes, or “buttons,” that are pressed against the borehole wall during the recording (Fig. F14). The electrodes are arranged in two diagonally offset rows of eight electrodes each and are spaced ~2.5 mm apart. A focused current is emitted from the four pads into the formation, with a return electrode near the top of the tool. Array buttons on each of the pads measure the current intensity variations. Processing transforms these measurements, which reflect the microresistivity variations of the formation, into continuous, spatially oriented, high-resolution images that mimic geologic structures behind the borehole walls. Further processing can provide measurements of dip and direction (azimuth) of planar features in the formation. FMS images are particularly useful for mapping structural features, dip determination, detailed core-log correlation, positioning of core sections with poor recovery, and analysis of depositional environments.

The FMS image is sensitive to structure within ~25 cm of the borehole wall and has a vertical resolution of 5 mm with a coverage of 22% of the borehole wall on a given pass. FMS logging commonly includes two passes, the images of which are merged to improve borehole wall coverage. To produce reliable FMS images, however, the pads must be firmly pressed against the borehole wall. The maximum extension of the caliper arms is 15.0 in. In holes with a diameter >15 in, the pad contact will be inconsistent and the FMS images can be blurred. The maximum borehole deviation where good data can be recorded with this tool is 10°. Irregular borehole walls will also adversely affect the images because contact with the wall is poor.

Magnetic Field Measurement

Downhole magnetic field measurements were made with the GPIT. The primary purpose of this sonde, which incorporates a three-component accelerometer and a three-component magnetometer, is to determine the acceleration and orientation of the FMS/sonic tool string during logging. The acceleration data allows more precise determination of log depths than is possible on the basis of cable length alone because the wireline is subject to both stretching and ship heave.

F14. Schematic diagram of FMS, p. 69.



Acceleration data is also used in processing of FMS data to correct the images for irregular tool motion.

Local magnetic anomalies, generated by high remanent magnetization of the basalts in the basement section of a borehole, can interfere with the determination of tool orientation. However, these magnetic anomalies can be useful to infer the magnetic stratigraphy of the basement section.

Aluminum Abundance

The AACT measures the wet weight percent of aluminum in the formation. It is generally similar to the NGT, but its spectrometer includes two more windows for a more detailed analysis of the spectrum. Aluminum abundance is determined by neutron-induced gamma-ray spectroscopy using a ^{252}Cf low-energy source (2 MeV) on the CNT-G mounted immediately above the AACT on the geochemical tool string. Aluminum activation occurs when thermal neutrons are captured by ^{27}Al and produces ^{28}Al . The latter decays with a half-life of 2.3 min, emitting 1.78-MeV gamma rays. The contribution to the gamma-ray spectrum from natural radiation is corrected using the counts from the NGT placed above the neutron source: when logging upward, the upper detector measures the natural radiation before activation, and the lower detector measures the induced radiation after activation. The naturally occurring component is then subtracted from the total measured after activation.

Chemical Composition

The chemical composition of the formation was measured with the GST. This is an induced gamma-ray device that measures some of the major element constituents of sedimentary and igneous rocks. The GST contains a pulsed source (minitron) of 14-MeV neutrons and a sodium iodide scintillation detector. Through scattering interactions with the atoms in the rock surrounding the borehole, the neutrons are progressively slowed until they reach thermal energy levels at which they can be captured by nuclei in the formation. When this occurs, the capturing nucleus emits a gamma ray of characteristic energy. Comparison of the spectra recorded downhole with a library of standard spectra on the ship provides an estimate of the elemental composition of the formation. The spectra are dominated by characteristic sets of gamma rays from six elements: Ca, Si, Fe, Cl, H, and S. As their sum is always unity, the results do not reflect the actual elemental composition. Instead, ratios (or yields) of these elements are used in interpreting the lithology and porosity of the formation and the salinity of the formation fluid. Shore-based processing is necessary to compute the absolute dry-weight fractions of the major oxides.

A boron sleeve surrounds the GST and increases the signal-to-noise ratio by shielding the path of fast neutrons from the borehole fluid, thus reducing the reading of iron from the tool housing. The measurement accuracy is dependent on logging speed, hole size, and porosity. The GST can be run inside the logging pipe, but corrections for the effect of the pipe are not always reliable. This through-pipe data, however, can be used from a qualitative point of view and offers useful information about the formation geochemistry in holes that otherwise could not be logged because of well-bore instability.

Log Data Quality

The quality of log data may be seriously degraded by excessively wide sections of the borehole or by rapid changes in the hole diameter. Resistivity and velocity measurements are the least sensitive to borehole effects, whereas the nuclear measurements (density, neutron porosity, and both natural and induced spectral gamma rays) are most sensitive because of the large attenuation by borehole fluid. Corrections can be applied to the original data to reduce the effects of these conditions and, generally, any departure from the conditions under which the tool was calibrated.

Logs from different tool strings may have depth mismatches, caused by either cable stretch or ship heave during recording. Small errors in depth matching can distort the logging results in zones of rapidly changing lithology. To minimize the effects of ship heave, a hydraulic WHC adjusts for rig motion during logging operations. Distinctive features recorded by the NGT, run on every log tool string, provide correlation and relative depth offsets among the logging runs and can be calibrated to distinctive lithologic contacts observed in the core recovery or drilling penetration (e.g., basement contacts). In Hole 801C, which is cased into basement, the point of entry into the bottom of the casing is also obvious on many of the tools and is a useful correlation point. Precise core-log depth matching is difficult in zones where core recovery is low because of the inherent ambiguity of placing the recovered section within the cored interval.

Reprocessing of Geochemical Logs

Raw count rates for six elements (Ca, Si, Fe, S, Cl, and H) are obtained in real time by the Schlumberger data acquisition software. In addition to these six elements, postcruise reprocessing inverts the gamma-ray spectrum at each depth for titanium, gadolinium, and potassium. Though gadolinium is present in concentrations of only a few parts per million, its neutron capture cross section is so large that it can account for 10%–30% of the total gamma spectrum. Inclusion of these additional elements improves the quality of the overall inversion, particularly improving the accuracy of calculated calcium abundance by converting sources of unaccounted variance to signals. However, the determined potassium concentrations are less accurate than those from the NGT, and the hydrogen concentrations are less accurate than those from the neutron tool.

When both the geophysical (triple combo) and geochemical (GLT) Schlumberger tool strings are run, additional reprocessing of geochemical logs is possible. The relative abundances of Ca, Si, Fe, Ti, Al, K, S, Th, U, and Gd are used to calculate a log of predicted photoelectric effect. The difference between this log and the actual log of photoelectric effect can be attributed to the only two major elements not directly measured, Mg and Na. Major elements are converted from volume percent to weight percent using logs of total porosity (bound water + pore water) and density. Major elements are expressed in terms of oxide dry weight percent, based on the assumption that oxygen is 50% of the total dry weight.

If the GLT data are available but not enough log types are run to permit complete solution for oxide weight percentage, one further processing step is made. Omitting chlorine and hydrogen, the yields of the other geochemical tool elements (Ca, Si, Fe, Ti, S, K, and Gd) are

summed, and each is expressed as a fraction of this total yield. This procedure corrects for porosity and count-rate variations. Although the absolute abundance of each element is not determined, downhole variations in relative abundance are indicated.

Core-Log Integration

The precision and reliability of the various logging measurements are governed by the resolutions of the various tools and the condition of the drill hole. Vertical resolutions of the various logging tools is generally ~46 cm, with several exceptions (Table T6).

Core-log integration during Leg 185 involved comparing lithologies in cores with the responses of the various logs within the corresponding drilled intervals. After calibrating the logs with the core recovery on a small scale, the logs were then used to interpret details of the sequences that were not recovered during coring.

The primary logging tools used in the core-to-log integration were the FMS high-resolution microresistivity image of the hole, the NGR spectrum, and the geochemical logs.

In Situ Temperature Measurements

Temperature measurements were taken at Site 1149 during Leg 185 to determine the amount of heat carried by the subducting sediments into the Izu-Bonin Trench. The discrete in situ measurements were made with the Adara tool, which is located in the coring shoe of the APC during piston-coring operations. The components include a platinum temperature sensor and a data logger. The platinum resistance temperature device is calibrated for temperatures ranging from -20° to 100°C , with a resolution of 0.01°C . In operation, the adapted coring shoe is mounted on a regular APC core barrel and lowered down the pipe by wireline. The tool is typically held for 5–10 min at the mudline to equilibrate with bottom-water temperatures and then lowered to the bottom of the drill string. Standard APC coring techniques are used, with the core barrel being fired out through the drill bit using hydraulic pressure. The Adara tool (and the APC corer) remains in the sediment for 10–15 min to obtain a temperature record. This provides a sufficiently long transient record for reliable extrapolation back to the steady-state temperature. The nominal accuracy of the temperature measurement is $\sim 0.1^{\circ}\text{C}$.

REFERENCES

- Archie, G.E., 1942. The electrical resistivity log as an aid in determining some reservoir characteristics. *J. Pet. Technol.*, 5:1–8.
- ASTM, 1989. *Annual Book of ASTM Standards for Soil and Rock: Building Stones* (Vol. 4.08): Geotextiles: Philadelphia (Am. Soc. Testing and Mater.).
- Baccelle, L., Bosellini, A., 1965. Diagrammi per la stima visiva della composizione percentuale nelle rocce sedimentarie. *Ann. Univ. Ferrara, N. Ser., Sez. IX, Sci. Geol. Paleontol.*, 1:59–62.
- Balsam, W.L., and Damuth, J.E., 2000. Further investigations of shipboard vs. shore-based spectral data: implications for interpreting Leg 164 sediment composition. In Paull, C.K., Matsumoto, R., Wallace, P., and Dillon, W.P. (Eds.), *Proc. ODP, Sci. Results*, 164: College Station, TX (Ocean Drilling Program), 313–324.
- Balsam, W.L., Damuth, J.E., and Schneider, R.R., 1997. Comparison of shipboard vs. shore-based spectral data from Amazon Fan cores: implications for interpreting sediment composition. In Flood, R.D., Piper, D.J.W., Klaus, A., and Peterson, L.C. (Eds.), *Proc. ODP, Sci. Results*, 155: College Station, TX (Ocean Drilling Program), 193–215.
- Balsam, W.L., Deaton, B.C., and Damuth, J.E., 1998. The effects of water content on diffuse reflectance measurements of deep-sea core samples: an example from ODP Leg 164 sediments. *Mar. Geol.*, 149:177–189.
- Baltuck, M., 1983. Some sedimentary and diagenetic signatures in the formation of bedded radiolarite. In Iijima, A., Hein, J.R., and Siever, R. (Eds.), *Siliceous Deposits in the Pacific Region*, Amsterdam (Elsevier), Dev. in Sedimentol. Ser., 36:299–315.
- , 1986. Authigenic silica in Tertiary and Upper Cretaceous sediments of the East Mariana Basin, Deep Sea Drilling Project Site 585. In Moberly, R., Schlanger, S.O., et al., *Init. Repts. DSDP*, 89: Washington (U.S. Govt. Printing Office), 389–398.
- Barnes, R.O., 1988. ODP in-situ fluid sampling and measurement: a new wireline tool. In Mascle, A., Moore, J.C., et al., *Proc. ODP, Init. Repts.*, 110: College Station, TX (Ocean Drilling Program), 55–63.
- Becker, K., Sakai, H., et al., 1988. *Proc. ODP, Init. Repts.*, 111: College Station, TX (Ocean Drilling Program).
- Behl, R.J., and Smith, B.M., 1992. Silicification of deep-sea sediments and the oxygen isotope composition of diagenetic siliceous rocks from the western Pacific, Pigafetta and East Mariana basins, Leg 129. In Larson, R.L., Lancelot, Y., et al., *Proc. ODP, Sci. Results*, 129: College Station, TX (Ocean Drilling Program), 81–117.
- Berggren, W.A., Kent, D.V., Swisher, C.C., III, and Aubry, M.P., 1995. A revised Cenozoic geochronology and chronostratigraphy. In Berggren, W.A., Kent, D.V., Aubry, M.-P., and Hardenbol, J. (Eds.), *Geochronology, Time Scales and Global Stratigraphic Correlation*. Spec. Publ.—Soc. Econ. Paleontol. Mineral., 54:129–212.
- Bernoulli, D., 1972. North Atlantic and Mediterranean Mesozoic facies: a comparison. In Hollister, C.D., Ewing, J.I., et al., *Init. Repts. DSDP*, 11: Washington (U.S. Govt. Printing Office), 801–871.
- Blum, P., 1997. Physical Properties Handbook: a Guide to the Shipboard Measurements of Physical Properties of Deep-sea Cores. *ODP Tech. Note*, 26.
- Boyce, R.E., 1976. Definitions and laboratory techniques of compressional sound velocity parameters and wet-water content, wet-bulk density, and porosity parameters by gravimetric and gamma-ray attenuation techniques. In Schlanger, S.O., Jackson, E.D., et al., *Init. Repts. DSDP*, 33: Washington (U.S. Govt. Printing Office), 931–958.
- , 1977. Deep Sea Drilling Project procedures for shear strength measurement of clayey sediment using modified Wykeham Farrance laboratory vane apparatus. In Barker, P.F., Dalziel, I.W.D., et al., *Init. Repts. DSDP*, 36: Washington (U.S. Govt. Printing Office), 1059–1068.

- Channell, J.E.T., Erba, E., Nakanishi, M., and Tamaki, K., 1995. Late Jurassic–Early Cretaceous time scales and oceanic magnetic anomaly block models. *In* Berggren, W.A., Kent, D.V., Aubry, M.-P., and Hardenbol, J. (Eds.), *Geochronology, Time Scales and Global Stratigraphic Correlation*. Spec. Publ.- Soc. Econ. Paleontol. Mineral., 54:51–63.
- Dean, W.E., Leinen, M., and Stow, D.A.V., 1984. Classification of deep-sea, fine grained sediments. *J. Sediment. Petrol.*, 55:250–256.
- Dick, H.J.B., Erzinger, J., Stokking, L.B., et al., 1992. *Proc. ODP, Init. Repts.*, 140: College Station, TX (Ocean Drilling Program).
- Doeglas, D.J., 1968. Grain-size indices, classification and environment. *Sedimentology*, 10:83–100.
- Doyle, P.S., Kennedy, G.G., and Riedel, W.R., 1974. Stratigraphy. *In* Davies, T.A., Luyendyk, B.P., et al., *Init. Repts. DSDP*, 26: Washington (U.S. Govt. Printing Office), 825–905.
- Doyle, P.S., and Riedel, W.R., 1979. Cretaceous to Neogene ichthyoliths in a giant piston core from the central North Pacific. *Micropaleontology*, 25:337–364.
- , 1985. Cenozoic and Late Cretaceous ichthyoliths. *In* Bolli, H.M., Saunders, J.B., and Perch-Nielsen, K. (Eds.), *Plankton Stratigraphy*: Cambridge (Cambridge Univ. Press), 965–994.
- Dumitrica-Jud, R., 1995. Early Cretaceous Radiolarian biostratigraphy of Umbria-Marche Apennines (Italy), Southern Alps (Italy and Switzerland) and Hawasina Nappes (Oman). *In* *INTERRAD Jurassic-Cretaceous Working Group, Middle Jurassic to Lower Cretaceous Radiolaria of Tethys: Occurrences, Systematics, Biochronology*. Mem. Geol. (Lausanne), 23:751–798.
- Ellis, D.V., 1987. *Well Logging for Earth Scientists*: New York (Elsevier).
- Erba, E., Channell, J.E.T., Claps, M., Jones, C., Larson, R., Opdyke, B., Premoli Silva, I., Riva, A., Salvini, G., Torricelli, S., in press. Integrated Stratigraphy of the Cismon APTICORE (Southern Alps, Italy): a “reference section” for the Hauterivian-Aptian interval at low latitudes. *J. Foraminiferal Res.*, Spec. Vol. dedicated to W.V. Sliter.
- Erba, E., Premoli Silva, I., and Watkins, D.K., 1995. Cretaceous calcareous plankton biostratigraphy of Sites 872 through 879. *In* Haggerty, J.A., Premoli Silva, I., Rack, F., and McNutt, M.K. (Eds.), *Proc. ODP, Sci. Results*, 144: College Station, TX (Ocean Drilling Program), 157–169.
- Fisher, A.T., Abrams, L., and Busch, W.H., 1992. Comparison of laboratory and logging data from Leg 129 and the inversion of logs to determine lithology. *In* Larson, R.L., Lancelot, Y., et al., *Proc. ODP, Sci. Results*, 129: College Station, TX (Ocean Drilling Program), 507–527.
- Gieskes, J.M., Gamo, T., and Brumsack, H., 1991. Chemical methods for interstitial water analysis aboard *JOIDES Resolution*. *ODP Tech. Note*, 15.
- Goldberg, D., 1997. The role of downhole measurements in marine geology and geophysics. *Rev. Geophys.*, 35:315–342.
- Govindaraju, K., 1989. 1989 compilation of working values and sample description for 272 geostandards. *Geostand. Newsl.*, 13 (spec. iss.).
- Gradstein, F.M., Agterberg, F.P., Ogg, J.G., Hardenbol, J., Van Veen, P., Thierry, J., and Huang, Z., 1995. A Triassic, Jurassic and Cretaceous time scale. *In* Berggren, W.A., Kent, D.V., Aubry, M.P., and Hardenbol, J. (Eds.), *Geochronology, Time Scales and Global Stratigraphic Correlation*. Spec. Publ.— Soc. Econ. Paleontol. Mineral., 54:95–126.
- Guex, J., 1977. Une nouvelle methode d'analyse biochronologique. *Bull. Soc. Vaudoise Sci. Nat.*, 73:309–322.
- , 1991. *Biochronological Correlations*: Berlin (Springer-Verlag), 1–250.
- Hoppie, B.W., Blum, P., and the Shipboard Scientific Party, 1994. Natural gamma-ray measurements on ODP cores: introduction to procedures with examples from Leg 150. *In* Mountain, G.S., Miller, K.G., Blum, P., et al., *Proc. ODP, Init. Repts.*, 150: College Station, TX (Ocean Drilling Program), 51–59.

- Ingram, R.L., 1954. Terminology for the thickness of stratification and parting units in sedimentary rocks. *Geol. Soc. Am. Bull.*, 65:937–938.
- INTERRAD Jurassic–Cretaceous Working Group, 1995. Middle Jurassic to Lower Cretaceous radiolaria of Tethys: occurrences, systematics, biochronology. *Mem. Geol. (Lausanne)*, 23:1–1172.
- Isaacs, C.M., 1982. Influence of rock compositions on kinetics of silica phase changes in the Monterey Formation, Santa Barbara area, California. *Geology*, 10:304–308.
- Isaacs, C.M., Pisciotto, K.A., and Garrison, R.E., 1983. Facies and diagenesis of the Miocene Monterey Formation, California: a summary. In Iijima, A., Hein, J.R., and Siever, R. (Eds.), *Siliceous Deposits in the Pacific Region*: Amsterdam (Elsevier), *Devl. in Sedimentol. Ser.*, 36:247–282.
- Jenkyns, H.C., 1986. Pelagic environments. In Reading, H.G. (Ed.), *Sedimentary Environments and Facies* (2nd ed.): Oxford (Blackwell Sci.), 343–397.
- JOI/USSSP JSC10-89, 1989. Multichannel seismic interpretation across geochemical reference section sites near the Bonin/Mariana arcs.
- Jud, R., 1994. Biochronology and systematics of Early Cretaceous radiolaria of the Western Tethys. *Mem. Geol. (Lausanne)*, 19:1–147.
- Karl, S.M., Wandless, G.A., and Karpoff, A.M., 1992. Sedimentological and geochemical characteristics of Leg 129 siliceous deposits. In Larson, R.L., Lancelot, Y., et al., *Proc. ODP, Sci. Results*, 129: College Station, TX (Ocean Drilling Program), 31–79.
- Karpoff, A.M., 1992. Cenozoic and Mesozoic sediments from the Pigafetta Basin, Leg 129, Sites 800 and 801: mineralogical and geochemical trends of the deposits overlying the oldest oceanic crust. In Larson, R.L., Lancelot, Y., et al., *Proc. ODP, Sci. Results*, 129: College Station, TX (Ocean Drilling Program), 3–30.
- Kastner, M., 1979. Silica polymorphs. In Burns, R.G. (Ed.), *Marine Minerals*. Mineral. Soc. Am., *Rev. Mineral.*, 6:99–111.
- Kozarek, R.J., and Orr, W.N., 1979. Ichthyoliths, Deep Sea Drilling Project Legs 51 through 53. In Donnelly, T., Francheteau, J., Bryan, W., Robinson, P., Flower, M., Salisbury, M., et al., *Init. Repts. DSDP*, 51, 52, 53 (Pt. 2): Washington (U.S. Govt. Printing Office), 857–895.
- Kvenvolden, K.A., and McDonald, T.J., 1986. Organic geochemistry on the *JOIDES Resolution*—an assay. *ODP Tech. Note*, 6.
- Lamont-Doherty Earth Observatory-Borehole Research Group, 1994. *Wireline Logging Services Guide*: Lamont-Doherty Earth Observatory-Borehole Research Group.
- Lancelot, Y., Larson, R.L., et al., 1990. *Proc. ODP, Init. Repts.*, 129: College Station, TX (Ocean Drilling Program).
- Langmuir, C.H., and Natland, J., 1986. Drilling old ocean crust at convergent margins: Argo Abyssal Plain and Western Pacific, *JOIDES Proposal*, 267-F:17.
- Larsen, H.C., Saunders, A.D., Clift, P.D., et al., 1994. *Proc. ODP, Init. Repts.*, 152: College Station, TX (Ocean Drilling Program).
- Larson, R.L., Fisher, A.T., Jarrard, R.D., Becker, K., and Ocean Drilling Program Leg 144 Shipboard Scientific Party, 1993. Highly permeable and layered Jurassic oceanic crust in the Western Pacific. *Earth Planet. Sci. Lett.*, 119:71–83.
- Lovell, M.A., Harvey, P.K., Brewer, T.S., Williams, C., Jackson, P.D., and Williamson, G., 1998. Application of FMS images in the Ocean Drilling Program: an overview. In Cramp, A., MacLeod, C.J., Lee, S.V., and Jones, E.J.W. (Eds.), *Geological Evolution of Ocean Basins: Results from the Ocean Drilling Program*. Geol. Soc. Spec. Publ. London, 131:287–303.
- Mazzullo, J.M., Meyer, A., and Kidd, R.B., 1988. New sediment classification scheme for the Ocean Drilling Program. In Mazzullo, J.M., and Graham, A.G. (Eds.), *Handbook for Shipboard Sedimentologists*. *ODP Tech. Note*, 8:45–67.
- McKee, E.D., and Weir, G.W., 1953. Terminology for stratification and cross-stratification in sedimentary rocks. *Geol. Soc. Am. Bull.*, 64:381–390.
- Munsell Color Company, Inc., 1975. *Munsell Soil Color Charts*. Baltimore, MD (Munsell).

- Norrish, K., and Hutton, J.T., 1969. An accurate X-ray spectrographic method for the analysis of a wide range of geological samples. *Geochim. Cosmochim. Acta*, 33:431–453.
- Ogg, J.G., Karl, S.M., and Behl, R.J., 1992. Jurassic through Early Cretaceous sedimentation history of the central equatorial Pacific and of Sites 800 and 801. In Larson, R.L., Lancelot, Y., et al., *Proc. ODP, Sci. Results*, 129: College Station, TX (Ocean Drilling Program), 571–613.
- Perch-Nielsen, K., 1985. Mesozoic calcareous nannofossils. In Bolli, H.M., Saunders, J.B., and Perch-Nielsen, K. (Eds.), *Plankton Stratigraphy*: Cambridge (Cambridge Univ. Press), 329–426.
- Pezard, P.A., 1990. Electrical properties of mid-ocean ridge basalt and implications for the structure of the upper oceanic crust in Hole 504B. *J. Geophys. Res.*, 95:9237–9264.
- Premoli Silva, I., and Sliter, W.V., 1994. Cretaceous planktonic foraminiferal biostratigraphy and evolutionary trends from the Bottaccione Section, Gubbio, Italy. *Paleontogr. Ital.*, 82:2–90.
- , 1999. Cretaceous Paleooceanography: evidence from planktonic foraminiferal evolution. In Barrera, E., and Johnson, C.C., (Eds.), *The Evolution of Cretaceous Ocean-Climatic System*. Spec. Pap.—Geol. Soc. Am., 332:301–328.
- Reasoner, D.J., and Geldreich, E.E., 1985. A new medium for the enumeration and subculture of bacteria from potable water. *Appl. Environ. Microbiol.*, 1:1–7.
- Reynolds, R.C., Jr., 1963. Matrix corrections in trace element analyses by X-ray fluorescence: estimation of the mass absorption coefficient by Compton scattering. *Am. Mineral.*, 48:1133–1143.
- , 1997. Estimation of mass absorption coefficients by Compton scattering: improvements and extensions of the method. *Am. Mineral.*, 52:1493–1502.
- Rider, M., 1996. *The Geological Interpretation of Well Logs*: (2nd ed.), Caithress (Whittles Publishing).
- Rock-Color Chart Committee, 1991. *Rock Color Charts*. Geol. Soc. Am.
- Roth, P.H., 1978. Cretaceous nannoplankton biostratigraphy and oceanography of the northwestern Atlantic Ocean. In Benson, W.E., Sheridan, R.E., et al., *Init. Repts. DSDP*, 44: Washington (U.S. Govt. Printing Office), 731–759.
- Sass, J.H., Kennelly, J.P., Jr., Smith, E.P., and Wendt, W.E., 1984. Laboratory line-source methods for the measurement of thermal conductivity of rocks near room temperature. *Open-File Rep.—U.S. Geol. Surv.*, 84–0091.
- Schlumberger, 1989a. *Formation MicroScanner Image Interpretation*: Houston, TX (Schlumberger Educ. Services).
- , 1989b. *Log Interpretation Principals/Applications*: Houston, TX (Schlumberger Educ. Services).
- , 1994. *IPL Integrated Porosity Lithology* (Schlumberger Wireline and Testing), SMP-9270.
- Serra, O., 1984. *Fundamentals of Well-Log Interpretation* (Vol. 1): *The Acquisition of Logging Data*: Dev. Pet. Sci., 15A: Amsterdam (Elsevier).
- , 1986. *Fundamentals of Well-Log Interpretation* (Vol. 2): *The Acquisition of Logging Data*: Dev. Pet. Sci., 15B.
- , 1989. *Formation MicroScanner Image Interpretation*: Houston, TX (Schlumberger Educ. Services) SMP-7028.
- Shepard, F., 1954. Nomenclature based on sand-silt-clay ratios. *J. Sediment, Petrol.*, 24:151–158.
- Shipboard Scientific Party, 1998a. Explanatory Notes. In Norris, R.D., Kroon, D., Klaus, A., et al., *Proc. ODP, Init. Repts.*, 171B: College Station, TX (Ocean Drilling Program), 11–44.
- , 1998b. Explanatory Notes. In Wefer, G., Berger, W.H., Richter, C., et al., *Proc. ODP, Init. Repts.*, 175: College Station, TX (Ocean Drilling Program), 27–46.

- , 1998c. Explanatory Notes. *In* Whitmarsh, R.B., Beslier, M.O., Wallace, P.J., et al., *Proc. ODP, Init. Repts.*, 173: College Station, TX (Ocean Drilling Program), 25–47.
- , 2000. Explanatory notes. *In* Coffin, M.F., Frey, F.A., Wallace, P.J., et al., *Proc. ODP, Init Repts.*, 183: College Station, TX (Ocean Drilling Program), 1–94.
- Sissingh, W., 1977. Biostratigraphy of Cretaceous calcareous nannoplankton. *Geol. Mijnbouw.*, 56:37–65.
- Smith, D.C., Spivack, A.J., Fisk, M.R., Haveman, S.A., Staudigel, H., and the Leg 185 Shipboard Scientific Party, 2000. Methods for quantifying potential microbial contamination during deep ocean coring. *ODP Tech. Note*, 28 [Online]. Available from World Wide Web: <<http://www-odp.tamu.edu/publications/tnotes/tn28/INDEX.HTM>>. [Cited 2000-05-23]
- Smith, W.H.F., and Sandwell, D.T., 1997. Global seafloor topography from satellite altimetry and ship depth soundings. *Science*, 277:1956–1962.
- Steiner, M.B., and Wallick, B.P., 1992, Jurassic to Paleocene paleolatitudes of the Pacific Plate derived from the paleomagnetism of the sedimentary sequences at Sites 800, 801, and 802. *In* Larson, R.L., Lancelot, Y., et al., *Proc. ODP, Sci. Results*, 129: College Station, TX (Ocean Drilling Program), 431–446.
- Thierstein, H.R., 1973. Lower Cretaceous calcareous nannoplankton biostratigraphy. *Abh. Geol. Bundesanst. (Austria)*, 29:1–52.
- , 1976. Mesozoic calcareous nannoplankton biostratigraphy of marine sediments. *Mar. Micropaleontol.*, 1:325–362.
- Thompson, G., and Bankston, D.C., 1970. Sample contamination from grinding and sieving determined by emission spectroscopy. *Appl. Spectros.*, 24:210–219.
- Vacquier, V., 1985. The measurement of thermal conductivity of solids with a transient linear heat source on the plane surface of a poorly conducting body. *Earth Planet. Sci. Lett.*, 74:275–279.
- van Andel, T., 1983. Sediment nomenclature and classification. *In* Heath, G.R. (Ed.), *Sedimentology, Physical Properties, and Geochemistry in the Initial Reports of the Deep Sea Drilling Project Volumes 1–44: An Overview*. World Data Cent. Mar. Geol. Geophys., Rep. MGG-1:3–25.
- Von Herzen, R.P., and Maxwell, A.E., 1959. The measurements of thermal conductivity of deep-sea sediments by a needle-probe method. *J. Geophys. Res.*, 64:1557–1563.
- Walker, D., 1973. Behavior of X-ray mass absorption coefficients near absorption edges: Reynold's method revisited. *Am. Mineral.*, 58:1069–1072.
- Wessel, P., and Smith, W.H.F., 1995. New version of the Generic Mapping Tools released. *Eos*, 76:329.

Figure F1. Examples of numbered core sections.

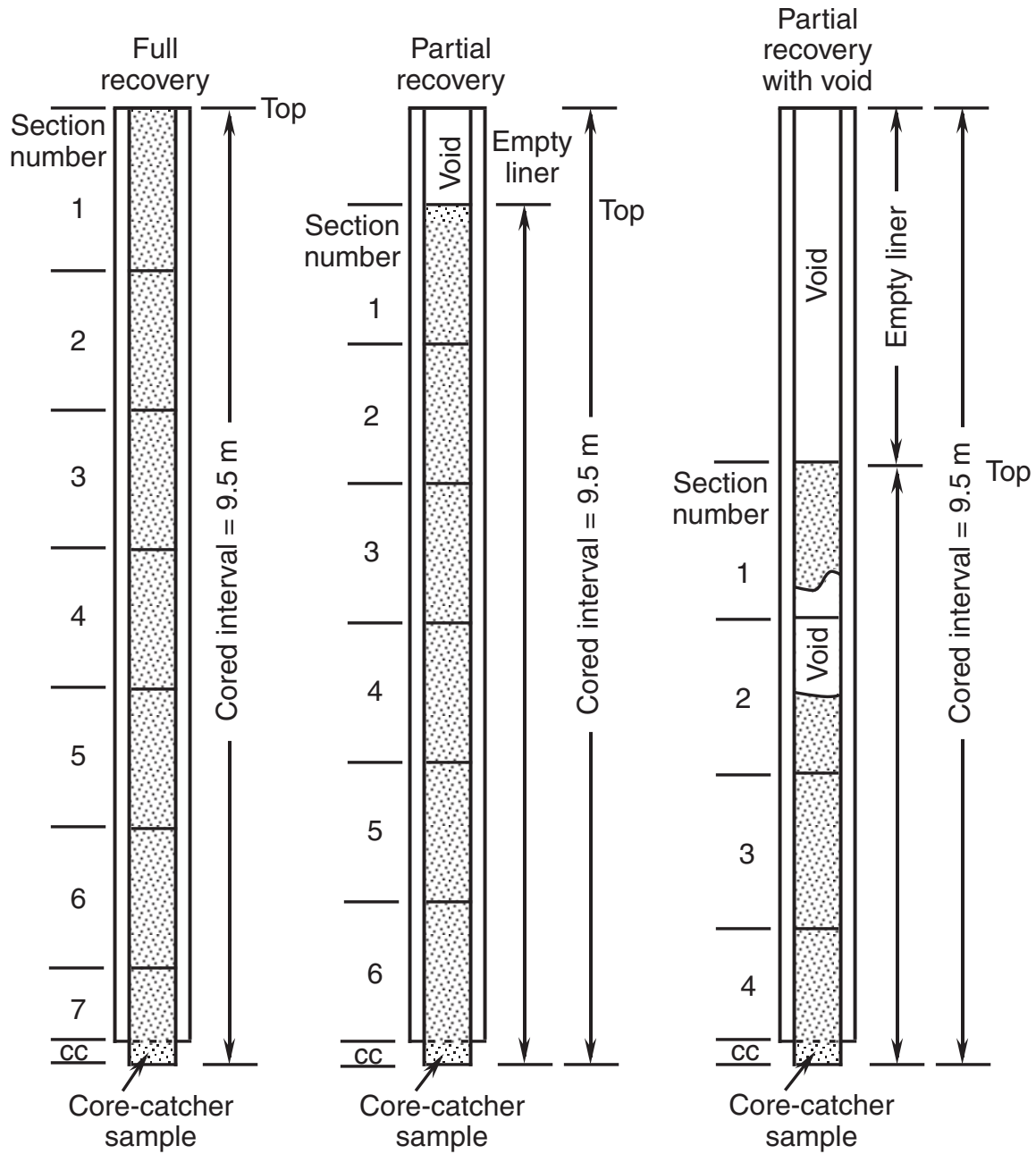


Figure F2. Track chart of the entire single-channel seismic (SCS) survey conducted during Leg 185 (bold line = SCS Lines 1, 2, and 3) and portions of C2005 MCS Lines 39 and 46 east of the Izu-Bonin Trench. Sonobuoy 171 is located on C2005 Line 46, 50 km west of Site 1149. Arrows locate hole positions for Site 1149 and proposed Site BON 10. Bathymetry is in meters below sea level from Smith and Sandwell (1997); GMT software, Wessel and Smith (1995).

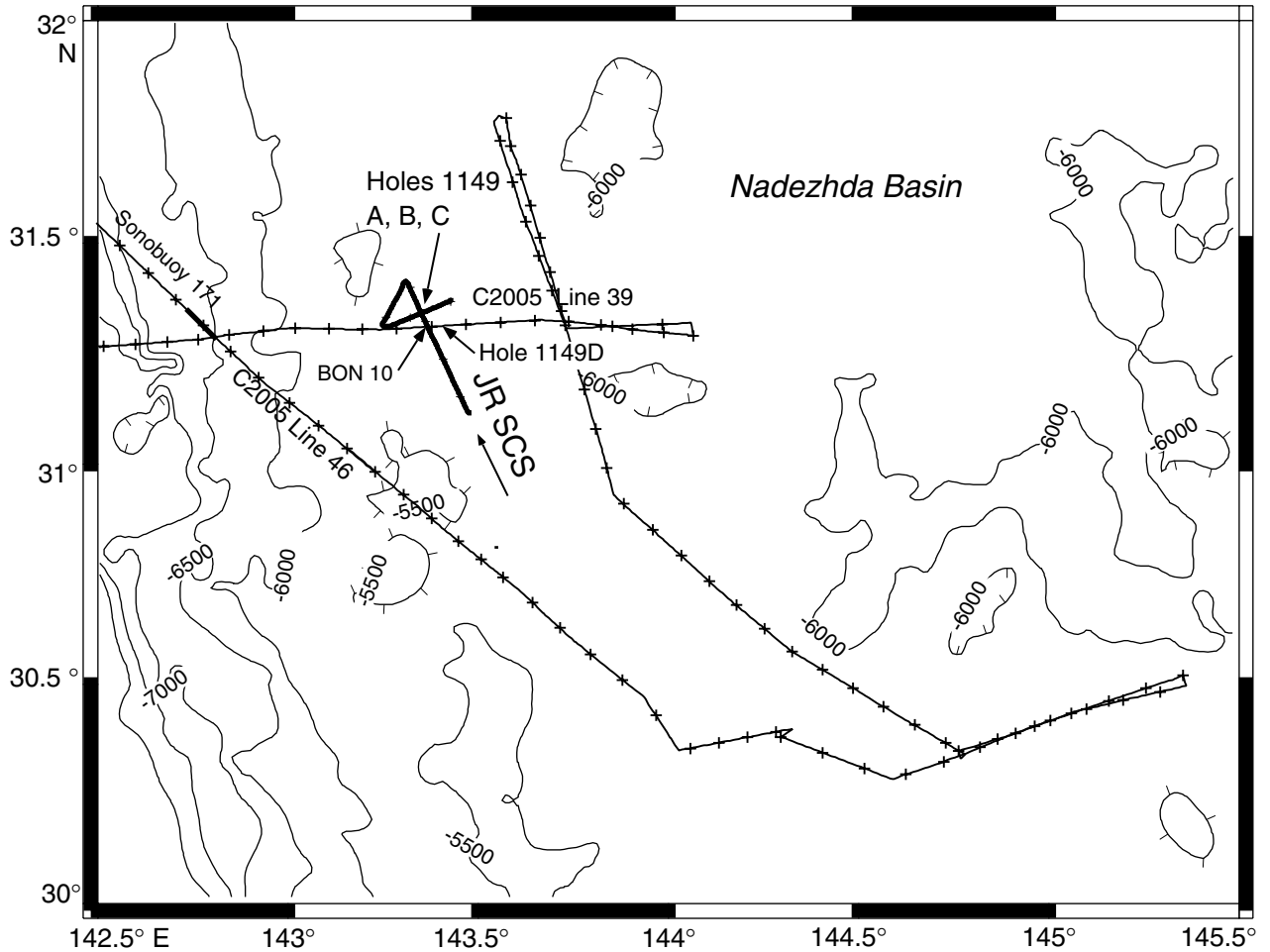


Figure F3. Key to symbols used to represent lithology, drilling disturbance, bioturbation intensity, sedimentary structures, accessories, and fossils in the barrel sheets.

Graphic Lithology

	Clay/Claystone		Nannofossil Chalk		Diatom-Rad Ooze
	Silty Clay/Claystone		Calcareous Chalk		Porcelanite
	Ash		Radiolarian Ooze		Chert

Structures, Lithologic Accessories, Ichnofossils, Fossils

	Planar Lamination		Wavy Lamination
	Mineralized Vein		Fault
	Dissolution Seams		Chondrites
	Silt Lamina		Green Clay Lamina
	Thin Ash Bed		Pumice

Disturbance

	Slightly Disturbed		Slightly Fragmented
	Moderately Disturbed		Moderately Fragmented
	Very Disturbed		Highly Fragmented
	Soupy		Drilling Breccia

Figure F4. Sediment classification used during Leg 185. Schematic for naming mixtures of detrital, carbonate, and siliceous sediments. The scheme shows examples for the principal names. The modifiers can be replaced by any valid textural or microfossil name.

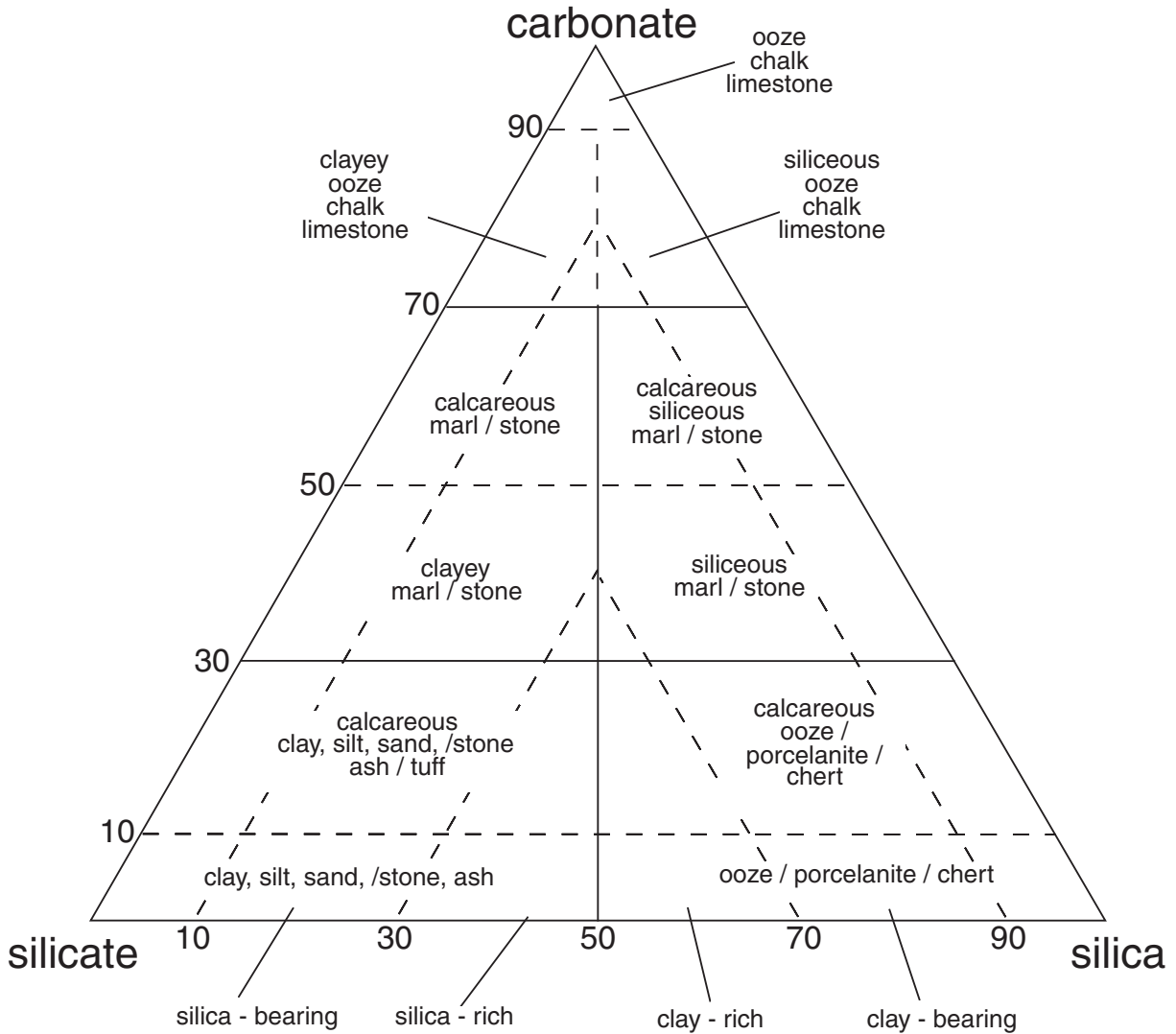
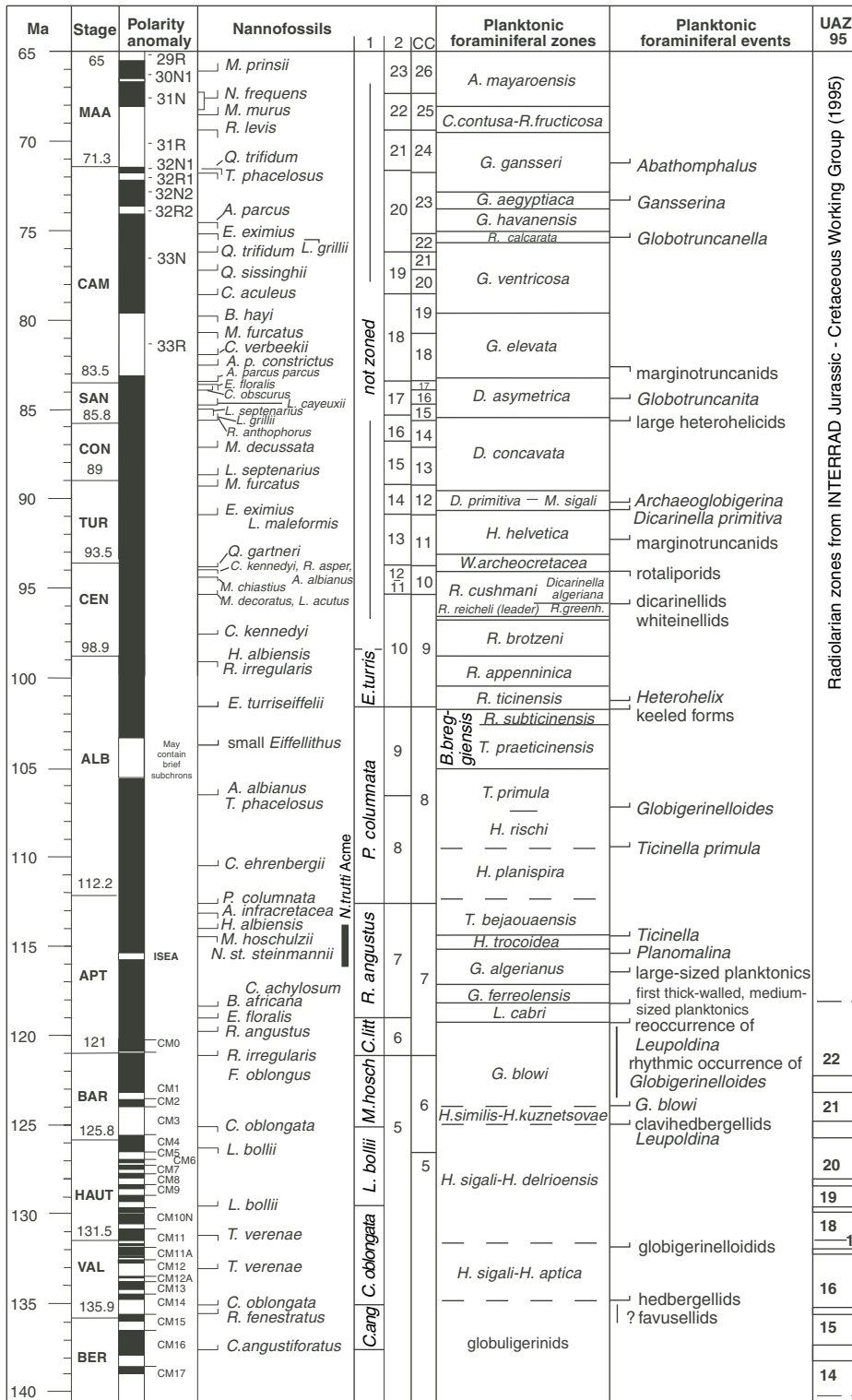


Figure F5. Cretaceous biostratigraphic scale used during Leg 185 (modified after Premoli Silva and Sliter, 1999). Magnetic sequence and absolute ages for the Late Cretaceous are after Gradstein et al. (1995); for the Early Cretaceous, after Channell et al. (1995).



1 = Thierstein, 1973; 2 = Roth, 1978; CC = Sissingh, 1977

(Modified from Premoli Silva and Sliter, 1999)

Figure F6. Example of a visual core description (VCD) form.

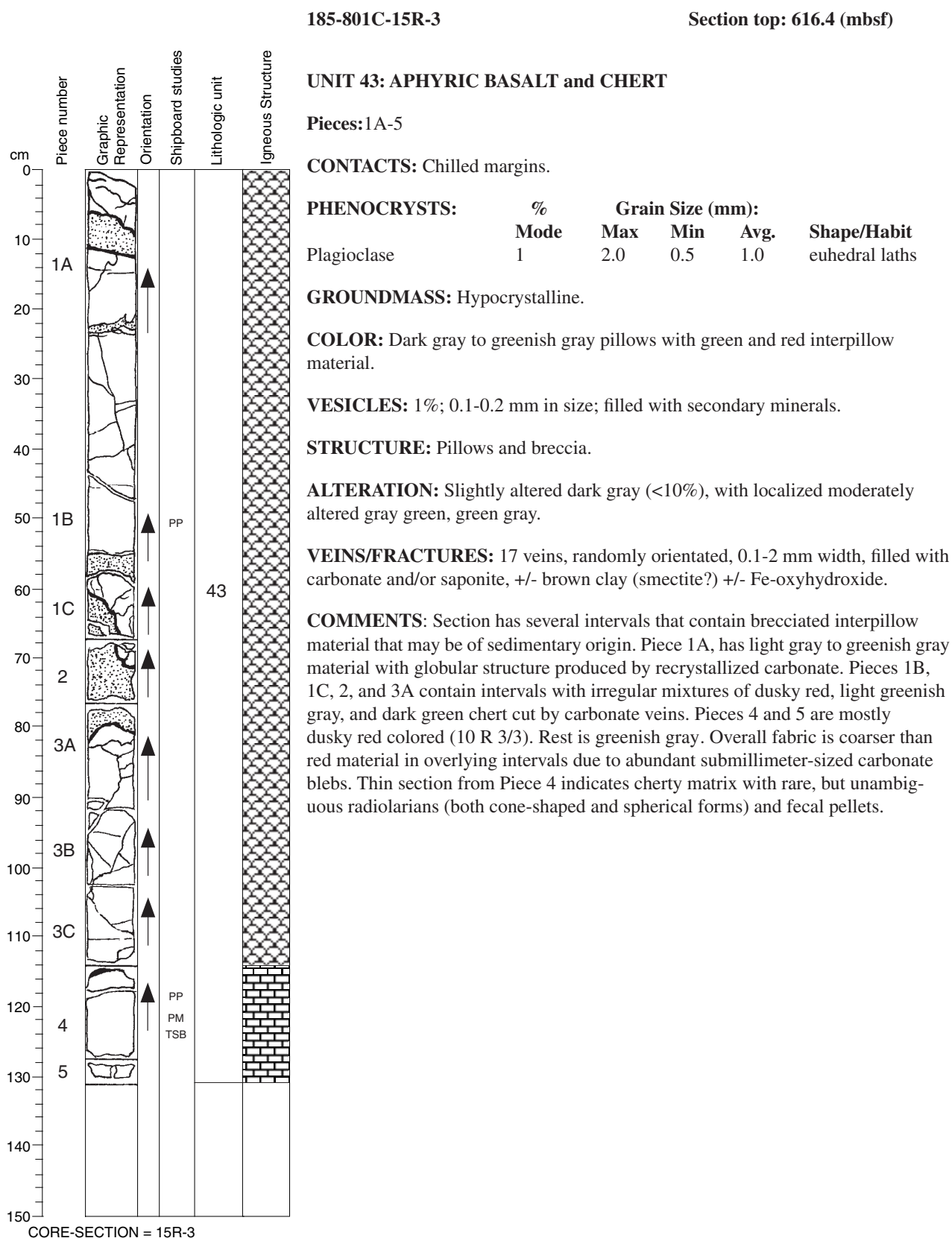


Figure F7. Hard rock VCD legend and types of igneous contacts.

Hard Rock VCD Legend

Graphic Representation Legend



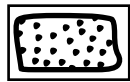
Glass or Chilled Margin



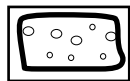
Fractures and Veins



Fracture Network

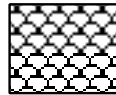


Breccia

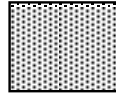


Vesicles

Structural Key



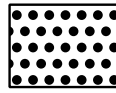
Pillow Basalt



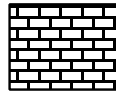
Pillows and Flows



Massive Basalt



Breccia



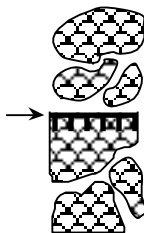
Sediment



Hydrothermal

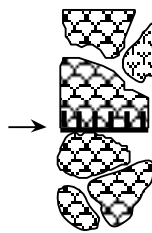
Contacts

A



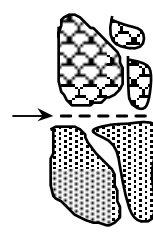
A. Upper boundary of the lower unit obtained.

B



B. Lower boundary of the upper unit obtained.

C



C. Contact between two units not recovered.

Figure F8. The profile of the field in the magnetically shielded area associated with the cryogenic magnetometer and AF demagnetization coils. The two centrally located peaks in an otherwise near-zero magnetic field region correspond to the bolted joints at which separate shielding metal segments are joined. The horizontal scale is in inches, corresponding to the instrument diagrams of the manufacturer. The cryogenic magnetometer occupies the region between 0 and 200 in; the AF demagnetization coils are located at ~225–255 in. The cores pass through the entire region.

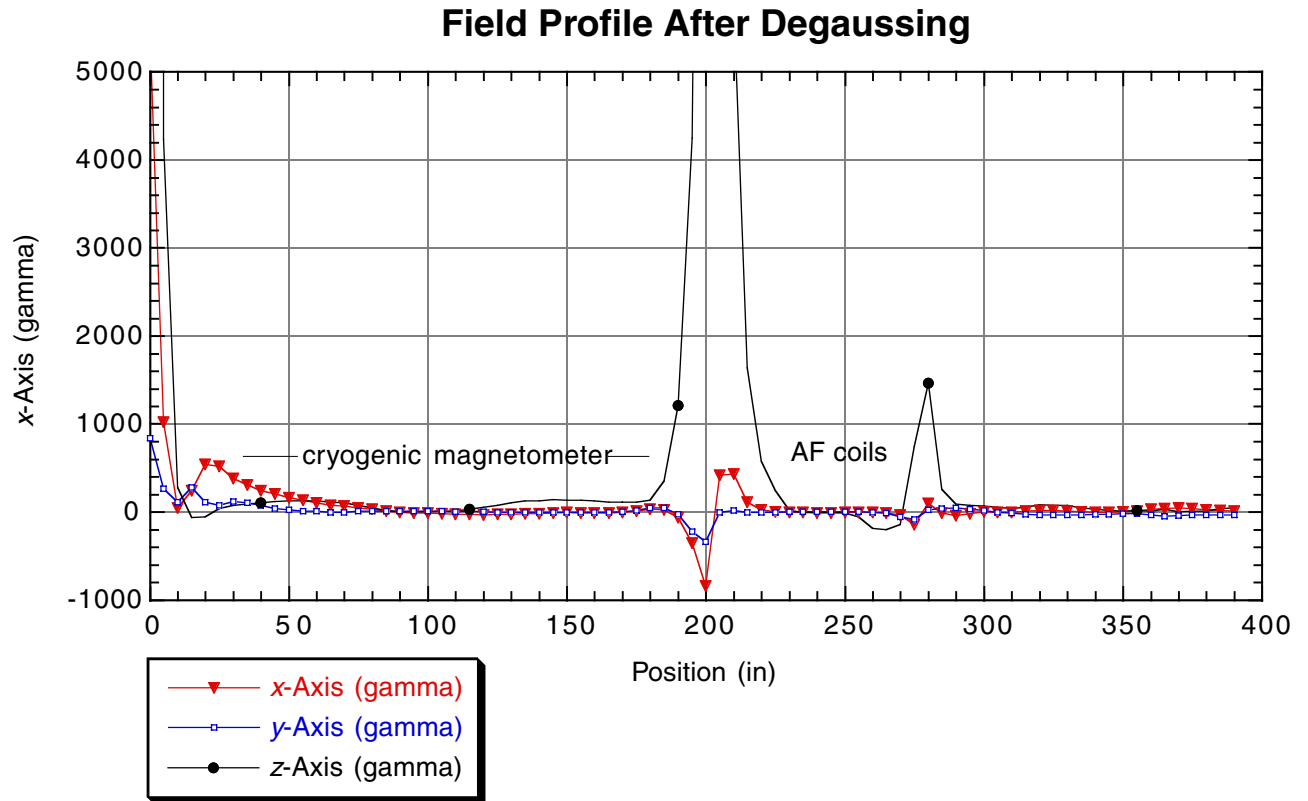


Figure F9. Comparison of inclinations of the cores from Hole 801C before demagnetization (solid circle), after 10 mT (open circle), and after 30 mT (solid square) to illustrate the progressive magnetization of the cores by the demagnetization coil (which has field inclination of approximately +90°).

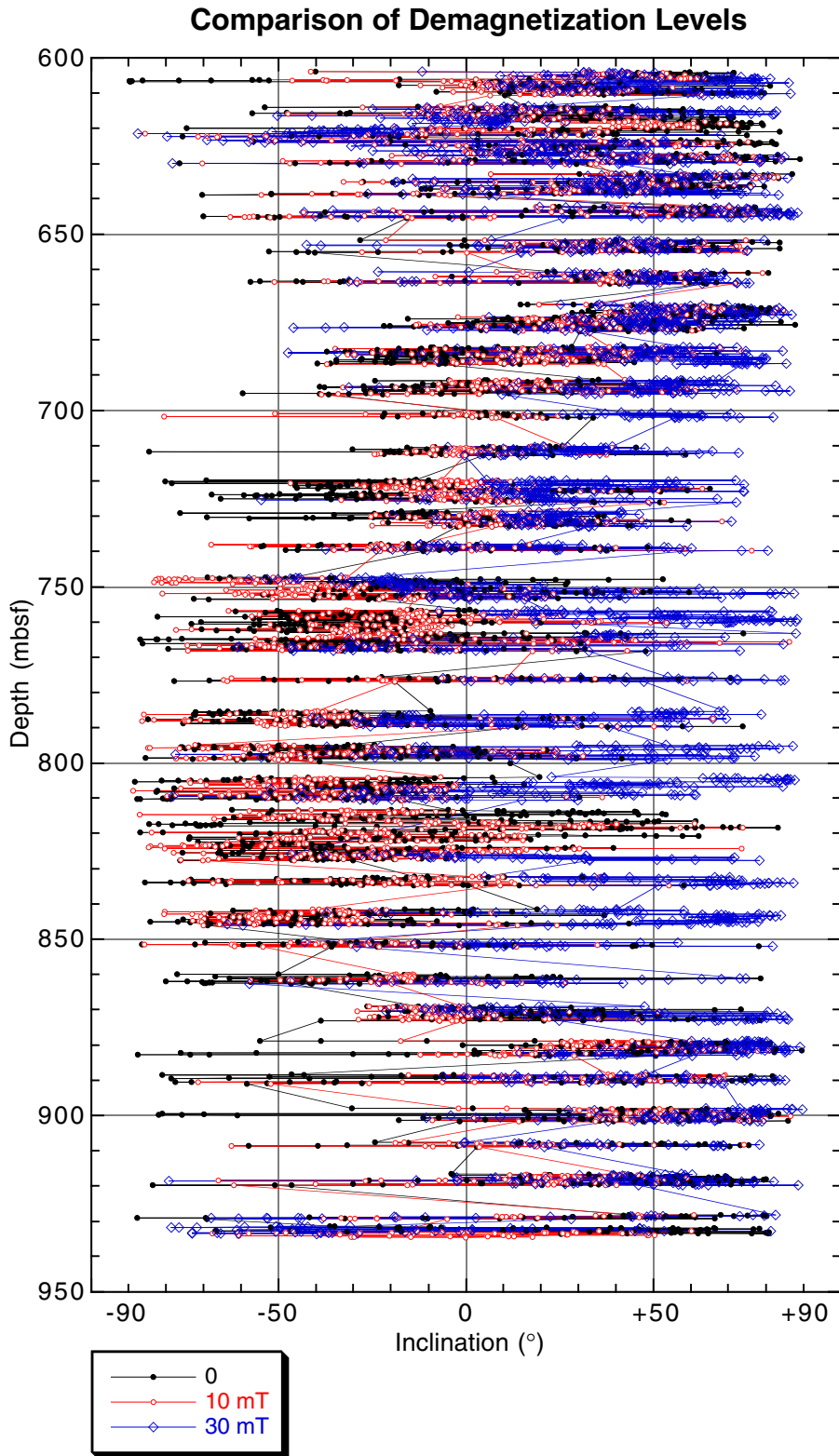


Figure F10. A. Whole-core (MST), half-core (AMST), and discrete sample measurements of susceptibility from Core 185-801D-1W. B. MST data corrected according to the Bartington correction formula and plotted with the AMST and discrete sample data of A.

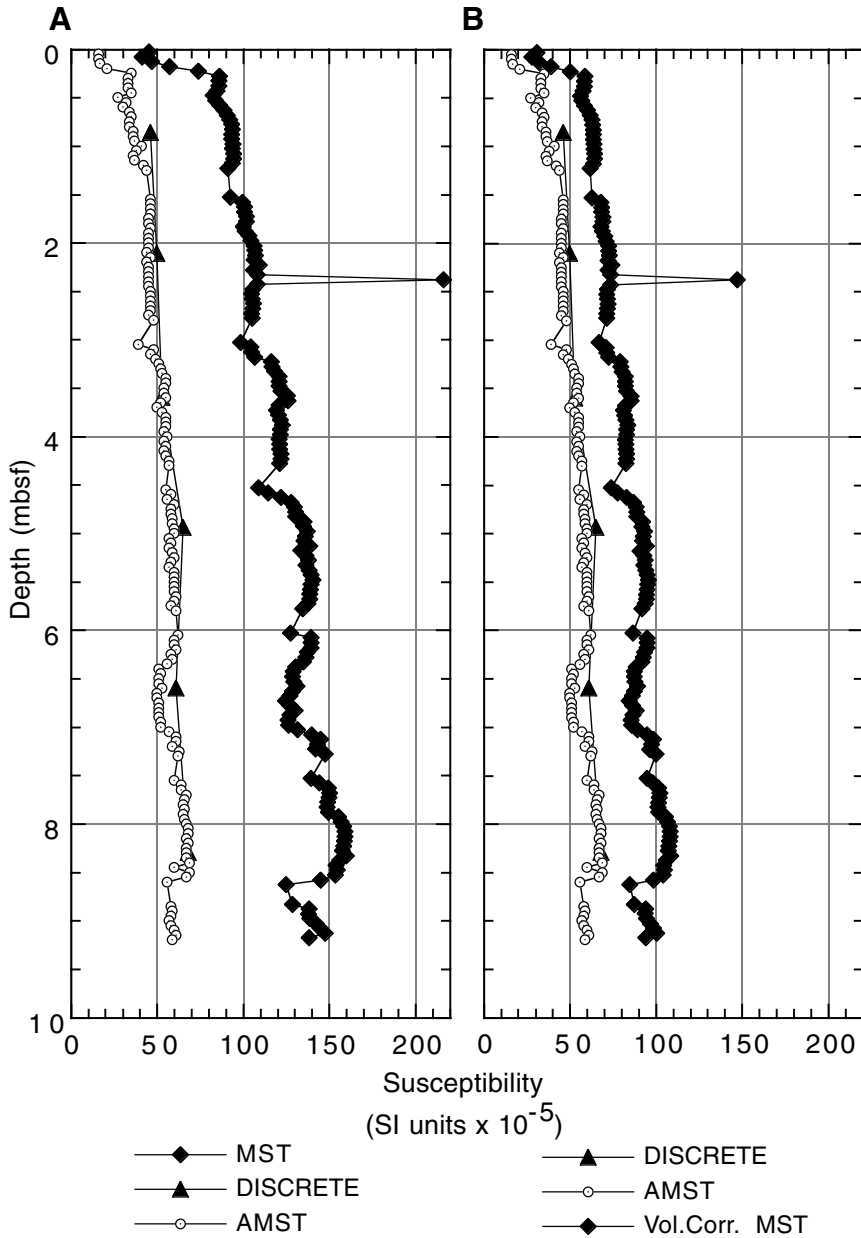


Figure F11. Equipment used for maintaining samples at in situ pressure. Equipment provided by Dr. A.A. Yayanos, Scripps Institution of Oceanography.

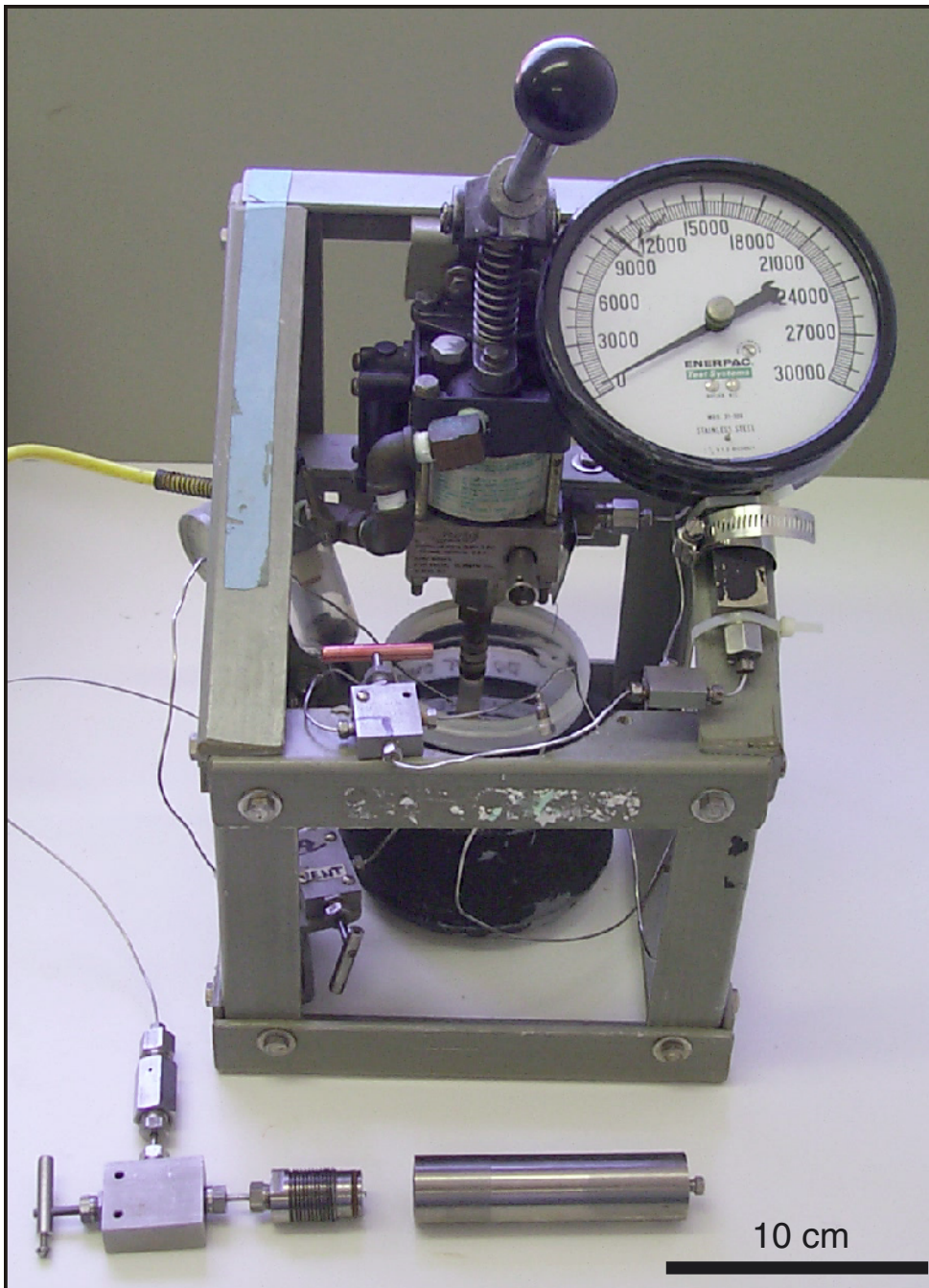


Figure F12. The triple combo and Formation MicroScanner/sonic tool strings used during Leg 185 (not to scale).

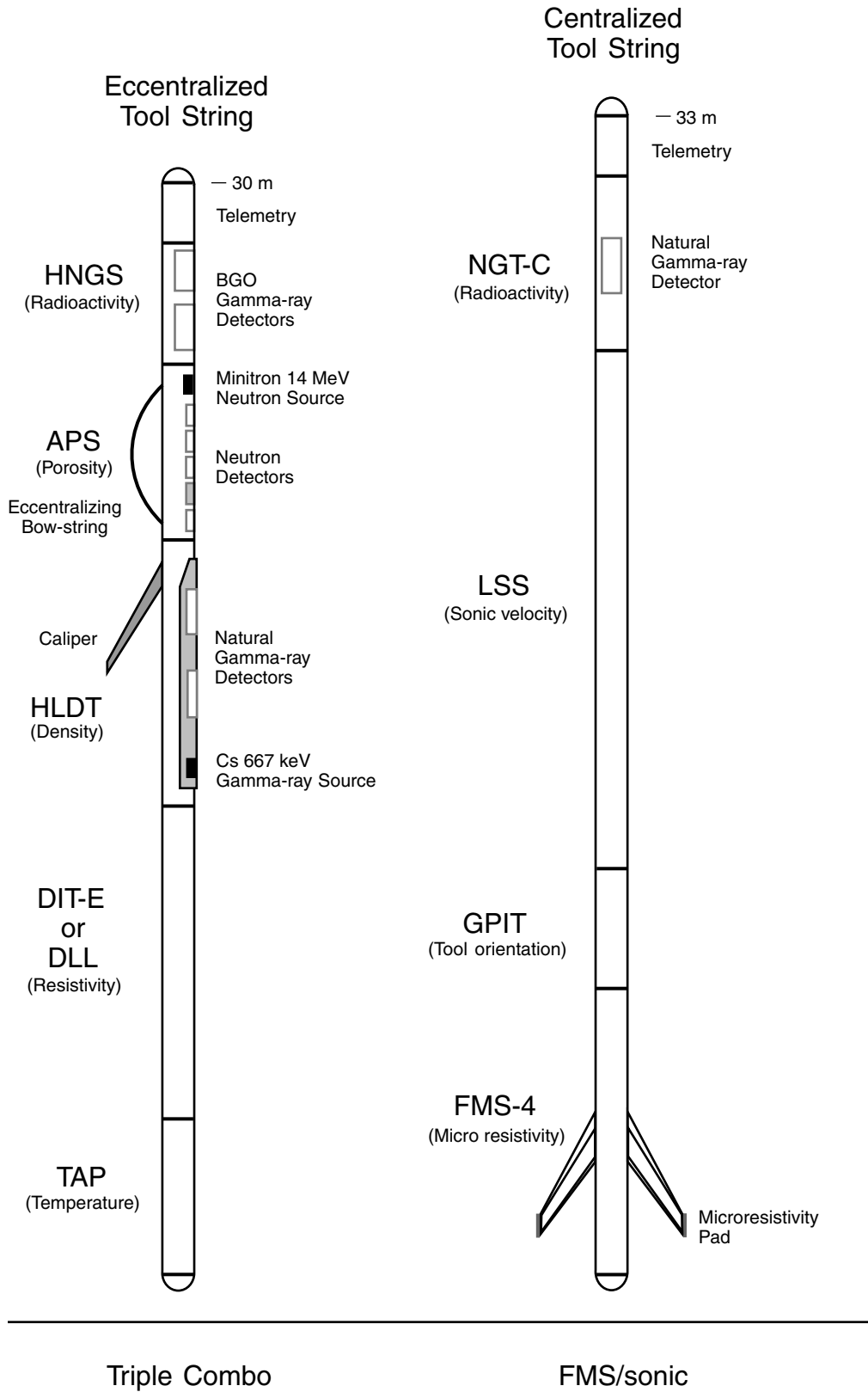
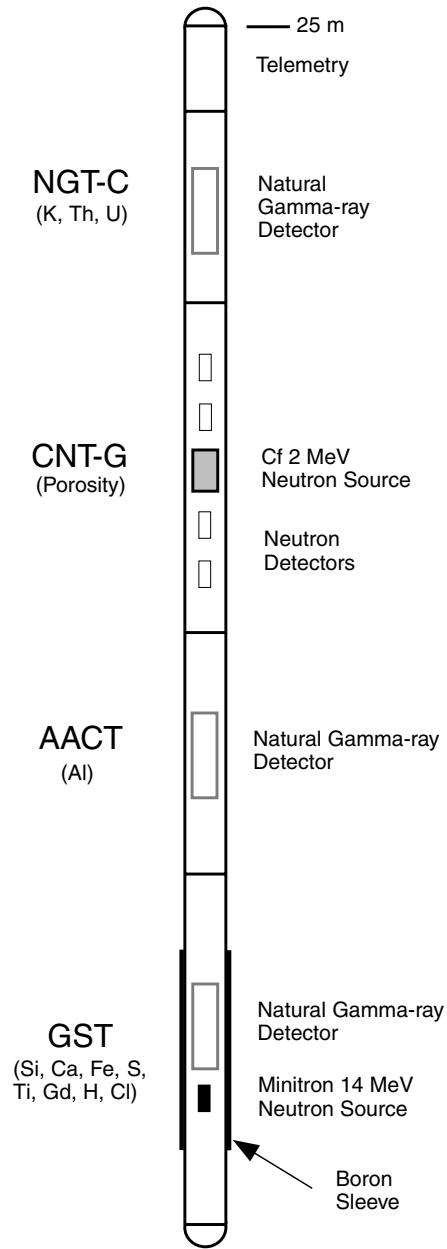


Figure F13. The geochemical logging tool string used during Leg 185 (not to scale).



GLT

Figure F14. Schematic diagram showing the basic principles of the Formation MicroScanner (FMS).

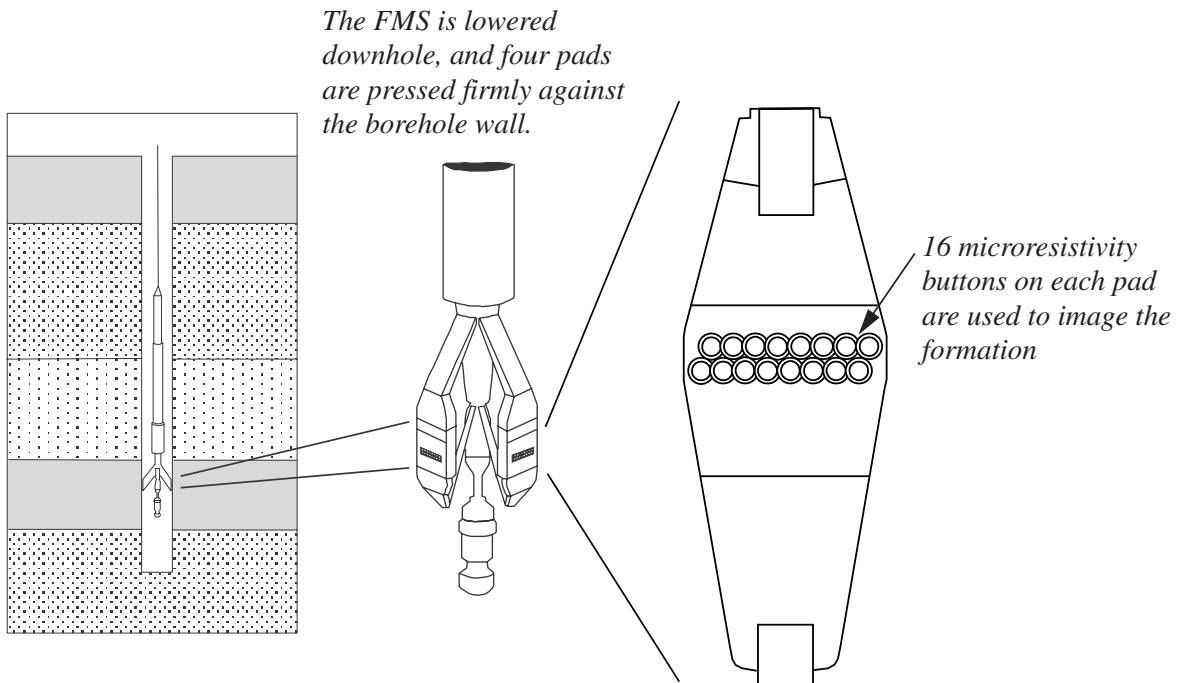


Table T3. Abbreviations used in the alteration and igneous core description logs.

Colors		Minerals		Mineral proportions	
Brn:	Brown	Am Si:	Amorphous silica	tr:	Trace (<1%)
Blk:	Black	Sm:	Smectite	X + Y:	≈50:50 x:y
G:	Gray	CO ₃ :	Calcium carbonate	X > Y:	70:30 x:y
Gn:	Green	Cp:	Chalcopyrite	X >> Y:	90:10 x:y
R:	Red	FeOx:	Iron oxyhydroxides	X >>> Y:	99:1 x:y
Or:	Orange	Ol:	Olivine	Other	
W:	White	Pl:	Plagioclase	ox:	Oxidized
G-Gn:	Gray-green	Py:	Pyrite	P:	Piece(s)
lt:	Light			V:	Vertical
dk:	Dark			Rbl:	Rubble
				→:	Altered to
				Bx:	Breccia

Note: Other minerals and colors are spelled out.

Table T5. Instrumental conditions for XRF major and trace element standard measurements.

Element	Line	Crystal	Detector	Collimator	Peak angle (°2θ)	Background offset (°2θ)	Total peak (s)	Count time background (s)	Analytical error (SD%)	Detection limit (%)
Major										
SiO ₂	SiKa1,2r	PET	FPC	Medium	109.21	NB	60	NB	0.20	0.030
TiO ₂	TiKa1,2r	LIF200	FPC	Fine	86.14	NB	100	NB	0.56	0.009
Al ₂ O ₃	AlKa1,2r	PET	FPC	Medium	145.12	NB	100	NB	0.55	0.041
Fe ₂ O ₃	FeKa1,2r	LIF200	FPC	Fine	57.52	NB	90	NB	0.42	0.007
MnO	MnKa1,2r	LIF200	FPC	Fine	62.97	NB	200	NB	2.12	0.006
MgO	MgKa1,2	TLAP	FPC	Medium	45.17	-0.80	200	200	0.40	0.050
CaO	CaKa1,2r	LIF200	FPC	Medium	113.09	NB	120	NB	0.25	0.003
Na ₂ O	NaKa1,2	TLAP	FPC	Medium	55.10	1.20	210	210	1.21	0.100
K ₂ O	KKa1,2r	LIF200	FPC	Medium	136.69	NB	175	NB	0.89	0.001
P ₂ O ₅	PKa1,2s	GE111	FPC	Medium	141.04	NB	175	NB	1.56	0.003
Trace										
Nb	Ka	LIF200	Scint	Fine	21.40	+0.35	100	100	2.0	1
Zr	Ka	LIF200	Scint	Fine	22.55	-0.35	100	100	0.7	1
Y	Ka	LIF200	Scint	Fine	23.80	-0.40	100	100	2.7	1
Sr	Ka	LIF200	Scint	Fine	25.15	-0.40	100	100	1.1	1
Rb	Ka	LIF200	Scint	Fine	26.62	-0.60	100	100	8.1	1
Zn	Ka	LIF200	Scint	Fine	41.81	-0.55	100	100	1.8	2
Cu	Ka	LIF200	Scint	Fine	45.03	-0.40	100	100	1.3	2
Ni	Ka	LIF200	Scint	Fine	48.67	-0.40	100	100	1.2	2
Cr	Ka	LIF200	FPC	Fine	69.35	-0.50	100	100	0.8	3
V	Ka	LIF220	FPC	Fine	123.06	-0.50	100	100	1.1	4
Ce	La	LIF220	FPC	Medium	128.16	-1.50	100	100	5.6	10
Ba	Kb	LIF220	FPC	Medium	128.78	-1.50	100	100	5.8	15

Notes: SD = standard deviation; NB = no background correction. The standard reference material BHVO-1 was used to quantify analytical error.

Table T6. Logging tools and their applications.

Tool	Acronym	Tool string	Principle	Synthetic seismogram*	Lithology mineralogy†	Porosity	Geochemistry elements	Other	Sample interval (cm)	Approximate vertical resolution (cm)
Sonic:										
Long spacing	LSS	FMS/sonic	Sonic travel time	G	F	G			15	61
Resistivity:										
Shallow focused	SFR	Triple combo	Spherically focused current	F	F	VG			15	76
Dual induction	DIT-E	Triple combo	Induced current	F	F	VG			15	150 and 200
Dual laterolog	DLL	Triple combo	Focused current	F	F	VG			15	61
Formation MicroScanner	FMS	FMS/sonic	Focused microcurrent	P	P	G		‡	0.25	0.5
General purpose	GPIT	FMS/sonic	Oriented magnetic field	P	F			**	0.25	1
Inclinometer										
Neutron porosity	APS	Triple combo	Absorption of bombarding neutrons	P	F	VG	H		5 and 15	30
	CNT-G	Geochemical							15	46
Aluminum activation clay tool	AACT	Geochemical	Absorption of bombarding neutrons	P	F	P	Al, Mn		15	46
Induced gamma ray	GST	Geochemical	Capture of bombarding neutrons	F	VG	F	Ca, Si, Fe, S,		15	46
							Ti, Gd, H, Cl			
Spectroscopy							K, Th, U	††	15	46
Natural gamma ray	HNGS	Triple combo	Natural gamma-ray emissions	P	VG				15	46
Spectroscopy	NGT	FMS/sonic and geochemical							15	46
Bulk density	HLDS	Triple combo	Absorption of bombarding gamma rays	G	G	G			15	46
Temperature/acceleration/pressure	TAP	Triple combo	Formation temperature tool acceleration pressure					‡‡ ***	1/s 4/s 1/s	
Caliper	LCAL	Triple combo	Hole diameter		P			†††	15	

Notes: * = logs other than sonic and density can be converted to pseudosonic/density, based on known log responses to lithology and porosity. † = percentages of minerals with abundances >3% are determined from simultaneous inversion of several logs. Usefulness of tool for application: VG = very good; G = good; F = fair; P = poor. ‡ = detailed mapping of fractures, faults, foliations, and formation structures; analysis of depositional environments; formation dip. ** = magnetic reversals, stratigraphy, fault zones. †† = used for depth matching of logs. ‡‡ = heat flux, detection of permeable layers. *** = information on tool motion for eventual integration into heave compensation system. ††† = quality control for other logs. Blank spaces = no data.

Table T7. Principal channels of the logging tools.

Tool	Parameter	Meaning	Units
HNCS		Hostile environment spectral gamma ray sonde	
	HSGR	Standard (total) gamma ray	gAPI
	HCGR	Corrected gamma ray (HSGR - uranium contribution)	gAPI
	HFK	Formation potassium	Fraction
	HTHO	Thorium	ppm
	HURA	Uranium	ppm
NGT-C		Natural gamma ray tool	
	SGR	Standard total gamma ray	gAPI
	CGR	Computed gamma ray (SGR minus uranium contribution)	gAPI
	POTA	Potassium	Fraction
	THOR	Thorium	ppm
	URAN	Uranium	ppm
APS		Accelerator porosity sonde	
	APLC	Near array porosity (limestone corrected)	Fraction
	FPLC	Far array porosity (limestone corrected)	Fraction
	SIGF	Neutron capture cross section of the formation (Sf)	cu
	STOF	Tool standoff (computed distance from borehole wall)	in
HLDS		High temperature lithodensity sonde	
	RHOB	Bulk density (corrected)	g/cm ³
	PEF	Photoelectric effect factor	barns/e ⁻
	DRHO	Bulk density correction	g/cm ³
	LCAL	Caliper measure of borehole diameter	in
DIT-E/SFR		Phasor dual induction-spherically focused resistivity tool	
	IDPH	Deep induction phasor-processed resistivity	Ωm
	IMPH	Medium induction phasor-processed resistivity	Ωm
	SFLU	Spherically focused log of resistivity	Ωm
DLL		Dual laterolog	
	LLd	Deep resistivity	Ωm
	LLs	Shallow resistivity	Ωm
TAP		High-resolution temperature/acceleration/pressure tool	
	T, A, P	Temperature/acceleration/pressure	°C, mm/s ² , psi
LSS		Long spacing sonic sonde	
	LTT1-4	Transit time (10', 8', 12', 10' respectively)	ms
	DTLN, DTLF	Transit time differential (10'-8', 12'-10')	ms/ft
	WF1-4	Sonic waveforms	
	ITT	Integrated transit time	s
GPIT		General purpose inclinometer tool	
	Fx, Fy, Fz	Magnetic field on x, y, z axis	oer
	FNOR	Intensity of the total magnetic field	oer
	HAZI	Hole azimuth	°
	DEVI	Deviation	°
FMS		Formation MicroScanner resistivity image	Ωm
CNT-G		Compensated neutron log	
	NPHI	Thermal porosity	Fraction
AACT		Aluminum activation clay tool	
	UWAL	Uncorrected Al wet%	Fraction
	ALUM	Corrected Al wet wt%	Fraction
GST		Induced-gamma spectrometry tool	
	CSIG	Capture cross section	cu
	CTB	Background yield	Fraction
	PHIG	GST porosity	Fraction
		Yield of Si, Ca, Fe, S, H, Cl	Fraction